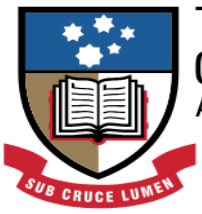

THE UNIVERSITY
OF ADELAIDE
AUSTRALIA

Investigation of tensile creep and tension stiffening behaviour for Ultra-High-Performance Fiber Reinforced Concrete (UHPFRC)

Prepared by

Mohammad Momeen Ul Islam
B.Sc (Civil Engineering) and M.Eng.Sc (Structural Engineering)

A dissertation submitted for the degree of

Master of Philosophy (Structural Engineering)

The School of Civil, Environment and Mining Engineering
The University of Adelaide
Australia

-April 2019-

ABSTRACT

Ultra-high-performance fiber reinforced concrete (UHPFRC) has improved properties over conventional concrete, such as high tensile strength, greater compressive strength and enhanced post cracking characteristics. The steel fibers in UHPFRC are recognized as providing resistance to crack widening in tension zones because of the fibers bridge adjacent cracks, which consequently enhances the tensile performance. Although, UHPFRC is capable of resisting the induced tensile stresses, it has still limitations under sustained tensile loads. It is also not well understood whether these characteristics would resist the induced tensile stress over a longer period or if they would leave the serviceability of the structure at risk. Therefore, the research presented in this study is concerned with the time-dependent tensile behaviour of UHPFRC.

The present study comprises of an experimental program based on the application of newly developed test rigs, preparation of the test specimens and investigations into the test results. The aims seek to provide an understanding of the instantaneous and time-dependent tensile behaviour of unreinforced and reinforced UHPFRC prisms. Instantaneous tensile tests were involved, applying axial tensile loads to UHPFRC prisms for both aged and unaged concrete. The time-dependent tensile behaviour of UHPFRC was investigated in terms of tensile creep and tension stiffening mechanisms under sustained tensile loads. The sustained tensile loads were considered as different percentages of cracking loads, such as 50% and 75% of the cracking loads of unreinforced UHPFRC specimens for the tensile creep test and 75%, 100%, 150%, and 200% of the cracking loads of reinforced UHPFRC specimens for the tension stiffening test. The cracking loads were determined from 28th day instantaneous tensile responses for both reinforced and unreinforced UHPFRC prisms. Two different test rigs were

used to conduct the tensile creep and tension stiffening tests under sustained tensile loads. The rigs were modified to overcome the limitations identified through the critical literature review.

The experimental results demonstrate that the tensile creep strain and tension stiffening mechanisms are greatly influenced by the shrinkage strain of UHPFRC. A significant portion of the measured total shrinkage was caused by autogenous shrinkage rather than drying shrinkage. The results demonstrate that higher sustained stress leads to higher tensile creep strain for the first 13 days, at a higher creep rate. Afterwards, the shrinkage strain dominates over the tensile creep strain. The extent of crack propagation and the deterioration of the bonds between the steel fibers and the cement matrix are also significantly affected by the sustained tensile loads.

.

STATEMENT OF ORIGINALITY

I certify that this work contains no material which has been accepted for the award of any other degree or diploma in my name, in any university or other tertiary institution and, to the best of my knowledge and belief, contains no material previously published or written by another person, except where due reference has been made in the text. In addition, I certify that no part of this work will, in the future, be used in a submission in my name, for any other degree or diploma in any university or other tertiary institution without the prior approval of the University of Adelaide and where applicable, any partner institution responsible for the joint-award of this degree.

I give permission for the digital version of my thesis to be made available on the web, via the University's digital research repository, the Library Search and also through web search engines, unless permission has been granted by the University to restrict access for a period of time.

Mohammad Momeen Ul Islam	16 April 2019
	Date

ACKNOWLEDGEMENT

I would like to express my sincere gratitude and appreciation to Dr Mohamed Ali Sadakkathulla and Dr Phillip Visintin, who supervise me in my M.Phil. research. Their invaluable advice, continuing supervision and support, encouragement, patience and weekly regular consultation were generous help throughout of M.Phil. reached me the final level.

I am extremely thankful to laboratory staffs Mr Ian, Mr. Jon Ayoub and Mr. Simon for their great assistance, help and suggestion to perform the experimental work. I want to give special thanks to Mr. Ian for his most great and valuable support and good cooperation in the mixing of concrete and instrumentation.

I want to give special thanks to Ms Alison-Jane Hunter (writing and language tutor, The University of Adelaide) for her support in language editing.

The financial support from the Adelaide Scholarships International (ASI) and the University of Adelaide are highly appreciated.

Finally, I am very much grateful to my parents, wife and my brother for their love, continuing support, motivation, understanding and encouragement during my M.Phil. start to final day. I dedicate this M.Phil. thesis to my parents.

TABLE OF CONTENT

LIST OF FIGURES

LIST OF TABLES

LIST OF EQUATIONS

CHAPTER 1 : INTRODUCTION

1.1 INTRODUCTION

In modern infrastructure, ultra-high-performance fiber reinforced Concrete (UHPFRC) has become appealing in construction industry because of its pseudo-static (partially ductile) mechanical properties and cost effectiveness (Li et al., 2001). UHPFRC principally consists of cement, silica fume, steel fibers and quartz sand (Makita and Brühwiler, 2014). It was first developed in France (Richard and Cheyrezy, 1995). Its compressive strength ranges from 100 to 150 MPa, as it contains steel fibers with a high tensile strength of 850 to 2000 MPa (Le, 2008). With the contemporary boom in the construction industry, UHPFRC is recognised in various important applications, such as bridge decks and girders, pavements (Fehling et al., 2008), marine construction, joint fills, wall facades, piles, stairs, urban furniture (Garas et al., 2010) as well as in blast and impact resistance applications (Pyo et al., 2016). There have been few experimental investigations conducted to study the long-term tensile behaviour of UHPFRC and the research in this field is mainly focused on the shear and flexural behaviour of UHPFRC. Therefore, there is a need to characterise the tensile behaviour of UHPFRC, which is a critical factor for understanding its performance under serviceability limit states related to the deflection and crack formation in UHPFRC structural members.

UHPFRC structural members are usually subjected to varying loading conditions and the material exhibits characteristics of deterioration in a reasonably ductile manner under compression, a partial ductile manner under tension and provides a distinctive energy absorption capability prior to crack formation, whilst cracks are found with small widths

before strain localization (Wille et al., 2014). According to Naaman et al. (2003), the tensile behaviour of UHPFRC can be classified into four levels, shown in Fig. 1.1 where Level 1

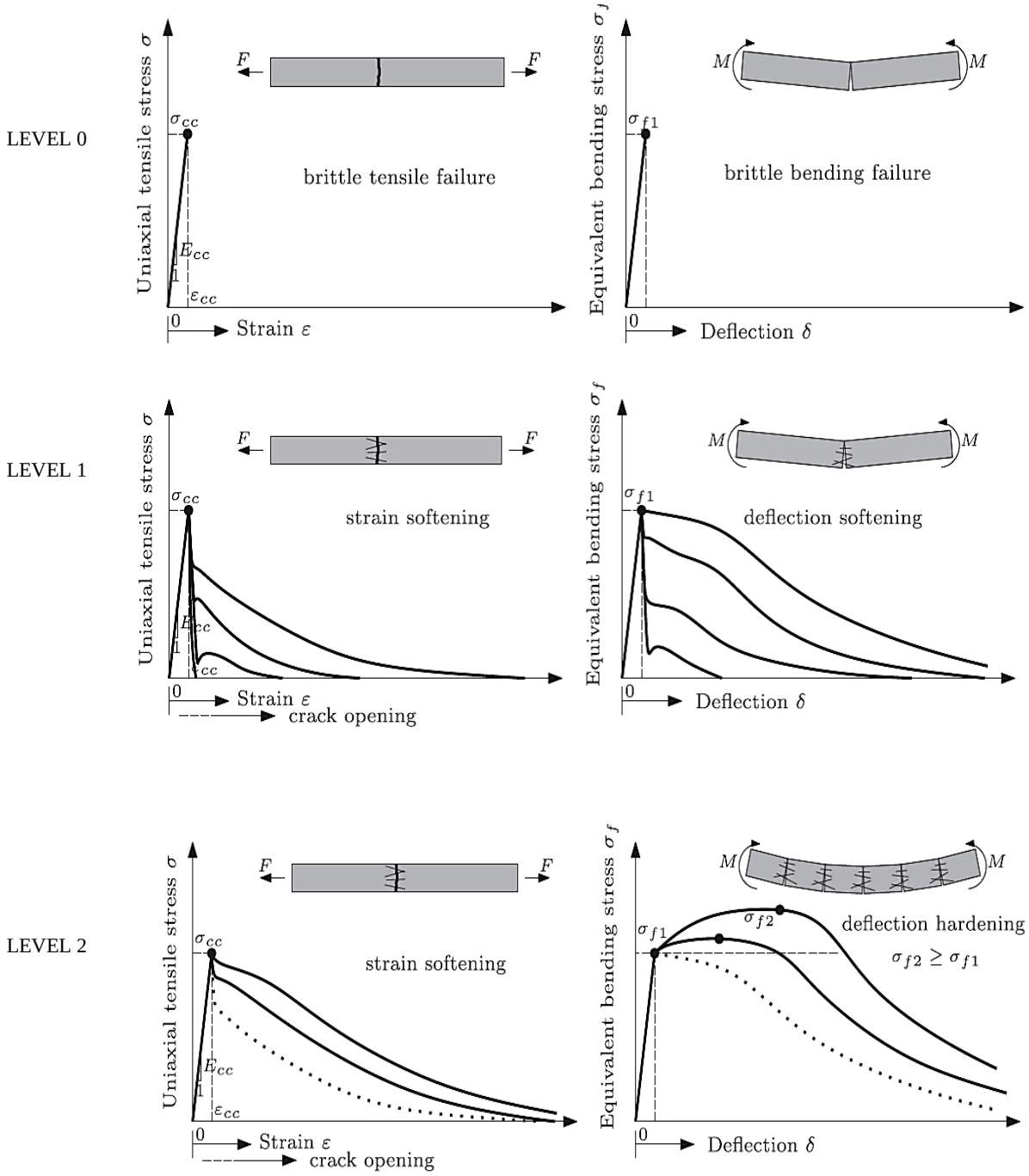

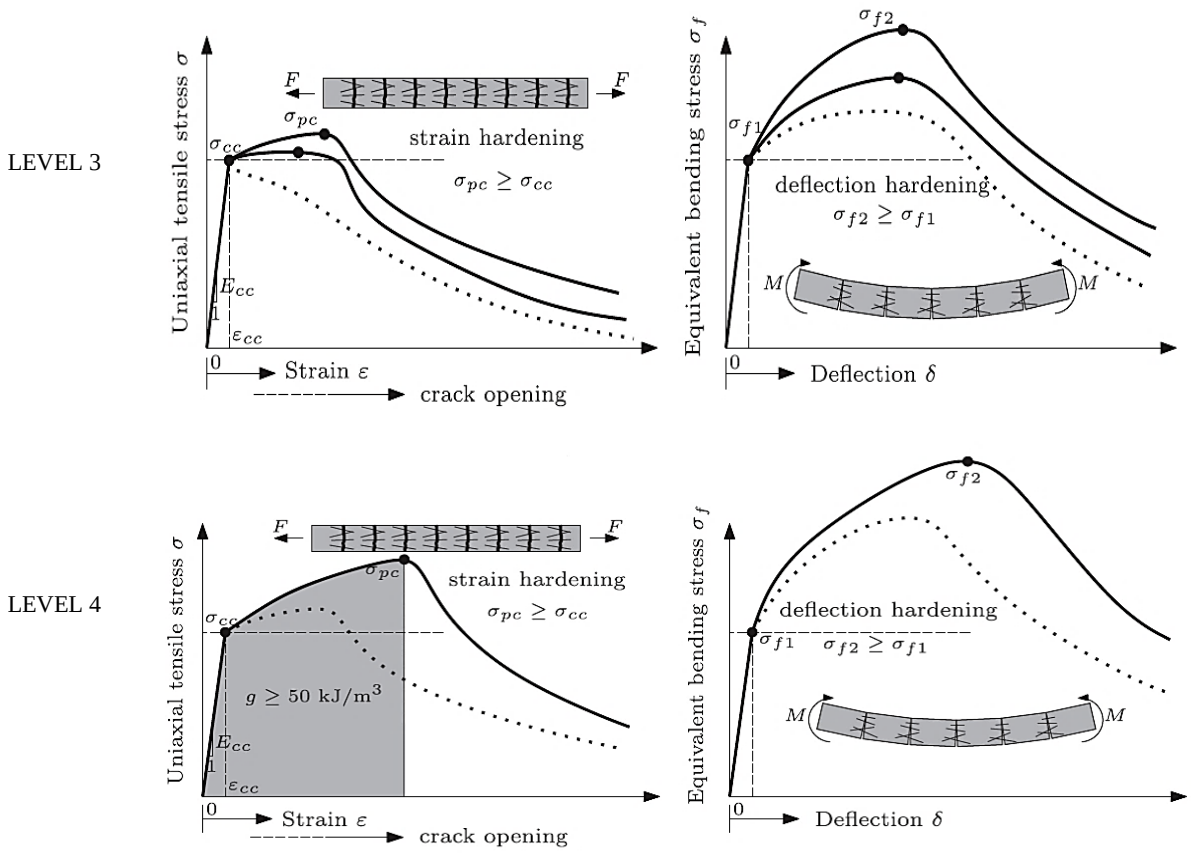

Fig. 1.1 Tensile behaviour of UHPFRC under direct tension where, σ_{cc} = cracking stress, ε_{cc} = associated strain, E_{cc} = elastic modulus, σ_{pc} = post cracking strength, σ_{f1} = modulus of rupture and σ_{f2} = equivalent bending strength (Wille et al, 2014, Naaman et al., 2003).

describes the controlling of cracks or softening for deflection with a moderate increase in mechanical properties, Level 2 shows hardening for deflection, Level 3 shows tensile strain hardening and Level 4 shows absorption of high energy. Level 0 has been added to show its character as a reference material without fiber. It is worth mentioning that the stress-strain relationship for UHPFRC is effective only prior to cracking and after the formation of cracks, the material's behaviour can be idealized as the relationship between the strain and the crack opening (Wille et al., 2014). The stress-strain curve principally comprises of three parts i.e. Part-I, Part-II and Part-III as shown in Fig. 1.2. Part–I is the elastic strain zone, characterized by the initial tensile strength up to the cracking stress $\sigma_{cc,}$ which is associated with an elastic

modulus of E_{cc} and a corresponding cracking strain of ε_{cc}. Part–II is the strain hardening slope within the region of (ε_{cc}, σ_{cc}) and (ε_{soft}, σ_{pc}), where there is a slow increase in stress coupled with a rapid increase in strain. This region has a strain hardening elastic modulus of E_{hc}. Part-III is the crack opening zone, which is characterized by the stress-crack width relationship. When UHPFRC exhibits the strain hardening property under tension, Part-II pertains to the multiple cracks leading to Part-III, which follows the softening curve along with crack localization. The unloading modulus E_{pc} distinguishes the strain softening (Part-III) and strain hardening (Part-II) zones.

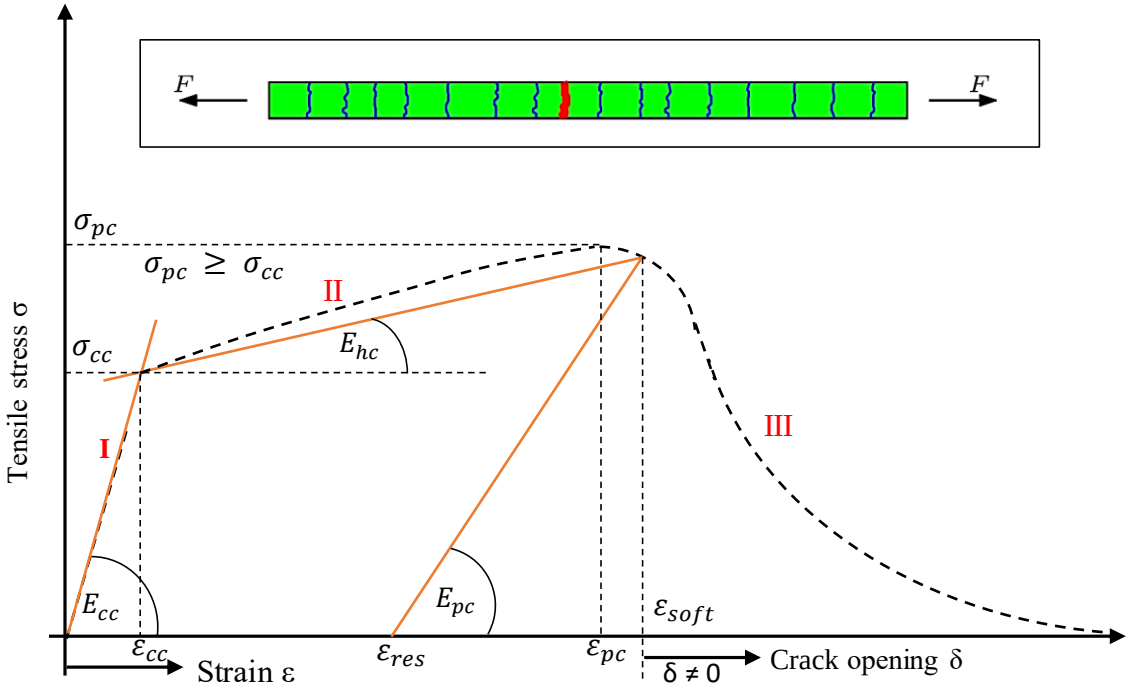

Fig. 1.2 Tensile properties of UHPFRC (Wille et al, 2014).

Generally, the UHPFRC structural members, i.e. beams, do not require provisional shear reinforcement, as the transverse pressure exerted by the longitudinal (main) reinforcement is resisted by the steel fibers in the surrounding concrete (Lagier et al., 2016). This resisting mechanism of anchoring the reinforcing bar is substantially carried out by the combined

action of the matrix and fibers. The individual resistance by the matrix and fibers is determined by the amount of tensile stress transferred to the interface, which is gained by the bond strength (Lee et al., 2010). Higher bond strength leads to the formation of narrower cracks with reduced spacing and low bond strength leads to the formation of larger cracks, while insufficient bond strength generates unexpected failure (Marchand et al., 2016). Thus, the bond characteristics control the cracking, tension stiffening and deflection of the RC member at its serviceability limit state (Sturm and Visintin., 2018). It is worth mentioning that the transfer of elastic stress is dominant before any crack occurs and debonding occurs across the bond at higher loading levels. Consequently, slip takes place and governs the transfer of stress at the matrix-fiber interface. Therefore, the bond characteristics are very important parameters in controlling any crack distributions and crack widths within the limitations of the serviceability state (Ebead et al., 2005). However, it is not well understood whether these bond characteristics will resist the induced tensile stress over a longer period or leave the serviceability of the structure at risk. Although UHPFRC is capable of resisting the induced tensile stresses, it has still limitations under sustained tensile loads. Zhao. et. al (2015) reported that UHPFRC shows time-dependent cracking under sustained tensile loads, which can be considered as the tensile creep behaviour of UHPFRC. This phenomenon leads to an increase in the crack width, redistribution of stresses and creep failure of the concrete structure. As the decay of the tensile resistance for UHPFRC is not well understood under sustained tensile loads, it is important to investigate tension stiffening and tensile creep simultaneously for better understanding of the tensile behaviour of UHPFRC.

UHPFRC possesses different material behaviours when compared with normal strength concrete (NSC) and high strength concrete (HSC) as it has a low water to binder ratio and contains higher fine additives in the absence of coarse aggregates (Yoo et al., 2013). This is

further complicated by rapid surface drying at an early age, which can result in the formation of premature shrinkage cracks. This could be due to the evaporation rate of the water from the surface of UHPFRC, which is higher than bleeding, so it results in a rapid condensation of the surface, while the interior volume of the UHPFRC remains fresh, leading to crack development. Moreover, shrinkage strains result in a change of member length before any load is applied and so the cracking load is reduced correspondingly (Bischoff 2003). As a result, the shrinkage strain has a significant importance in determining the tensile behaviour of UHPFRC, especially for understanding tensile creep (Rossi et al, 2013) and the tension stiffening mechanism (Bischoff, 2001). Therefore, the present study aims to investigate the time-dependent tensile behaviour of UHPFRC in terms of tensile creep and the tension stiffening mechanism and its associated effects. In this investigation, several experiments relating to the tensile behaviour of UHPFRC are presented and the results are discussed. Both reinforced and unreinforced UHPFRC prisms were tested to determine the tensile behaviour of UHPFRC, under instantaneous and sustained tensile loading conditions. To achieve this testing process, different percentages of cracking loads were selected as sustained tensile loads to investigate the time-dependent tensile behaviour of UHPFRC, such as 50% and 75% of cracking loads of unreinforced UHPFRC specimens for tensile creep tests and 75%, 100%, 150%, and 200% of cracking loads of reinforced UHPFRC specimens for tension stiffening tests. Two different types of test rig were designed and newly developed to carry out the tensile creep and tension stiffening tests for long-term, under-sustained, tensile loading conditions. Instantaneous loads were applied for both short-term and long-term aged concrete to determine the material properties of UHPFRC. UHPFRC prisms were used to determine both autogenous shrinkage and total drying shrinkage, which was considered in terms of its influence on tensile creep and the tension stiffening mechanism.

1.2 RESEARCH OBJECTIVES

The proposed research aims to investigate the mechanical material properties, tensile creep strain, tension stiffening mechanism and shrinkage strain for UHPFRC.

The following objectives were set:

1. Evaluating the mechanical material properties (compressive strength, tensile strength and modulus of elasticity) of UHPFRC.
2. Evaluating the time-dependent shrinkage strain value of UHPFRC.
3. Quantifying the instantaneous tensile response (direct tension) and time-dependent tensile behaviour (tensile creep) of unreinforced UHPFRC prisms.
4. Quantifying the instantaneous and time-dependent tension stiffening and cracking behaviour of reinforced UHPFRC prisms.

1.3 SCOPE OF THESIS

This thesis is organized into the following five chapters:

Chapter - 1 provides the general background, objectives of the research and the scope of the thesis.

Chapter - 2 presents the general knowledge, definitions, factors, limitations and current state of the art relating to this study. Furthermore, a review of the earlier research on tensile creep, shrinkage and tension stiffening of ultra-high-performance fiber reinforced concrete (UHPFRC) are discussed. A review of the earlier methods, equations and reports relating to this study is provided.

Chapter - 3 provides a clear picture of the methodology for the experiments that were conducted for this thesis. Detailed methods for evaluating the material properties, direct tensile strength and shrinkage are discussed. A newly designed steel frame is introduced to conduct tensile creep and tension stiffening tests for UHPFRC in the long term.

Chapter - 4 gives a detailed presentation of the experimental results for the various experiments that were conducted, such as for compressive strength, splitting tensile strength, modulus of elasticity, direct tensile strength as material properties and for time-dependent test shrinkage; tensile creep and tension stiffening test results are also described in this chapter. The results are analysed and validated with the previous research work in this chapter.

Finally, **Chapter - 5** provides a summary of the completed research for this study and it also contains the future research recommendations.

CHAPTER 2 LITERATURE REVIEW

2.1 INTRODUCTION

In this chapter, those aspects related to the research reported in the literature on material properties and tensile behaviours of ultra high-performance fiber reinforced concrete (UHPFRC) are summarized and reviewed critically. The mechanical properties of UHPFRC that are considered for the review include compressive strength, splitting tensile strength, modulus of elasticity and direct tensile strength subjected to instantaneous loading. Subsequently, the long-term tensile behaviours of UHPFRC, such as tensile creep and the tension stiffening mechanism under sustained tensile loads along with shrinkage, are reviewed critically. Special attention is paid to the different testing techniques and methods of measurement pertaining to tensile creep and the tension stiffening tests.

2.2 ULTRA HIGH-PERFORMANCE FIBER REINFORCED CONCRETE (UHPFRC)

UHPFRC is a versatile material that possess very high compressive strength (generally greater than 150 MPa) (Denarié et al., 2011), which is associated with higher tensile ductile characteristics. The enhanced ductile properties in UHPFRC are the result of using mixed recipes with a lower water to binder ratio and incorporation of steel fibers. The lower water to binder ratio (w/b) helps to densify the cement matrix, which consequently reduces the porosity in UHPFRC. These particular characteristics make this material suitable for application in various design purposes. It also provides the freedom to design potential structural elements with various shapes and degrees of slenderness due to the material's

capacity to avoid conventional steel reinforcement (Esteban et al., 2010). As the steel fiber in UHPFRC provides tensile capacity across the cracked sections, it also helps to enhance the shear capacity of the bending members. UHPFRC is also well known for its cost effectiveness because of the possibility of eliminating shear stirrups when designing reinforced concrete members (Graybeal et al., 2006).

2.2.1 **Advantages of UHPFRC**

Sustained effort over the past few decades to improve the properties of cementitious materials incorporating steel fibers, have led to the development of the novel material, UHPFRC. Some of the advantages of UHPFRC reported in the literature include its low permeability, high compressive strength, higher tensile strength and durability. It has very low permeability, which protects the concrete from the ingression of chloride and other aggressive agents, ultimately resisting corrosion of the reinforcing bars (Charron et al., 2007). UHPFRC, with correct and suitable fiber mixes, provides very low absorption to liquids and a dense matrix. Generally, the compressive strength of UHPFRC reaches more than 150 MPa and up to 20 MPa direct tensile strength, with considerable softening and strain hardening characteristics (Denarié et al., 2011). Due to these advantages, UHPFRC is currently being widely used in construction, for items such as bridges, nuclear waste, roofs, piers and structures that require blast resistance (Arafa et al., 2010). Moreover, UHPFRC exhibits better durability properties with lower maintenance costs during its service life than conventional concrete (Arafa et al., 2010) which makes it possible to design concrete structures without any shear reinforcement because of its advanced flexural strengths (Madhoun, 2013).

2.2.2 **Ingredients for manufacturing UHPFRC:**

The materials for UHPFRC have different characteristics from conventional concrete, as the large aggregates are omitted, and sand is the largest granular material, ranging from 150 to 600 microns (Mohammed et al., 2015), along with silica fume and a large amount of cement as binders. According to Aziz et al. (2012), UHPFRC can be produced after consideration of the following principles: (i) there should be an elimination of coarse aggregates to produce an homogeneous mix, (ii) heat treatment should be applied (iii) fibers should be added, whilst maintaining a low water to binder ratio yields some non-hydrated cement that can later react as a high elastic micro-aggregate and, (iv) an optimum grain size distribution should be ensured to gain the highest packing density.

The basic materials, such as Portland cement, silica fume, sand, superplasticizer, water, steel fibers, fillers and supplementary cementitious materials are used to manufacture UHPFRC.

2.3 **MATERIAL PROPERTIES**

2.3.1 Compressive strength

In modern structural engineering, compressive strength is one of the most vital parameters of concrete as an indicator for its structural performance. Generally, there are two standard methods for determining the compressive strength: one is by testing cubes and the other is by testing cylinders. France, Australia, North America, New Zealand and Japan specify cylinders as the standard specimen in their national codes, whereas Europe and rest of the countries prefer cubes to determine the compressive strength (Graybeal et al., 2008).

Graybeal et al. (2008) conducted an experiment to determine an alternate reliable test of specimen details for UHPFRC, whose compressive strength ranged from 80 MPa to 200 MPa.

They investigated the suitability of using both cube specimens (75 mm diameter and 100 mm height) and cylinder specimens (50 mm × 70.7 mm × 100 mm) for compressive strength tests. They suggested the use of cube specimens over cylinder specimens, where the cylinder's edge preparation and the capacity of the machine were of concern. It was recommended to use 100 mm cubes and cylinders with 75 mm or 100 mm diameters to determine the compressive strength of UHPFRC.

Now a days, UHPFRC is produced with a precisely optimized blend of nano materials such as: silica fumes, quarts flour and silica sand. However, its production is achieved by optimizing the following: the characteristics of the cementing medium, characteristics of the aggregates, proportions of the paste, paste aggregate interactions, mixing, consolidating and curing. Wille and Naaman (2011) showed that increasing the silica fumes replacement from 0% to 25% significantly increased the compressive strength up to 158 MPa. Moreover, they tested glass powder replacement values and concluded that a replacement value of 20-30 % of cement resulted in a compressive strength of 240 MPa.

Yu et al. (2014) conducted intensive experimental works in evaluating the compressive strength of different UHPFRC mixes. They also reported that, with the addition of steel fibers, the compressive strength of UHPFRC might be significantly enhanced, whilst the strength was found to increase from 94.2 MPa to 148.6 MPa after the addition of steel fibers. A significant amount of strength was achieved by Richard and Cheyrezy (1995) by using a 10% volume fraction of steel fibers along with 50 MPa pressure, adopted at an elevated temperature of 400° C, to reach a compressive strength of 800 MPa. They reported that the elimination of coarse aggregate, associated with an optimized granular mixture, exhibits a denser cement matrix, which results in a higher compressive strength for UHPFRC.

2.3.2 Tensile strength

In the reported literature, the tensile characteristics can mainly be obtained through three methods: (1) a direct tension test using dog bone. (2) the standard prism test for the modulus of rupture or a beam flexural strength test and, (3) splitting tensile strength. Of these three methods, the direct tension method is preferred by the researchers as this yields the complete stress (σ)- strain (ε) curve prior to the cracking and stress (σ) – crack width (W_{cr}) relationship in post cracking.

2.3.2.1 Direct tension test

For a specimen under direct tension (shown in Fig. 2.1), the fracture energy can be denoted as the zone under the stress-strain curve to formulate a unit zone of the crack surface, which can be represented by the following Equation 2.1 (Peterson, 1980).

$$G_f = \int_0^{\delta_{max}} f_t d\delta_t \quad \text{---------- Equation 2.1}$$

where f_t is a function of tensile displacement δ_t and $\delta_{max\,t}$ is the maximum tensile effective displacement when f_t reaches to zero. Hillerborg et al., (1976) reported that the energy absorbed by the concrete members under tension is associated with the descending area of the stress displacement shown in Fig. 2.2.

Principally, stress increases with the increase in deformation until reaching the ultimate stress and then starts to decrease with the increase of deformation. The descending branch characteristics in Fig. 2.3 are termed as the strain softening (Hillerborg, 1985). This strain softening behaviour takes place in a small area of the concrete specimen, termed the fracture process zone. With the progress of the fracture process zone, the strain distribution becomes

ineffective along the concrete specimen. The deformation keeps increasing with the continuous formation of the damage zone and decreases with the relaxation of the specimen. This zone, denoted in the graph, expresses the amount of energy that is absorbed in a tensile

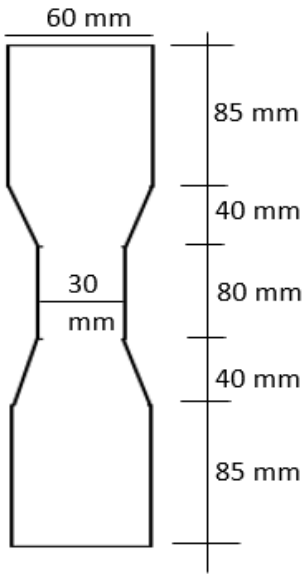

Fig. 2.1 Dog bone specimen sample for direct tensile test (Ding et al., 2018).

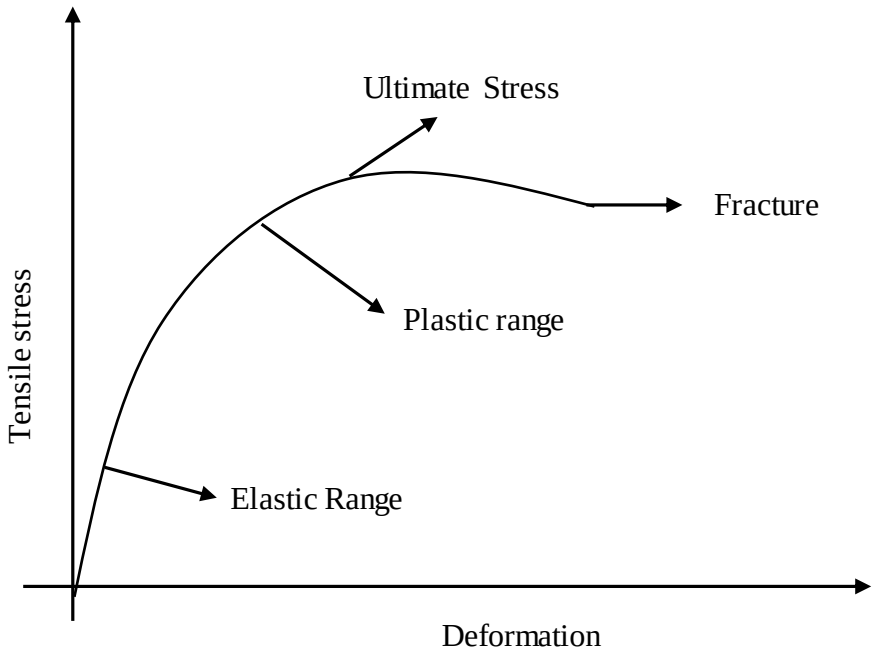

Fig. 2.2 Stress strain relation of Concrete (Hillerborg et al., 1976).

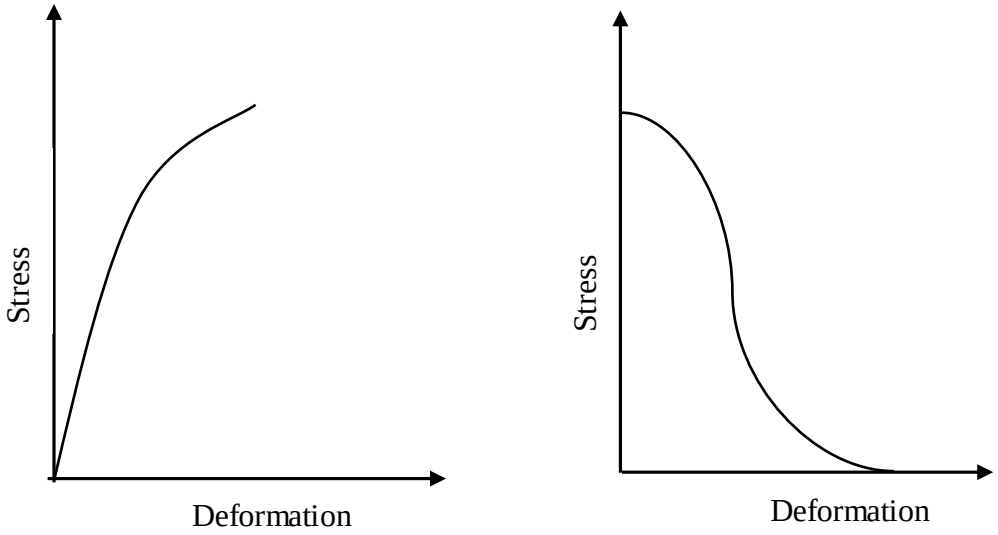

Fig. 2.3 Ascending and descending behaviour within the damage zone of concrete under direct tension (Hillerborg, 1985).

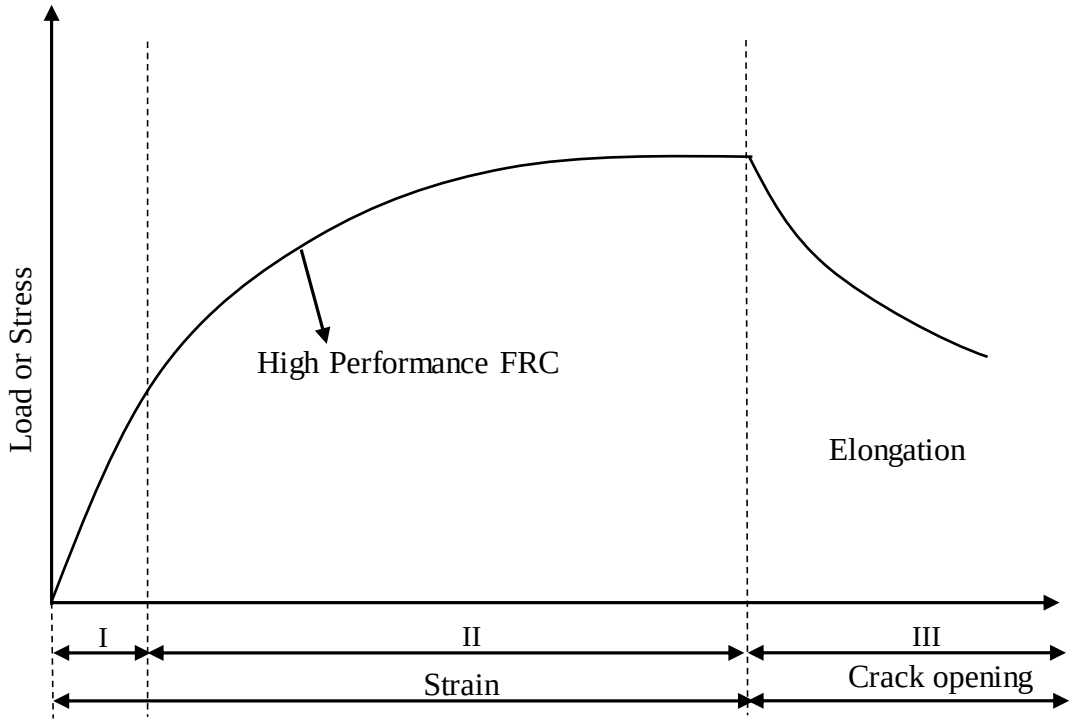

Fig. 2.4 Stress-strain relation for UHPFRC (Martin et al., 2007).

test. This absorbed energy is categorized into two portions, shown in Fig. 2.3, where the ascending portion shows the amount of energy per unit volume and the descending curve represents the amount of energy absorbed in the fracture zone (Hillerborg, 1985). Marzouk et al. (1995) performed an experiment for high strength concrete (HSC) under direct tension. They reported that HSC presents higher brittle failure than NSC. It was also observed that a sharp failure shows as a descending curve after the maximum stress is reached in a stress-strain diagram. Fig. 2.4 shows the stress-strain relationship for UHPFRC where the fibers in UHPFRC exhibit a region of inelastic strain hardening, and also the area between the ultimate load and the end of the elastic line, which can be termed the multiple cracking phase. It consists of three phases: phase I (the micro cracking stage), phase II (the strain hardening stage) and phase III (the softening stage) (Martin et al., 2007).

2.3.3 Flexural strength

Flexural strength, which is an important material property of concrete, generally known as the modulus of rupture, can be defined as the maximum tensile stress in a specimen prior to its failure in a flexure test (Ashby, 2011). This test is adopted for a specimen with either a rectangular or a circular cross-section, and provides the maximum stress obtained from the materials at the yielding point. This can be expressed in terms of stress σ, as shown in Fig. 2.5. The flexural test can be determined following two standard test methods, namely (i) standard test method ASTM C78 (2010) (third-point loading) and (ii) ASTM C293 (2010) (center-point loading).

For a rectangular beam specimen under three-point loading, the flexural strength can be expressed as Equation 2.2:

$$\sigma = \frac{3FL}{2bd^2} \quad \text{---------- Equation 2.2}$$

where, F = the applied load at the fracture point, b = the width of the specimen, d = the depth of the specimen and L = the effective span of the beam.

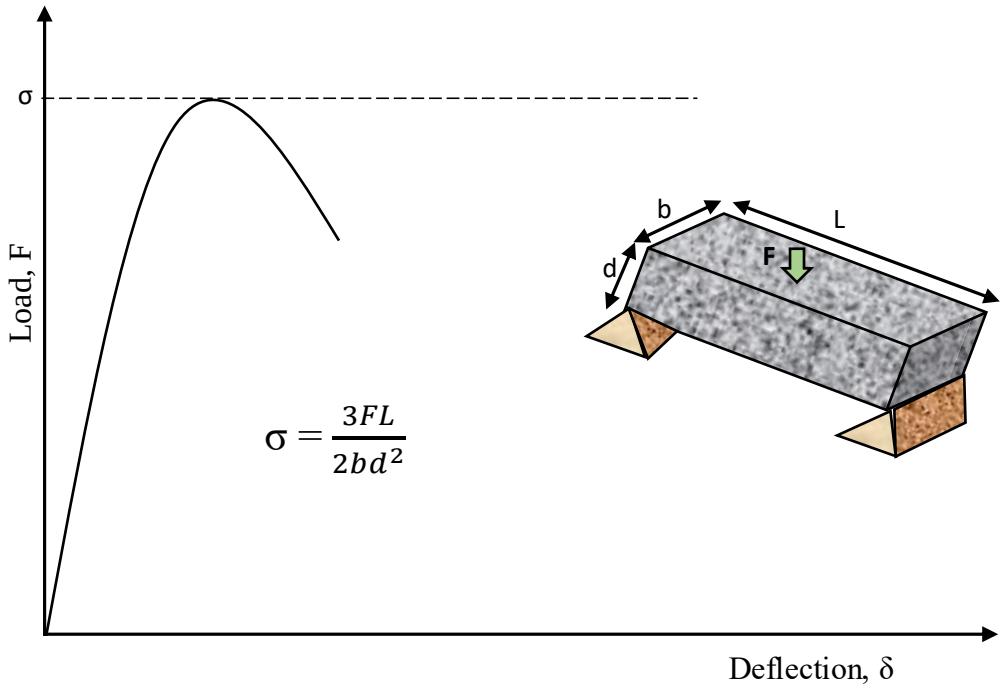

Fig. 2.5 The flexural beam test.

When the specimen is under four-point loading (when the loading span length is one third of the support span), the following equation (Equation 2.3) gives the flexural strength

$$\sigma = \frac{FL}{bd^2} \quad \text{---------- Equation 2.3}$$

Yang et al. (2009) conducted a flexural strength test for UHPFRC prisms where the applied loading condition was four-point bending. They observed the formation of a single failure crack at the bending failure between two loading heads. Prior to the failure of the specimen, several transverse cracks were visible on the tension faces of the specimen, while only one

crack was widening continuously at the weakest section. This single crack was progressing to weaken the bridging effect of the steel fibers in UHPFRC and it propagated to the top surface of the prism specimen. The crack tip was found to end just below any one of the plates. They reported the maximum flexural strength of 24 MPa at 28th day for UHPFRC with a corresponding compressive strength of 124 MPa.

Yu et al. (2014) performed the flexural strength test for UHPC both with steel fibers and without fibers. They reported that the addition of the steel fibers in UHPC significantly increased the flexural strength from 16.7 MPa to 32.7 MPa at 28th day, whilst the compressive strength ranged from 78 MPa to 158 MPa. They concluded that adding the steel fibers in UHPC contributes to bridging the cracks and retards the crack propagation, which directly increases the flexural strength.

2.3.4 Splitting tensile strength

A splitting tensile strength test is performed to determine the tensile capacity of concrete indirectly. This test measures the tensile strength of concrete by compressing the cylinder through a centre line. High compressive stress is produced by the loading conditions adjacent to the loading point, where the tensile stress acts horizontally. It is assumed that the compressive stress acts at about a 1/6 depth of the cylinder and the remaining 5/6 depth is under tensile stress because of the Poisson ratio effect. UHPFRC provides significantly higher tensile strength than the normal concrete both before and after cracking. Basically, the tensile capacity allows for a higher tensile load prior to the cracking in structural applications. There are several test methods to determine the tensile strength directly and indirectly (Graybeal et al., 2003). ASTM C496 (2011) is the standard test method to determine the indirect tensile strength and hence the tensile capacity. According to ASTM C496 (2011),

while tensile capacity can also be increased to 0.70 to 1.37 MPa/min, it can also be modified to 3.45 MPa/min whilst applying the loads.

Different test methods have been reported by previous researchers such as Kanstad et al., (1999), Kasai et al., (1971), Hellman (1969), Lauba (1990) and Bellander (1976) for conducting a splitting tensile strength test.

2.3.4 Modulus of elasticity (MOE)

The modulus of elasticity (MOE) can be determined from the slope of the linear elastic portion in a stress strain diagram. The MOE of UHPFRC is obtained from the same specimen used for the compressive strength test and it is usually described in standard ASTM C318 (2013).

The MOE can also be obtained from the known compressive strength (f'_c) value for design purposes, using empirical formulas. An equation (Equation 2.4) is represented by ACI 318 (2010), which is related to the 28th day compressive strength (f'_c) of normal strength concrete (NSC) and for the unit weight (w_c) of 1440 kg/m^3 to 2400 kg/m^3.

$$E_c\,(MPa) = w_c \times 4853 \times \sqrt{f'_c} \quad \text{---------- Equation 2.4}$$

High strength concrete (HSC) possess higher compressive strength when compared with NSC; ACI 363 (2011) provides a modified equation (Equation 2.5) for normal strength concrete with compressive strength ranging from 21 MPa to 83 MPa.

$$E_c\,(MPa) = 5.88 \times 10^6 \times \sqrt{f'_c} + 1.47 \times 10^8 \quad \text{---------- Equation 2.5}$$

Both these equations can be used when the compressive strength is less than 83 MPa. However, in the case of UHPC, an equation was prescribed by the Cattenom nuclear power plant reports, where 196 cylinders with a 2.76-inch diameter were used to present the

relationship between the MOE and the compressive strength. The equation (Equation 2.6) is as follows, where f'_c is the compressive strength of UHPC after thermal treatment at 28th day.

$$E_c(MPa) = 3.85 \times 10^6 \times 147 \sqrt[3]{f'_c} \quad \text{---------- Equation 2.6}$$

If the test data is not available for estimating the MOE of the UHPC, it can be obtained from empirical relationships, including the following equations (Equation 2.7, Equation 2.8 and Equation 2.9):

For thermally treated concrete,

$$E_c(MPa) = 7.35 \times 10^6 \times 147 \sqrt[3]{f'_c} \quad \text{---------- Equation 2.7}$$

(Voort et al., 2008)

$$E_c(MPa) = 5.16 \times 10^7 \times 147 \sqrt[3.14]{f'_c} \quad \text{---------- Equation 2.8}$$

(Kollmorgen, 2004)

For non-thermally treated concrete,

$$E_c(MPa) = 6.79 \times 10^6 \times 147 \sqrt{f'_c} \quad \text{---------- Equation 2.9}$$

(Graybeal, 2006)

2.4 SHRINKAGE

Concrete shrinkage occurs in unrestrained and unloaded specimens. The shrinkage strain is time-dependent. There are various types of shrinkage and these occur in two stages, one at an early stage (less than 24 hours after casting) and another one is in the long term (more than 24 hours).

It was reported by Gilbert and Ranzi, (2010); Gribniak et al., (2008); and Lam, (2002) that concrete shrinkage could be categorized into four major components, namely plastic shrinkage, chemical shrinkage, carbonation shrinkage, drying shrinkage and autogenous shrinkage. Plastic shrinkage strain is on the moisture which is lost from freshly cast concrete

to the surrounding environment, whereas autogenous shrinkage, drying shrinkage and carbonation shrinkage occur in hardened concrete after setting. Autogenous or chemical shrinkage occurs at the early phases of drying because of chemical reactions within the cement paste and binder; this includes the hydration of cement without any moisture movement to the outside environment. In the case of carbonation shrinkage, there should be a chemical reaction between the different products of cement hydration and the atmospheric carbon dioxide. According to Holt and Leivo (2004), different shrinkage stages and types are as illustrated in Fig. 2.6, where drying shrinkage at initial stages has a negligible effect when compared with the shrinkage for long-term. Drying shrinkage in concrete usually occurs over a long period of time and it increases with time at a continuous declining rate. There are several factors influencing the drying shrinkage to occur. These are the water binder ratio, types of binders, aggregate types, relative humidity, and the shape and size of the structure. To analyse the effect of shrinkage on concrete structures, two types of shrinkage are mainly considered: drying and autogenous shrinkage (Gribniak et al., 2008; Holt and Leivo, 2004). The ratio of drying and autogenous shrinkage is shown in Fig. 2.7 (Sakata and Shimomura, 2004) for normal strength concrete where the drying shrinkage governs the autogenous shrinkage. Generally, the autogenous shrinkage is approximately 10 to 20% of the total shrinkage strain (Silliman and Newtson, 2006a), whilst the drying shrinkage is assumed to be the most crucial factor.

Reinforced concrete members, such as beams, or slabs, which are embedded with reinforcements, and other concrete members supported with joints, may provide a restraining effect to the shrinkage, leading to shrinkage induced curvature. Hence, the curvature induced by shrinkage can often cause significant deflection of the member, which is load independent. Therefore, shrinkage starain is one of the important factors that affects time-dependent

deflection in RC flexural members (Gilbert et al., 2010; Jafarifar et al., 2014; Jayasinghe, 2011).

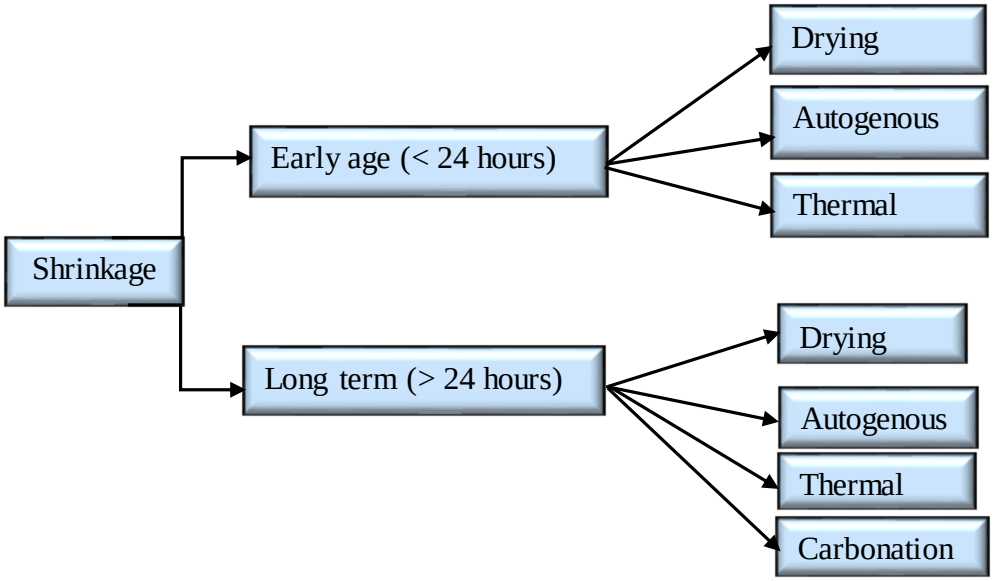

Fig. 2.6 Shrinkage stages and types of concrete.

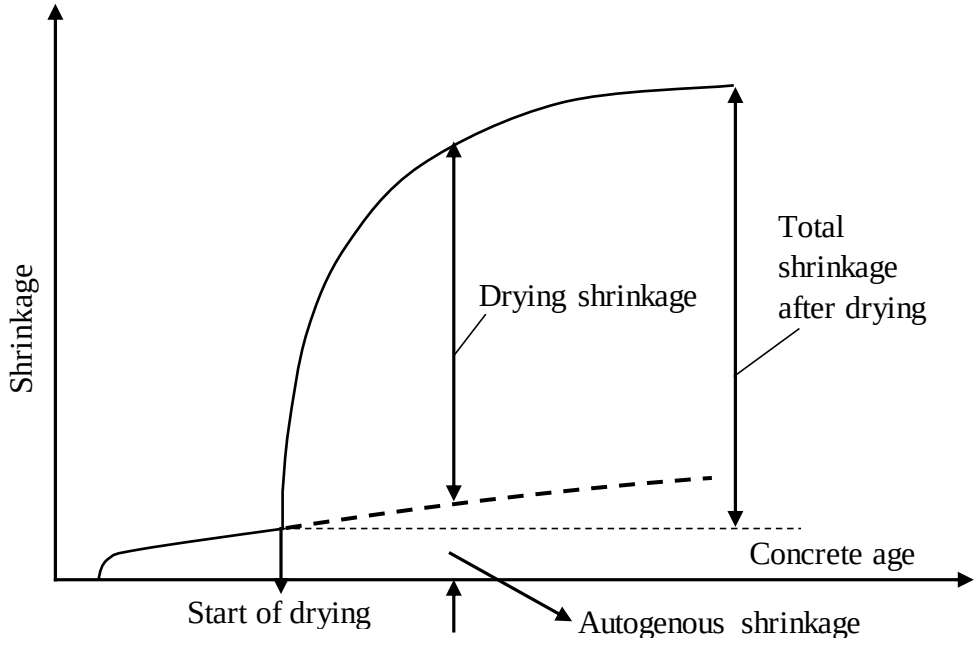

Fig. 2.7 Shrinkage strain components in normal strength concrete (Sakata et al., 2004; Gribniak et al., 2008).

The importance of evaluating shrinkage values has been reported to a number of recent studies intended at understanding the basic mechanisms leading autogenous shrinkage in UHPC and its influence on performance. For example, experimental programs performed by Yoo et al. (2014) and Şahmaran et al. (2015) observed the effects of curing conditions, mixing proportions, specimen restraints and geometry on autogenous shrinkage starin of UHPC specimens methodically. Research has determined several factors for reducing both the value of shrinkage strain, as well as the period over which they progress. For example, Rößler et al. (2014) have reported that by curing at a temperature of 20 °C, a decrease of 85% in autogenous shrinkage strain is possible, in comparison with those gained at 90 °C heat curing. Other researchers have found that drying shrinkage could be reduced through the addition of superabsorbent polymers into the mix for moisture retaining. These exerts water over the time, substituting that lost because of drying and hydration, causing in a decrease of 75% for the shrinkage strain.

2.5 TENSILE CREEP

2.5.1 Definition and mechanism

Creep is stress and time dependent strain under prolonged constant or sustained loads. To define creep clearly, two identical specimens can be considered in similar ambient conditions, where one specimen could be under external load and the other one load free. The strain difference between these two specimens is generally considered to be creep.

Creep is classified into two types in terms of ambient humidity; namely basic creep and drying creep. Basic creep occurs when the concrete specimen is sealed to prevent the moisture transfer from the surface of the concrete to the surrounding environment. Drying creep occurs

when the concrete surface is exposed to the environment and moisture stabilizes between the environment and the surface of the concrete. It is generally considered that the magnitude of drying creep is much higher than that of basic creep. Again, depending on the loading condition, creep can be defined into two categories, namely compressive creep and tensile creep. Compressive creep occurs when the specimen is under constant or sustained compressive loads and tensile creep occurs under sustained tensile loads. The mechanism of creep has been studied for several decades, but it is still not well understood.

There are various theories for explaining the creep mechanism in the literature, such as plastic theory, visco-elastic and viscous theory, mechanical deformation theory, seepage theory, micro-cracking theory and solid solution theory (Neville et al., 1981) but it is generally agreed that none of these theories can account for every kind of observed phenomena. The main mechanism of creep can be described as follows (Neville et al., 1981): firstly, sliding or shearing of the gel particles causes the viscous flow of the cement paste. Next, the redistribution of water in pores under stress and seepage cause the consolidation. Finally, the delayed elasticity is found due to the restraint behaviour of the cement paste on the skeleton elastic deformation formed by the gel-crystals and aggregate.

2.5.2 Factors effecting tensile creep

There are several factors, such as closure of voids in the concrete, viscous flow of the cement-water paste, crystalline flow in aggregates, and water flowing out of the cement "gel" due to drying and loading, and the bond strength at the interfacial transition zone (ITZ), which may change during the prolonged period of a tensile creep test, and which will complicate the stability of the concrete specimen while under loading. Consequently, this instability causes the non-linearity and scattering of the recorded data. Hence, performing the tensile creep test over a long term has always been difficult. Moreover, UHPC with fiber exhibits different

material responses, such as developing pseudo-ductile properties, high tensile strength and compressive strength, in comparison with normal strength and high-performance concrete (Yoo et al., 2013).

The tensile creep mechanism is complex and depends on a variety of factors, such as the temperature, humidity, load effects, water binder ratio (w/b), progressive debonding, pull out of fibers, modulus of elasticity of fibers, and crack propagation under sustained loading (Bazant el al., 1982; Byfors, 1980; Neville, et al., 1981; Gettu et al., 2017). This is further complicated by other factors, such as the porosity of the concrete, distribution of the fibers, type and volume of fiber and the bond at the interfacial transition zone of the fiber and cement matrix, stress level, strength of concrete (as creep in higher-strength concrete is less than that in lower-strength concrete) and aggregate content (as an increase in either the aggregate content or the maximum aggregate size reduces creep) (Gilbert et al., 2002).

It is also worth noting that creep increases with the decrease in relative humidity and it depends on the ratio of the volume to the exposed surface area of the concrete specimen. However, this dependence of creep on the volume to surface area ratio and relative humidity can be minimized with an increase in concrete strength. Furthermore, creep also depends on the loading history, particularly on the stress-strain ratio and the age of the concrete. It is considered that when the concrete stress is less than about $0.5f_c'$ (where f_c' is the compressive strength), the creep strain shows a linear relationship with the stress. It is also greater for early age loaded concrete specimens than later age loaded specimens.

2.5.3 Test methods for tensile creep

Various test rigs have been developed to investigate the tensile creep behaviour of concrete and the most common form of rig that has been developed to perform the test is a dead load

lever arm system developed by Bissonnette et al. (1995; Garas et al. (2010); Ranaivomanana et al. (2013); Reinhardt et al. (2006); Switek et al. (2009).

Garas et al. (2010) developed a test set up, as shown in Fig. 2.8**,** where three UHPC specimens were placed in a series of individual frames with a maximum sustained tensile load capacity of 66.68 kN. This test set up was modified following the previous test set up developed by Bissonnette et al. (1995), where the required minimum number of specimens prescribed by the ASTM C512 (2011) was adhered to.

The rig was built such that the dead load-based lever arm was connected to the end of the dead load point through a metal ball knob, and the other end was connected to the frame via a ball bearing as a pinned or hinge connection. This type of connection helps to minimize the friction loss while applying the tensile dead load. To apply the tensile dead load, a 455 mm × 455 mm × 25 mm steel plate was used and the steel plates weighted from 382.5 N to 402 N. Four sets of steel plates (shown in Fig. 2.9) were inserted into the two opposite ends (cross section 75 mm × 75 mm) of each test specimen, whilst the gauge length of each set was 250 mm. Mechanical demec gauges were used to determine the creep of the specimen with an accuracy of ± 10-micro strains.

Ranaivomanana et al. (2013) determined the tensile creep for high strength concrete using the loading device illustrated in Fig. 2.10. This loading device was designed to apply loads for two specimens simultaneously, with associated hydraulic jacks. Longitudinal deformation of the specimen was measured by inductive transducers positioned at the reservation (Fig. 2.11) that was created while casting, by placing a removable metal inside the mould. LVDT was also used in this loading device at the upper portion of the specimen (Fig. 2.10) to measure the deformation of the specimen. The entire strain measurement and loading was maintained following the RILEM recommendations (RILEM subcommittee 4, 1998).

Kamen et. Al. (2009) used a temperature stress testing machine (TSTM) to determine the basic tensile creep of the UHPFRC specimen, where two different devices were adopted. The

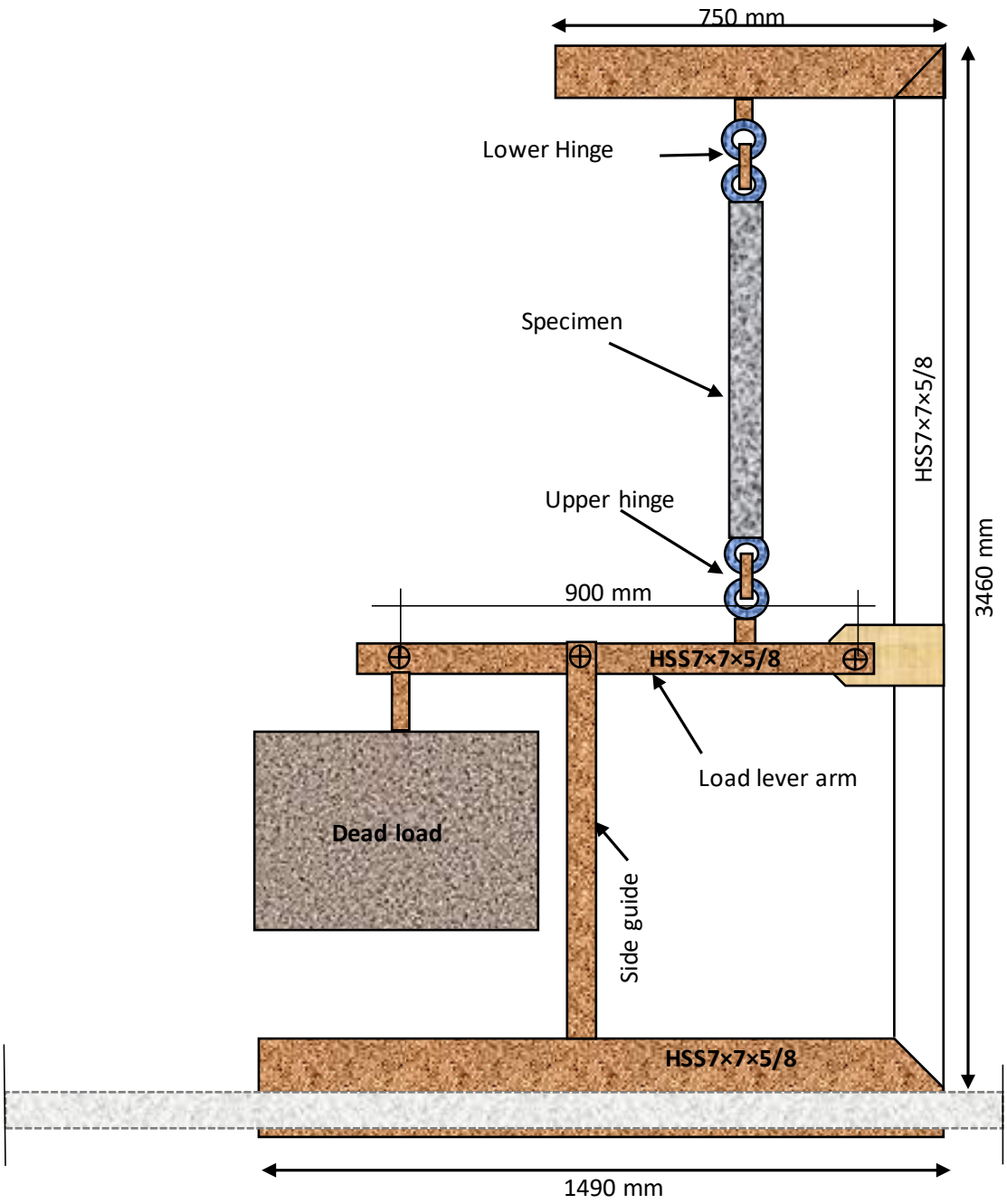

Fig. 2.8 Tensile creep test frame built at Georgia Tech (Garas et al, 2010).

main function of these two devices was to determine the free shrinkage and total deformation under restrained deformation. To determine the basic tensile creep, several layers of self-adhesive tape were used to restrict the moisture transformation from the surface of the concrete. A specific environmental condition was maintained prior to the commencement of the tensile creep experiments. While conducting the experiments, it is recommended to use replicate specimens to determine both autogenous shrinkage and total strain values. The tensile creep is determined by subtracting the autogenous shrinkage from the total strain.

Some studies (Garas et al., 2012; Garas et al., 2010; Ranaivomanana et al., 2013) deducted the immediate strain just after applying the load (termed instantaneous strain) along with autogenous strain from the total strain to determine the actual tensile creep. These investigations considered the free shrinkage of the specimen at similar ambient conditions for tensile creep specimens. However, the reliability of both types of experiment (considering autogenous shrinkage and free shrinkage) without considering the instantaneous strain fails to provide a precise tensile creep result.

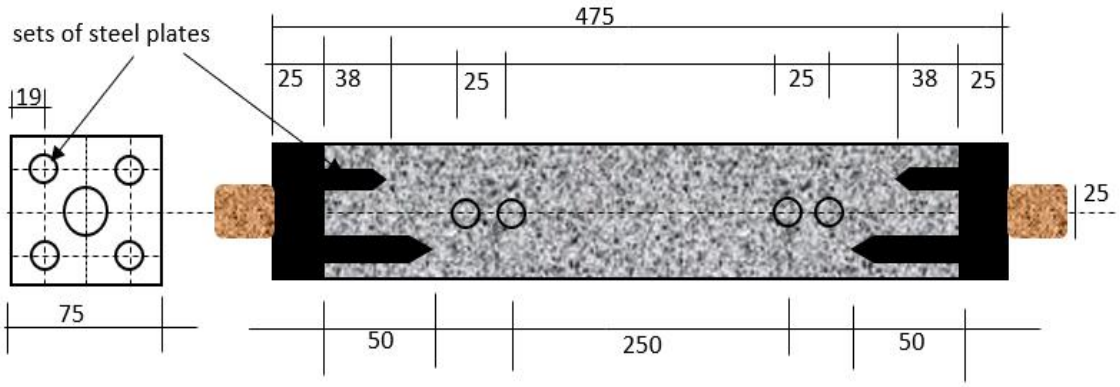

Fig. 2.9 Tensile creep specimen (Garas et al., 2010).

Different specimen shapes were also adopted to determine the tensile creep. The most common specimen type used was a rectangular prism (Garas et al., 2012; Garas et al., 2010; Ranaivomanana et al., 2013). Other researchers used dog bone shaped specimens (Østergaard et al., 2001; Reinhardt et al., 2006), cylinders (Błyszko, 2017; Garas et al., 2009) and cubes (Zhao et al., 2016) to determine the tensile creep.

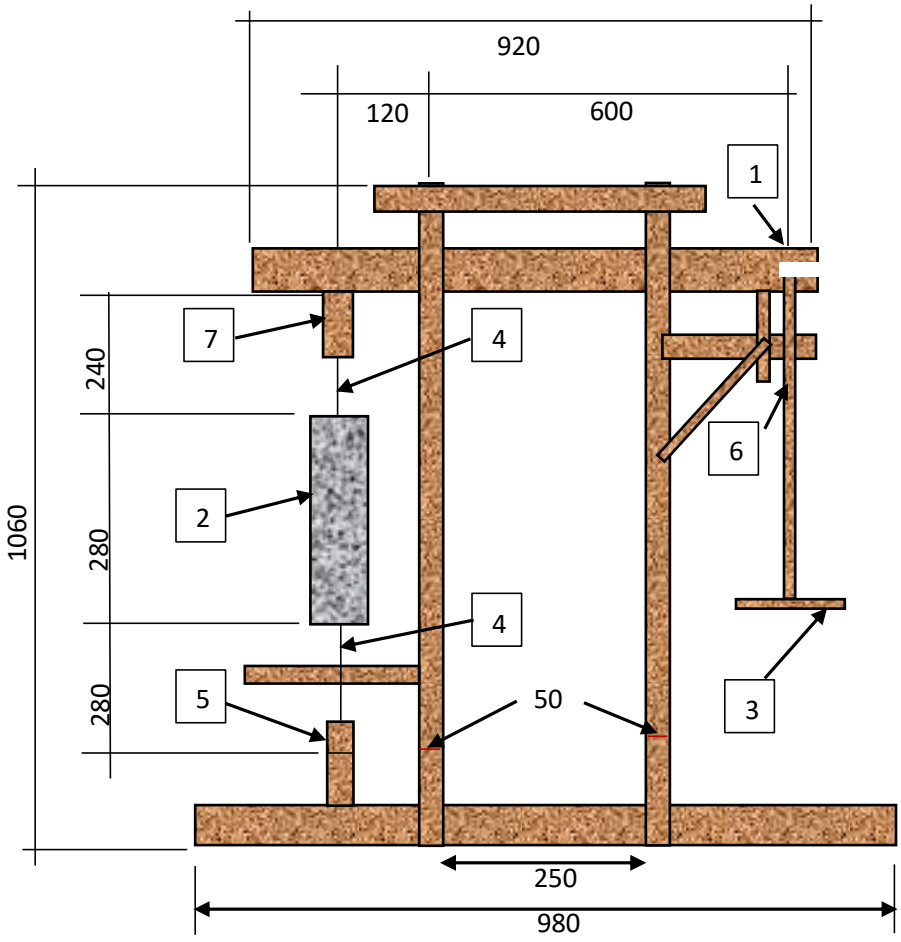

Fig. 2.10 Tensile creep test set up (all dimensions are in mm) following lever arm mechanism where (1)lever arm, (2)70 × 70 × 280 mm prismatic specimen, (3) platen, (4) cable, (5) screw system to control the horizontality of the lever arm, (6) stopping device and (7) cylindrical roller (Ranaivomanana et al., 2013).

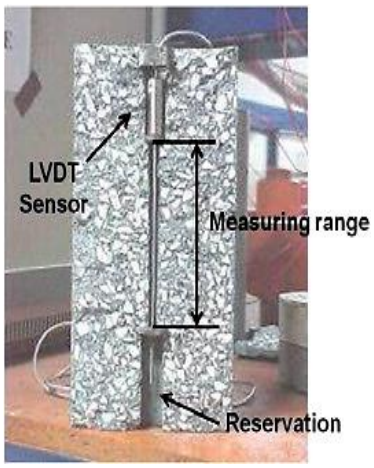

Fig. 2.11 Test set up for the specimen (Ranaivomanana et al., 2013).

2.5.4 Investigation on tensile Creep

Several types of research work have been conducted to determine the tensile creep of UHPFRC. It has been observed that steel fiber provides better crack resistance than synthetic fibers where the angle of the fibers influences both the tensile strength and the permeability of the concrete. The expected fiber hook angle should be 39º. A fiber hook angle of more than 39º causes a reduction in tensile strength and an increase in permeability (Plagué et al., 2017). Twisted types of fibers exhibit better mechanical properties than specimens with straight fibers at high strain rates and the strain capacity can be increased using all types of fibers (Pyo et al., 2016). Steel fiber has been used more often to strengthen and prevent the cracks in concrete. Steel fiber shows higher creep during the first 24 hours than concrete without fiber (Błyszko, 2017). To avoid high creep at an early period, polypropylene fibers can be used, which eliminate the formation of cracks at an early age. It was also found that short steel fibers decrease the tensile creep of UHPFRC when compared with NSC and HSC (Garas et al., 2009). It has also been reported that steel fibers with high elasticity reduce the tensile creep value of plain concrete more effectively than steel fibers with a lower elastic modulus (Zhao et al., 2016). Moreover, adding fibers in concrete non-uniformly may cause

a weak bond in the interfacial transition zone of fibers and concrete, which leads to poor crack resistance of the concrete member. Fig. 2.12 shows the distribution of steel fibers in UHPFRC, whilt Fig. 2.12a and Fig. 2.12b show the homogeneous distribution of steel fibers inside the concrete and Fig. 2.12c shows the obvious nonhomogeneous distribution of the steel fibers. It was reported that nonhomogeneous distribution of the steel fibers may cause internal defects inside the concrete and also affect the performance of the concrete member negatively, including concrete creep (Zhao et al, 2016).

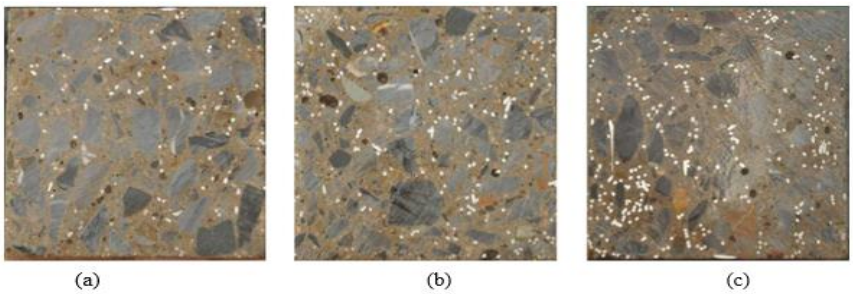

Fig. 2.12 Fiber distribution feature images of different steel fiber reinforced concretes (Zhao et al., 2016).

Table 1 shows the previous tensile creep test results for different types of concrete. Garas et al. (2009) performed the tensile creep test for UHPC for a shorter term of 14 days, where they found the specific tensile creep values ranged from 28.44 to 51.78 με/MPa at 7^{th} day and 34.22 to 57.44 με/MPa at 14^{th} day for different UHPC mixes. Hence, they developed an advanced method to determine the tensile creep for a longer period of one year. The tensile creep test results for different UHPC mixes were 54 με/MPa to 176 με/MPa at 365^{th} day where the corresponding maximum tensile strength was 10.30 MPa at 7^{th} day.

In another study, Garas et al. (2012) cured the UHPFRC creep specimen thermally prior to testing. They found that thermally treated UHPC specimens suffered lower tensile creep than the corresponding non-thermally cured specimens. They concluded that the tensile creep of

UHPFRC could be more sensitive to the thermal treatment compared with the tensile strength, whereas for non-thermally treated UHPFRC specimens the tensile creep strain showed a much more sensitive inclination to the fiber/matrix interfacial bond strength.

Kamen et al. (2009) evaluated the tensile creep behaviour of UHPFRC at an early age, where the tensile creep was 40 με/MPa at 35 hours and 135 με/MPa at 46 hours. It was reported that the tensile creep occurred rapidly for the first 72 hours, after which it stabilised. Another study by Switek et al., 2009 evaluated the basic tensile creep of UHPFRC under three different stress levels. The basic tensile creep was 29 με/MPa to 33 με/MPa at the 13th day.

Table 1 Experimental results of tensile creep from previous research works.

No.	**Concrete type**	**Tensile strength, f_t at 28th day**	**Tensile creep test results**	**Test Period**	**Reference**
1	UHPC	6.50 MPa	54 με/MPa to 176 με/MPa	1 year	(Garas et al., 2010)
2	UHPC	6.50 MPa	28.44 28.44 to 124.66 με/MPa and 35.22 με/MPa to 57.44 με/MPa	7th day and 14th day	(Garas et al., 2009)
3	UHPFRC	11.5 MPa	29 με/MPa to 33 με/MPa	13th day	(Switek et al., 2009)
4	UHPFRC	14 MPa	40 με/MPa and 135 με/MPa	35 h and 46 h	(Kamen et al., 2009)
5	NSC	3.16 MPa	60 με/MPa to 200 με/MPa (at 25% of tensile strength), 40 με/MPa to 200 με/MPa (at 45% of tensile strength)	5th day and 12 hours	(Østergaard et al, 2001)
6	NSC	5.6 MPa	60 με/MPa to 200 με/MPa	45th day	(Bissonnette et al, 1995)

Bissonnette and Pigeon (1995) obtained tensile creep results for different mixes of NSC. These values ranged from 60 με/MPa to 200 με/MPa at 45th day. Østergaard et al. (2001) also evaluated the basic tensile creep for NSC where, for an applied load of 45% of the tensile strength, the tensile creep ranged from 40 με/MPa to 200 με/MPa. They also varied the strength stress ratio at different loading conditions, which yielded basic tensile creep values ranging from 60 με/MPa to 200 με/MPa. Higher specific tensile creep was found when applied load was reduced from 45% to 25% of the tensile strength.

2.6 TENSION STIFFENING

Tension stiffening is the direct result of interactions between the tensile reinforcement and concrete, attributed to the additional stiffness of a reinforced concrete member in facilitating the tensile stresses carried by the concrete. To determine the deflection of a reinforced concrete member precisely, it is important to consider the tension stiffening effect.

Fig. 2.13 shows the mechanism for tension stiffening on the deformation of a concrete member where the tensile load is applied to the reinforced concrete member. Initially, the deformation of the concrete follows the uncracked response, prior to the formation of the crack in the linear elastic stage. When the increased load reaches the tensile strength of concrete, the reinforced concrete member exhibits the first crack. Once the crack is formed, the concrete is assumed to carry no tension at the cracked section. Nonetheless, the concrete is still able to develop tensile stresses adjacent to the crack section, as the load is transferred from the reinforcing bar to the surrounding concrete. If the reinforced concrete member carries no stress at the cracked regions, the load deflection curve should follow the line ACD, shown in Fig. 2.13. In the case of UHPFRC, the fiber suffers extreme tensile stress in the concrete, remaining at the modulus of rupture after the formation of cracks. The load

deflection curve should then follow the line AE. But in reality, the corresponding response is in between these two-lines ACD and AE, following the solid line AB. This difference between the zero-tension response and actual response can be termed as the tension stiffening. Hereafter, the stress in the concrete varies between the cracks, along with the member length, resulting in reduced tensile stress in the concrete. Subsequently, the tensile capacity of the concrete reduces with the increased strain because of the formation of more cracks. This is reflected by the reduction in tension stiffening for increasing loads. With the stabilization of cracking, i.e. no more development of transverse cracks, the decrease in the average concrete stress, along with the tension stiffening, is observed to continue at a slower rate. This is due to the loss of bond strength caused by internal cracking. At the yielding point, the tension stiffening drops to zero, as the reinforcement is unable to transmit the tensile force across the cracks, which is greater than the yielding force.

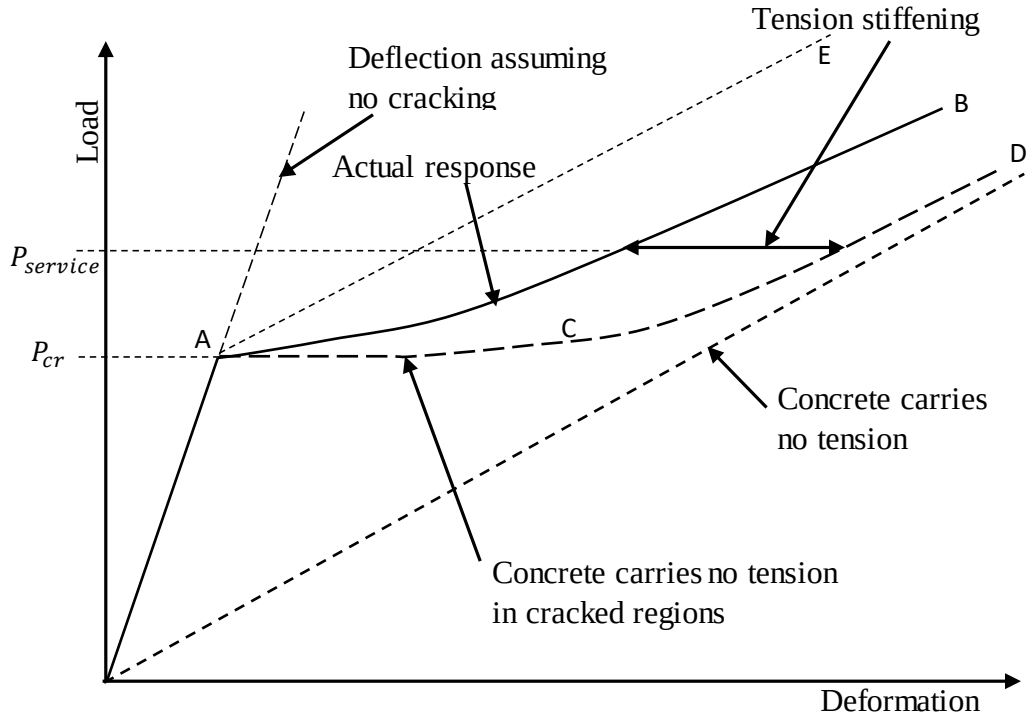

Fig. 2.13 Typical load versus deflection relationship for reinforced concrete member (Gilbert, 2007).

Hereafter, the stress in the concrete varies between the cracks along with the member length, resulting in reduced tensile stress in concrete. Subsequently, the tensile capacity of the concrete is reduced with the increased strain because of the formation of more cracks which is reflected by the reduction of tension stiffening for increasing loads. With the stabilization of cracking i.e. no more development of transverse cracks, the decrease of average concrete stress along with the tension stiffening is observed to continue at a slower rate. This is due to the loss of bond strength causing from internal cracking. At the yielding point, the tension stiffening drops to zero as the reinforcement is unable to transmit the tensile force across the cracks which is greater than the yielding force.

Earlier, Illston and Stevens (1972) conducted experiments where 60 beams were loaded for a duration of 2 years to investigate the time-dependent effect of a high strength concrete cover on crack width. It was observed that the initial crack spacing was about 2.3 times that of the concrete cover, where the formation of crack was at a slower rate due to the reduction of the average concrete tensile strains. They reported that this was linked to the time-dependent load-deflection curve changes, along with the shrinkage and steel strain.

In 1979, Clark and Cranstown reported that the decrease in tension stiffening is not only due to the function of strain but also the bar spacing of the reinforced concrete member. They found that the deterioration in tension stiffening is significant when the bars are spaced widely in a concrete member, especially when spaced about 1.5 times the slab depth. It was also reported that the tension stiffening effect is independent of the bar diameter when the ratio of reinforcement remains unchanged (Sooriyaarachchi et al., 2005).

Al-Fayadh (1997) and Abrishami et al. (1996) found that the tension stiffening effect increases for high strength concrete at the onset of crack formation and also at the linear

elastic stage. They also reported that the crack spacing for higher strength concrete is comparatively larger than for conventional concrete.

Hung et al. (2019) conducted experiments to investigate the tension stiffening effect on steel-reinforced UHPC composites where the crack propagation, effect of the bar size and effect of the loading conditions were reported. They concluded that the fibers in UHPC caused multiple cracking to a single localized crack in association with the strain localization, contributing to the reduction of ultimate strain and yield strain under tensile loads. Moreno et al. (2014) conducted tension stiffening tests for HPFRC (high-performance fiber reinforced concrete) to investigate the plastic and elastic responses up to the fracture. They concluded that multiple cracking occurred prior to the yielding of reinforcement for HPFRC, where the splitting cracks were observed at lower strain levels. It was observed that when the splitting cracks occurred prior to the pull out of the fibers, the strain elongated more evenly and several transverse cracks were found to grow widely at the same time, resulting in a delay to the reinforcement fracture, while exhibiting higher deformation.

A few other pieces of research have also been conducted to investigate the time-dependent tension stiffening effect, long-term. Ranzi and Gilbert (2010) performed a long-term experiment where the specimens were subjected to sustained loading for about 2 years. They reported the average concrete strain and steel strain along with the progress of any cracks during the entire test period.

2.7 SUMMARY

Based on the literature review conducted in this chapter, the following major findings are reported:

UHPFRC does not require shear reinforcement as the steel fiber is capable of carrying tensile loads. This concept is considered when designing concrete structures, such as beams and

girders. However, very little guidance or work is reported on the long-term behaviour of UHPFRC pertaining to tensile creep and tension stiffening mechanisms. This indicates that there is a scope for investigating long-term tensile behaviour, especially the tensile creep and tension stiffening mechanisms of UHPFRC.

Most of the limited research work available related to the tensile creep tests of UHPFRC were conducted for the shorter term, i.e. for several hours (Altoubat and Lange, 2001; Østergaard et al., 2001) up to a maximum 14 days (Garas et al., 2009; Switek et al., 2009; Kamen et al., 2009). It is important to understand whether the material could withstand tension stresses induced by sustained loads for a longer time period.

From the literature review, it can be observed that the dead load-based lever arm test rig was used by most of the researchers for conducting the tensile creep test. It has some limitations, such as restrictions in adopting multiple numbers of specimens simultaneously for testing, and also for possessing a limited load capacity for long-term testing. The principle purpose of the rig was to investigate the tensile creep of UHPFRC for short term testing (Garas et al., 2009, 2012; Østergaard et al., 2001; Rossi et al., 2013). Some other researchers followed a similar rig that was used for the compressive creep test (Kolver et al., 1999; Kristiawan, et al., 2006a).

There are available test methods to determine compressive creep and the most acceptable standard test method is ASTM C512 (2011), whilst no standard test method has been found for testing tensile creep. Moreover, most of the studies investigated the tensile creep of UHPFRC with a limited number of specimens. Based on the standard test method, ASTM C512 (2011), to evaluate the creep of concrete there should be at least two non-loaded specimens associated with two loaded specimens replicated from the same batch of concrete to determine the creep and also the shrinkage of the specimen. However, with the current

available tensile creep test methods, only a limited number of specimens can be tested and therefore these test set ups require modification for increasing the number of specimens that are prescribed by ASTM C 512 (2011).

To date, no research work has been conducted to investigate the tension stiffening effect of UHPFRC associated simultaneously with tensile creep. It is important to understand the crack propagation of reinforced UHPFRC specimens under sustained tensile loads, along with the tensile creep of unreinforced UHPFRC specimens to evaluate the complete tensile behaviour.

2.8 RESEARCH GAPS

Based on the above-mentioned discussion and considering the time and resources constraints, the intention is to focus the current study on the following research gaps in these related knowledge areas.

i. There is very limited information available on long-term tensile behaviour of UHPFRC from previous research work and this study aims to investigate long-term tensile behaviours, such as tensile creep and the time-dependent tension stiffening effects of UHPFRC in detail.

ii. Previous investigations indicate that the progress of tensile creep is very slow and there was difficulty in applying sustained tensile loads for tensile creep specimens for a longer time period (> 14 days). Therefore, in this study, it is proposed to formulate ways and means for investigating tensile creep under sustained loads for a longer term.

iii. Previously, many researchers used the dead load lever arm or frame to apply the sustained tensile loads, where the specific tensile dead load was applied using the gravitational force/weight or water tank. Several factors were neglected when applying the sustained

tensile loads, such as the friction loss while applying the load, stability of the applied gravity based dead load and the direct impact of the dead load on the specimens. In this study, a test method will be developed to overcome these negative factors in a more sophisticated way to apply the loads to the specimens to generate precise test data.

CHAPTER 3 : TEST SPECIMENS, INSTRUMENTATION AND TEST PROCEDURE

3.1 OVERVIEW

In this chapter, the experimental program used to quantify the shrinkage, direct tension, tensile creep and tension stiffening to evaluate the tensile behaviour of UHPFRC are described in detail.

An overview of the tests to be completed is described in Table 2 where the test type, test name, characterization of specimens, loading type and duration are given. The experimental program of this study was designed to achieve the following objectives:

1. To quantify the instantaneous tensile response (direct tension) and time dependent tensile behaviour (tensile creep) of UHPFRC.
2. To quantify the instantaneous and time dependent tension stiffening and cracking behaviour of UHPFRC.
3. Evaluating the time-dependent shrinkage value to determine the shrinkage effect on both tensile creep and tension stiffening of UHPFRC.

The design and preparation of the specimens for these tests (direct tension test, tensile creep test and tension stiffening test) will be discussed later in this chapter.

To produce the UHPFRC, specific concrete mix design was followed according to the previous research work by Sobuz et al., (2016) which will be discussed later. Initially, all the specimens were cured in specific ambient condition (temperature 23 ± 2^0 C and relative humidity $50 \pm 5\%$) for 28 days and later these specimens were utilized for conducting direct tension and tension stiffening tests. The shrinkage strain magnitudes were obtained from the

very beginning of the experimental program to investigate the shrinkage effect on the tensile behavior of UHPFRC. Note that the tensile creep, tension stiffening and shrinkage tests were performed simultaneously, the details of which are presented schematically in Fig. 3.1 as flow chart. Tension stiffening test was performed for reinforced UHPFRC specimens at 28^{th} day to determine the associated cracking load. This cracking load was used to calculate sustained tensile loads to be applied in tests for determining the time dependent tension stiffening of UHPFRC. Different percentage of cracking loads were selected as sustained tensile loads to investigate the time dependent tensile behaviour of UHPFRC such as 50% and 75% of cracking loads of unreinforced UHPFRC specimen for tensile creep test and 75%, 100%, 150%, and 200% of cracking loads of reinforced UHPFRC specimen for tension stiffening test. Two different types of test rigs were designed and developed to carry the tensile creep and tension stiffening test for long term under sustained tensile loading conditions. While applying these sustained tensile loads, the associated strain gradients of cracking load from load vs strain curve at 28^{th} day direct tension and tension stiffening tests were estimated and maintained to reach the appropriate loading state. The procedure for determining the associated strain gradients will also be discussed in this chapter.

Table 2 Test matrix for the entire experimental program.

Test type	Applied Load types	Specimen size (mm)	Label of each specimen	Number of replicate specimens	Amount of Loading (% of cracking load)	Sustain–ed loading period	Age of testing
Direct tension test	Direct tensile loads	75 × 80 × 500 (prism)	C_1,C_2	2	Up to 120 kN at 0.18 kN/min	-	At 28th day
	Sustained tensile loads (for Tensile creep test)	75 × 80 × 500 (prism)	C_3	2	50%	180th day	-
			C_4				
			C_5	2	75%		
			C_6				
			C_7	2	Non-loaded		
			C_8				
	Direct tensile loads test	75 × 80 × 500 (prism)	C_3, C_4, C_5,C_6, C_7, C_8	6	Up to 120 kN at 0.18 kN/min	-	At 180th day
Tension stiffening test	Direct tensile loads	75 × 75 × 660 (prism)	S_1, S_2	2	Up to 120 kN at 0.18 kN/min	-	At 28th day
	Sustained tensile loads	75 × 75 × 660 (prism)	S_3	2	75% (T20)	180th day	-
			S_4				
			S_5	2	100% (T40)		
			S_6				
			S_7	2	150% (T60)		
			S_8				
			S_9	2	200% (T80)		
			S_{10}				
			S_{11}	2	Non-loaded		
			S_{12}				
	Direct tensile loads	75 × 75 × 660 (prism)	S_3, S_4, S_5,S_6,S_7, S_8 S_9, S_{10}, S_{11},S_{12}	10	Up to 120 kN at 0.18 kN/min	-	At 180th day
Shrinkage test	Drying Shrinkage	75 × 75 × 660 (prism)	D_1, D_2	2	-	-	Up to 180th day
	Autogenous shrinkage test	75 × 75 × 660 (prism)	A_1, A_2	2	-	-	Up to 180th day

Percentage of loadings refer to the related percentage of cracking loads from direct tension and tension stiffening test at 28th day.

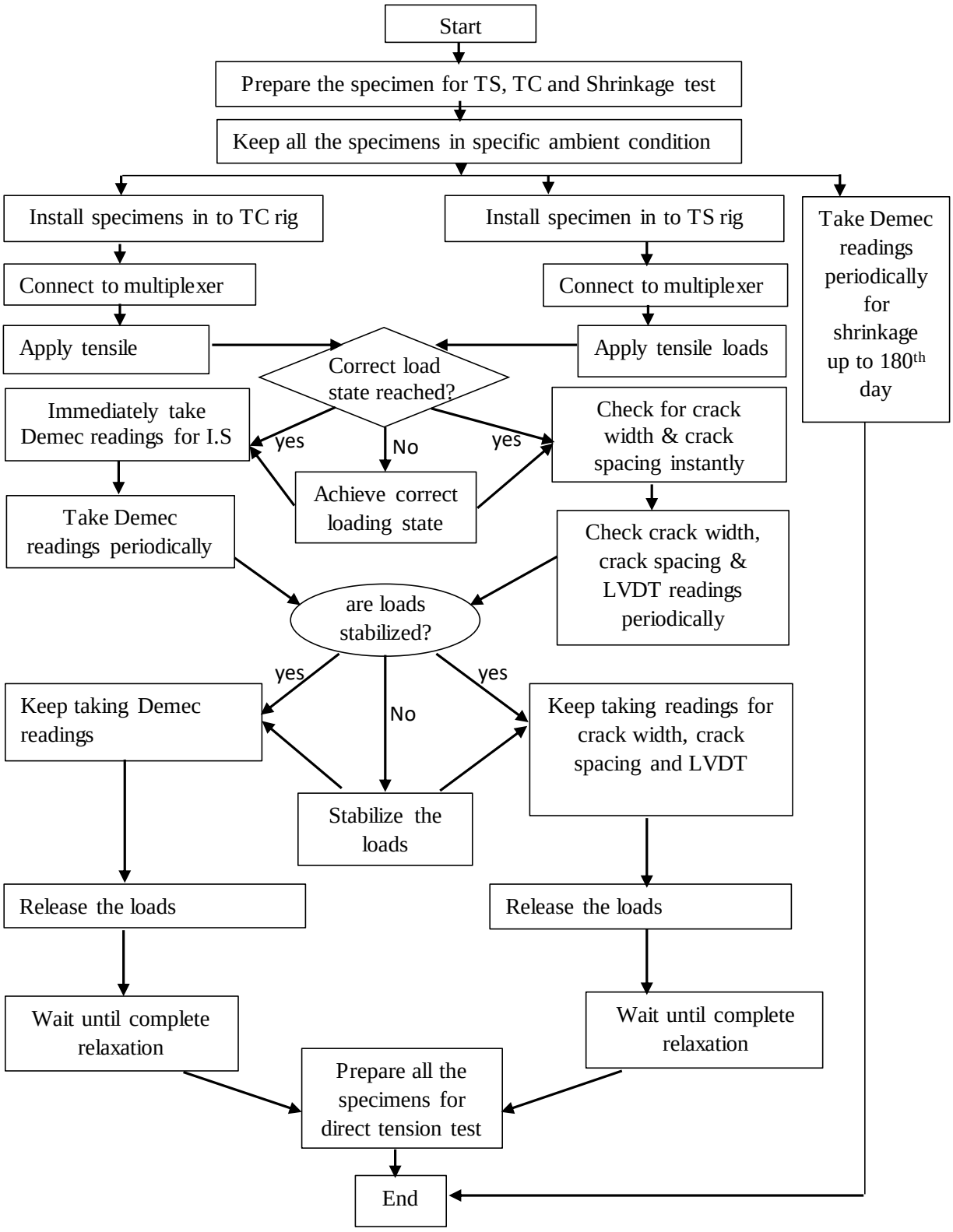

Fig. 3.1 Flow chart for simultaneous Tensile creep (TC), Tension stiffening (TS) and shrinkage test procedure.

3.2 CONCRETE MIXING AND CASTING

3.2.1 Mix recipe

UHPFRC was produced using different ingredients such as sulfate resistant cement, silica fume, sand, water, superplasticizer and short steel fibers. The sulfate resisting cement with fineness index of was 365 m^2/kg and the undensified silica fume with bulk density of 625 kg/m^3 were used as blinders for all the mixes. The short steel fiber with diameter of 30 mm and diameter of 1 mm (shown in Fig. 3.2b) was used with the maximum ultimate strength of 1100 MPa. The superplasticizer was third-generation high range water reducer with an added retarder to achieve improved workability of UHPFRC. The mix proportions details are given in Table 3 as below

Table 3 Mix proportion for UHPFRC.

Constituents	Weight (kg)	Ratio
Sulfate Resistant cement	220	0.790
Sand	280	1.00
Water	33.5	0.120
Silica fume	59	0.210
Super-plasticizer	17	0.061
Short steel Fiber	58	0.207
Total	667.5	2.387

3.2.2 Mixing procedure

Initially, all the dry ingredients such as sulfate resistant cement, silica fume and sand were weighed and mixed in the concrete mixer machine. The dry materials were properly mixed, water and superplasticizer were added, and it was mixed further 15 minutes to attain the desired consistency of the mix., The short steel fibers were added, and the resultant concrete was mixed for another 8 minutes produce the appropriate UHPFRC. Fig. 3.2 shows the fresh UHPFRC just after casting and the short steel fibers which were used to produce UHPFRC.

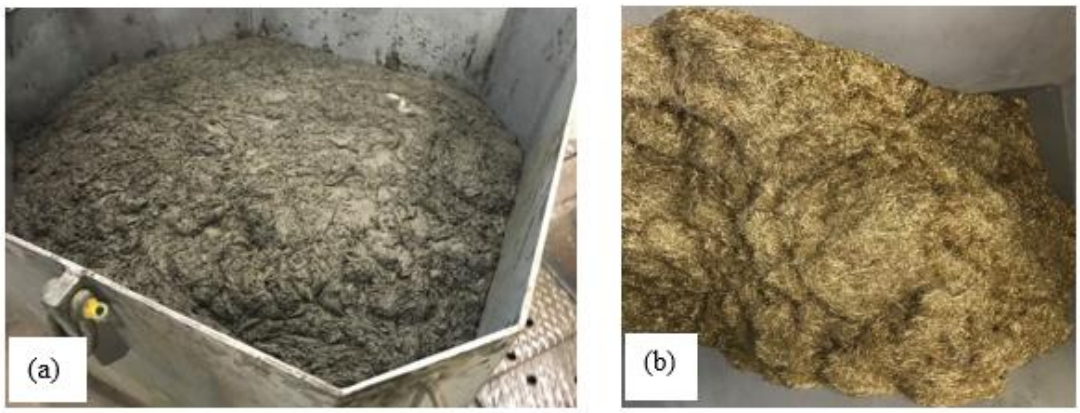

Fig. 3.2 (a) Fresh concrete mix of UHPFRC at laboratory and (b) picture of steel fibers.

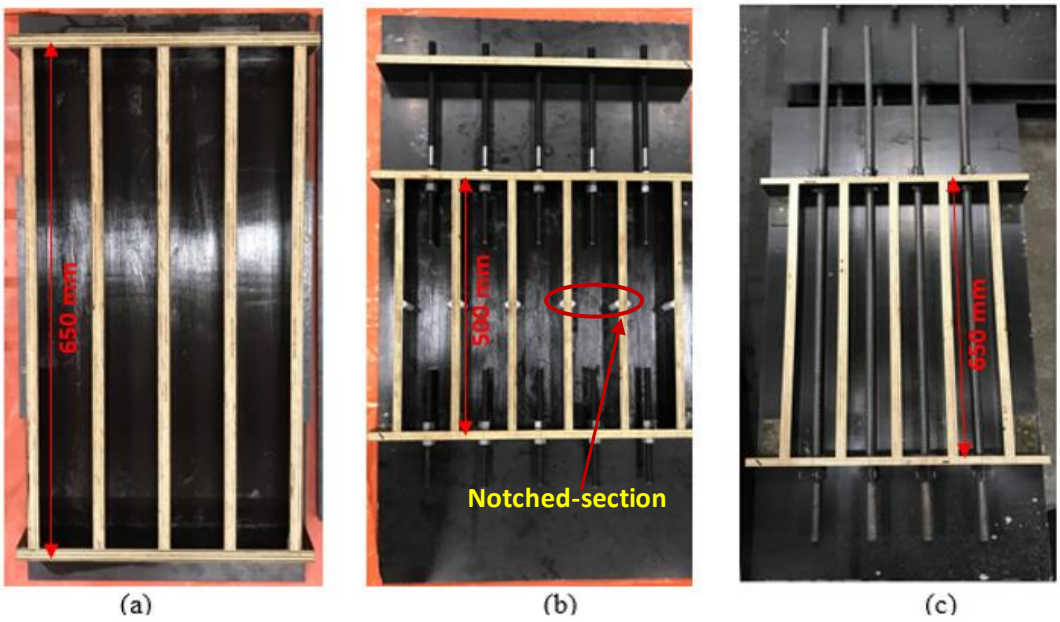

Fig. 3.3 Different types of moulds for (a) shrinkage test specimen (b) direct tension test specimen and (c) tension stiffening test specimen.

Moulds were prepared to the desired specimen size shown in Fig. 3.3 for various testing purposes and also cleaned and oiled prior to the casting. The fresh UHPFRC was transported from the concrete mixer through wheelbarrows to the casting site shown in Fig. 3.4. The

fresh UHPFRC was poured in to the moulds from wheelbarrows and the needle vibrator was used to compact the concrete and it was troweled to yield an even surface.

After demoulding, all the test specimens were transferred in the fog room with a constant temperature 23 ± 2^0 C and relative humidity $50 \pm 5\%$ during the entire test period. While taking the data for every test result, the specimens were kept in to the same ambient condition to avoid the effect of changed ambient environmental conditions for studying the long-term performance.

Fig. 3.4 Immediately after pouring concrete mix in to the moulds for different test specimens.

3.3 TEST SPECIMEN

3.3.1 Direct tension test specimens

Fig. 3.5 shows the cross-sectional details of the specimen used to perform the direct tension test. These specimens of 75 mm × 80 mm in cross-section with a height of 500 mm and a pair of specimens were used to conduct the direct tension test.

Threaded rods were used to facilitate the gripping in MTS machine which were inserted from the top and bottom of the specimen (namely top gripping and bottom gripping rod) through

the centre line and extended up to 100 mm to the inside of the specimen. The threaded reinforcements were inserted to the moulds prior to the casting shown in Fig. 3.3b, extending

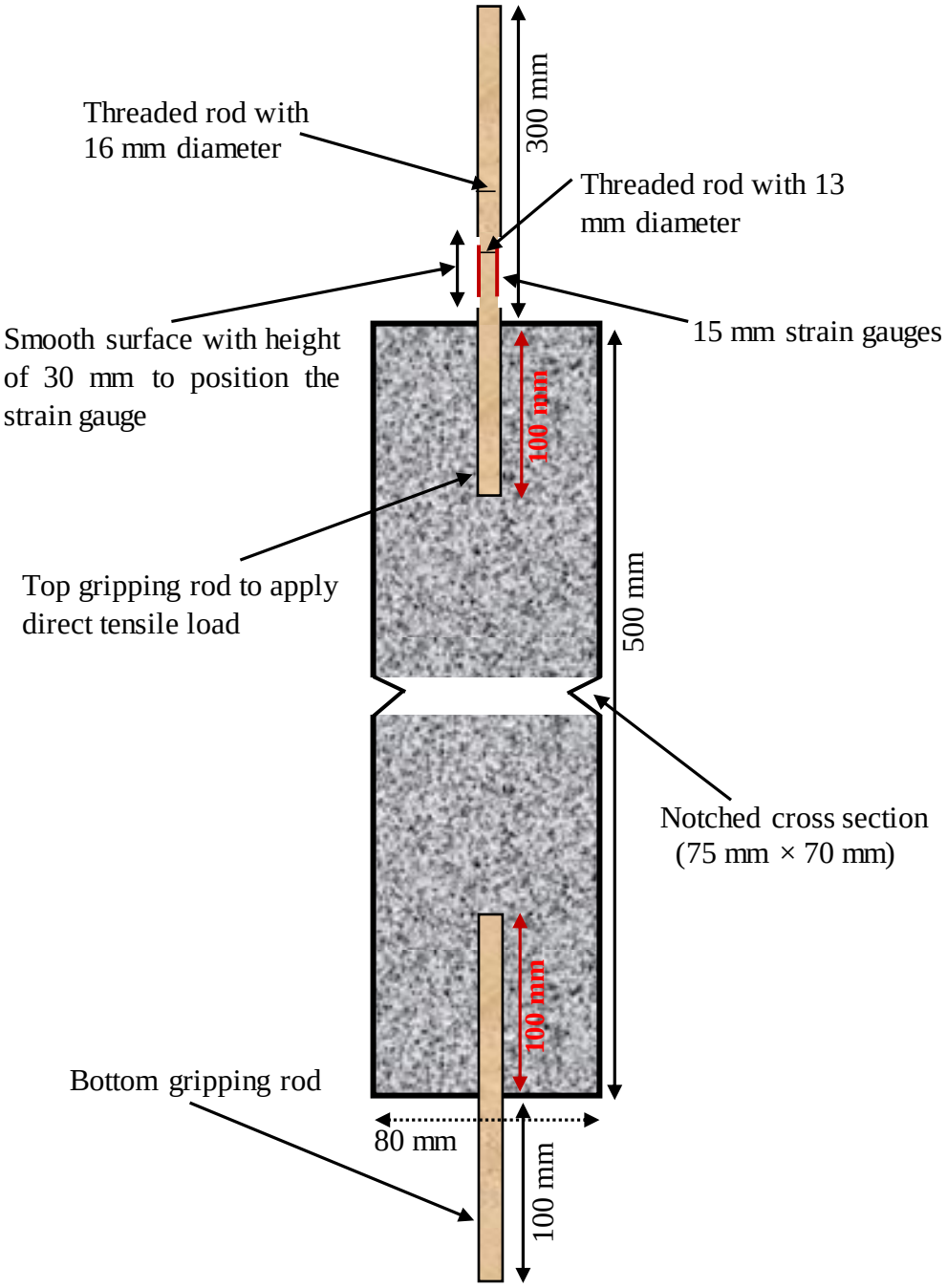

Fig. 3.5 Specimen preparation for direct tensile strength test of unreinforced specimen.

up to 300 mm from the top edge of the specimen and 100 mm from the bottom edge. The threaded reinforcement was 16 mm in diameter and immediately above the top edge of each specimen, the threaded reinforcement was kept smooth with 13 mm diameter of 30 mm length to bond the 15 mm strain gauge. These strain gauges were used to measure the strain magnitudes for reinforcement under the axial tensile loads. A notched section was created by using notch at the middle of each specimen prior to casting as shown in Fig. 3.3b and the purpose of the notched section was to force the formation of the crack at this location. The strain magnitudes of the UHPFRC concrete specimens at the notched section were determined using 30 mm strain gauges and the strain gauges were positioned at the middle of the specimen which was prepared by cleaning the surface and made smooth before pasting the strain gauges.

3.3.2 Tensile creep test specimens

For tensile creep test, the specimen was prepared similar to the direct tension test (shown in Fig. 3.5) whereas the additional mechanical demec gauges were mounted as shown in

Fig. *3.6* to determine the time dependent deformation of the tensile creep specimen. The demec discs were glued to the opposite sides of the specimen and were positioned 202 mm apart by using the standard gauge meter length prior to applying the sustained loads. Each demec disc was located at equal distance x (= 101) mm from the centre line of the notched section.

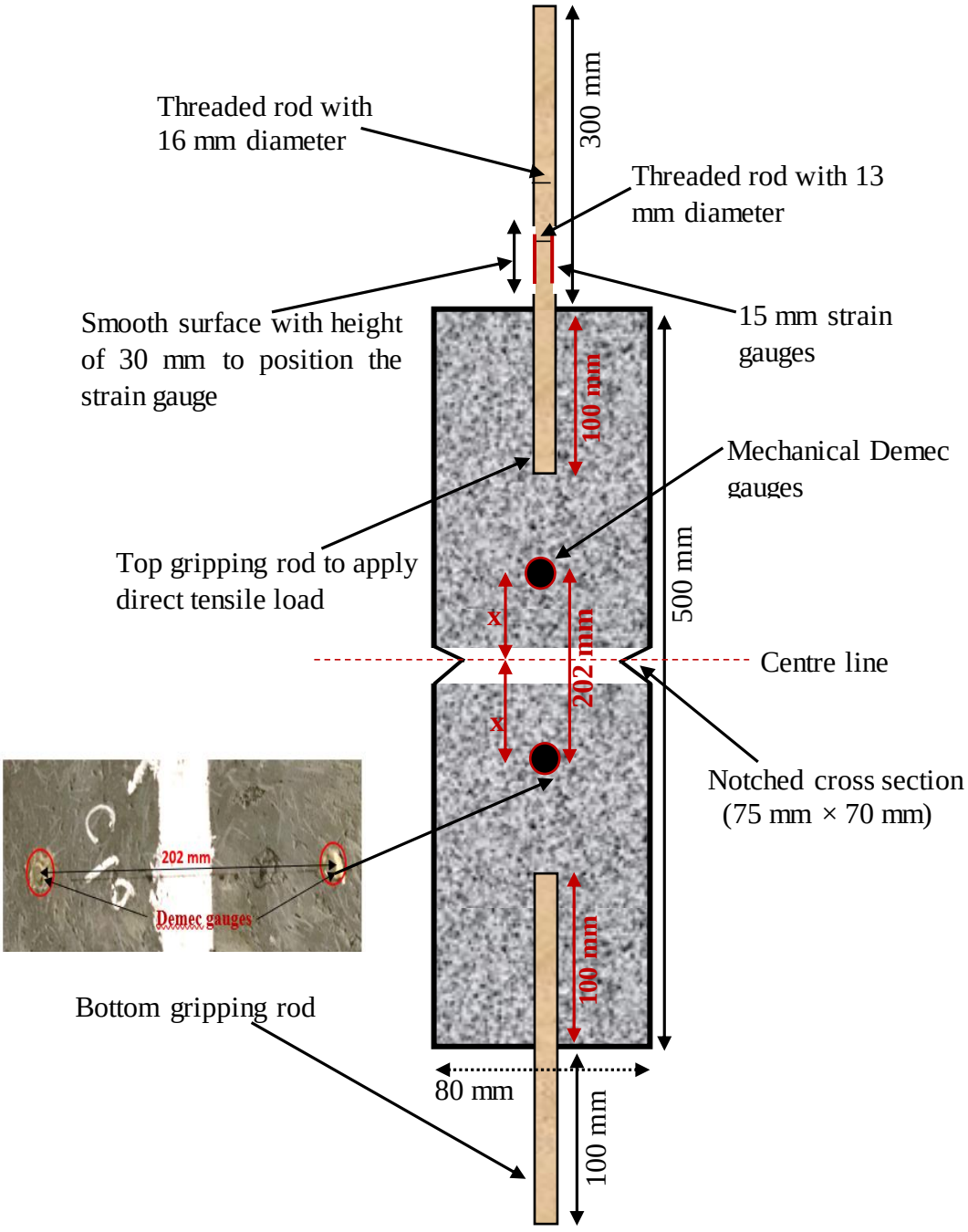

Fig. 3.6 Specimen preparation for tensile creep test.

3.3.3 For Tension stiffening test

The reinforced UHPFRC specimens were used to determine the instantaneous tension stiffening effect as shown in Fig. 3.7 where each of the specimen size was 75 mm × 75 mm × 650 mm.

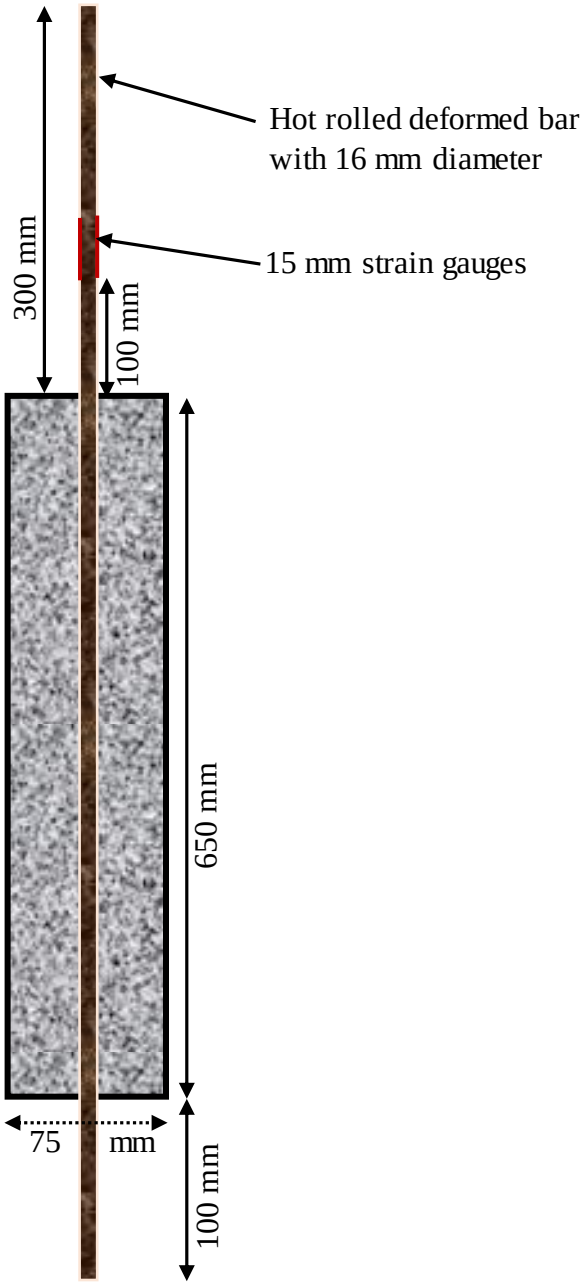

Fig. 3.7 Specimen preparation for direct tensile strength test of reinforced concrete specimen.

The deformed steel rebar with a diameter of 16 mm were inserted to the mould across the longitudinal centre line prior to the casting as shown in Fig. 3.3c. The reinforcement was extended to a distance of 300 mm from the top of the specimen and 100 mm from the bottom of the specimen. The strain magnitudes of the reinforcement were determined by using 15 mm strain gauges and the strain gauges were bonded about 100 mm above the top edge of the concrete specimen. The rod surface was grinded to acquire even and smooth surface without compromising the load carrying capacity of the rod. The surface of the concrete was grinded with abrasive grinding paper to gain the smooth surface without disturbing the concrete specimen shown in Fig. 3.8. The excessive length (150 mm) of reinforcement was cut down from top of each specimen to fit in to the designated rig of universal testing machine (MTS machine).

Fig. 3.8 Electronic strain gauges on reinforcement.

Fig. 3.9 shows the specimen details to determine the time dependent tension stiffening effect of UHPFRC where each of the specimen size was 75 mm × 75 mm × 650 mm. Two rods were attached to the opposite side of each specimen with four equal leg angles to determine the time dependent total average concrete deformation. The equal leg angles were glued to

the specimen surface by plastic bond. The electrical strain gauges were bonded to the reinforcement to determine the strain which were at 100 mm from the top surface of the specimen.

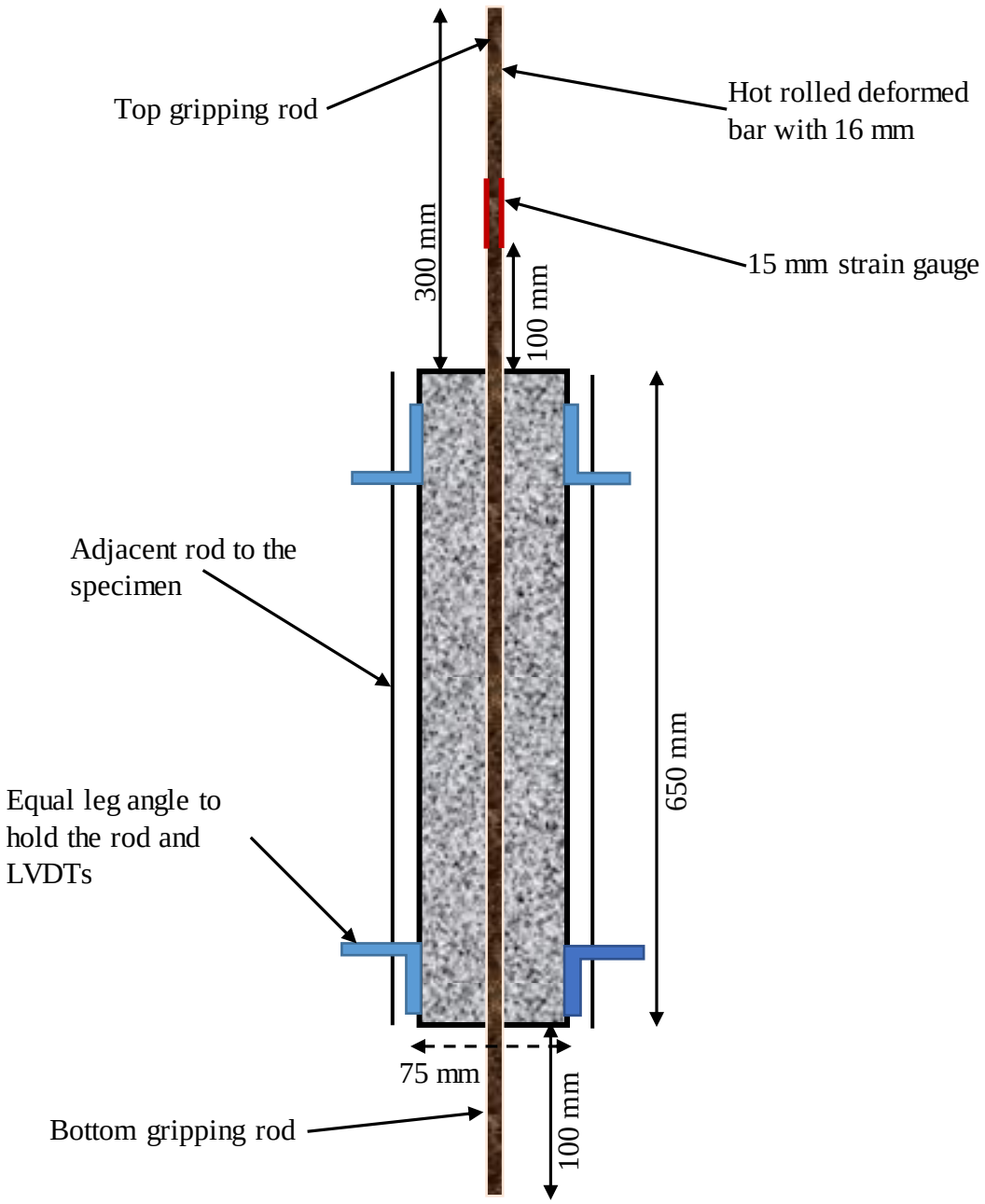

Fig. 3.9 Specimen preparation for tension stiffening test.

3.4 MATERIAL PROPERTIES

The mechanical properties including compressive strength, splitting tensile strength and modulus of elasticity test were conducted at 7^{th}, 14^{th}, 28^{th}, 56^{th}, 90^{th} and 120^{th} day. A total of 18 cylinders (100 mm diameter × 200 mm height) were used to determine the concrete properties.

The compressive strength test was performed according to ASTM C39 (2014a) while splitting tensile strength test and modulus of elasticity tests were carried out according to ASTM C496 (2011) and ASTM C 469 (2014), respectively. Fig. 3.10 shows the set up for compressive strength and splitting tensile strength tests. However, in this study the concrete mix proportions were not varied, and the concrete ingredients were also not changed to keep the feasibility of the experiments and to gain the main objectives.

Fig. 3.10(a) test set up for compressive strength test (b) test set up for splitting tensile strength test and (c) grinding both ends of test specimen.

3.5 SHRINKAGE TEST PROCEDURE

In this study, to evaluate the drying shrinkage and autogenous shrinkage, the square prisms of size 75 mm × 75 mm × 650 mm were used. The same type of prisms was also used for

conducting the tension stiffening tests to determine the actual shortening of the specimen. It is important to consider free shortening of the prisms as shrinkage strains result in a change of member length even before any load is applied, and hence, the member cracking load is also reduced (Bischoff 2003). Moreover, according to ASTM C512 (2002), there should be at least two specimens without any applied external loads from same batch of concrete mix to determine the shrinkage magnitude for creep test. A total of six specimens were cast, and out of these, two specimens were used to determine drying and autogenous shrinkage.

To measure the autogenous shrinkage, the entire specimen was sealed with aluminium foil paper immediately after demoulding as shown in Fig. 3.11a, as it restricts the moisture transfer from the surface of the specimen to the surrounding environment. The specimens

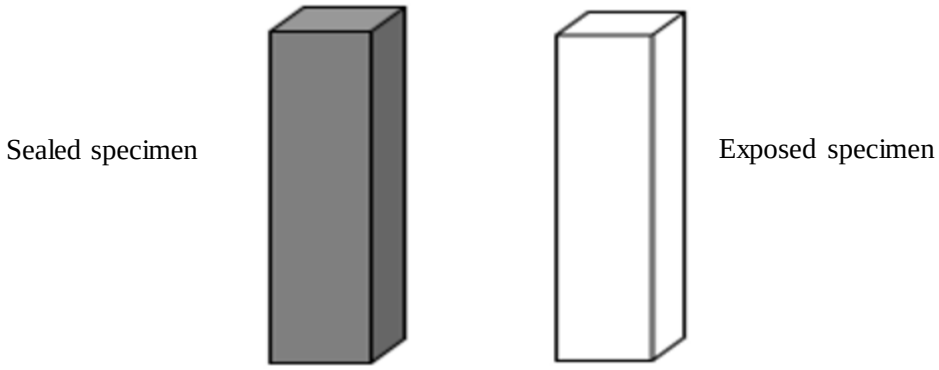

(a)

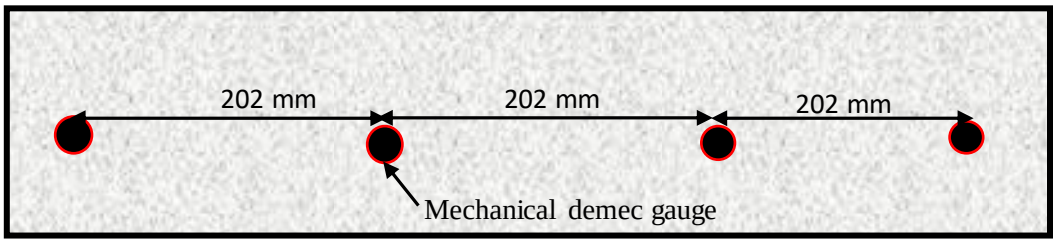

(b)

Fig. 3.11 (a) sealing of specimen for shrinkage test and (b) Location of mechanical Demec points on the specimen.

were also covered with wet cloths just after pouring of concrete to prevent the drying of the specimen. The mechanical demec discs were positioned (Fig. 3.11b) at a standard gauge length of 202 mm interval to cover the entire specimen length. Two opposite smooth surfaces were selected to position the demec discs and average demec readings were used to estimate the autogenous shrinkage strain values. Adhesive was used to bond the demec disc to the surface of the specimens. A similar set up was organized to determine the total drying shrinkage excepting that all the specimen surfaces were exposed to the adjacent environment as shown in Fig. 3.11a. The demec readings were taken for a period of 180 days at regular interval.

3.6 DIRECT TENSION TEST

3.6.1 Instrumentation

A test rig shown in Fig. 3.12, was used to install the direct tension test specimen inside the universal testing machine (MTS machine). Prior to mounting the specimens to the MTS, the specimens were prepared according to the test requirements shown in Fig. 3.5.

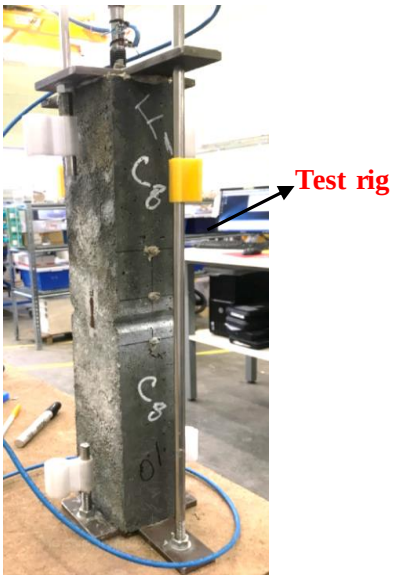

Fig. 3.12 Test rig for direct tension test available at CEME laboratory, The University of Adelaide.

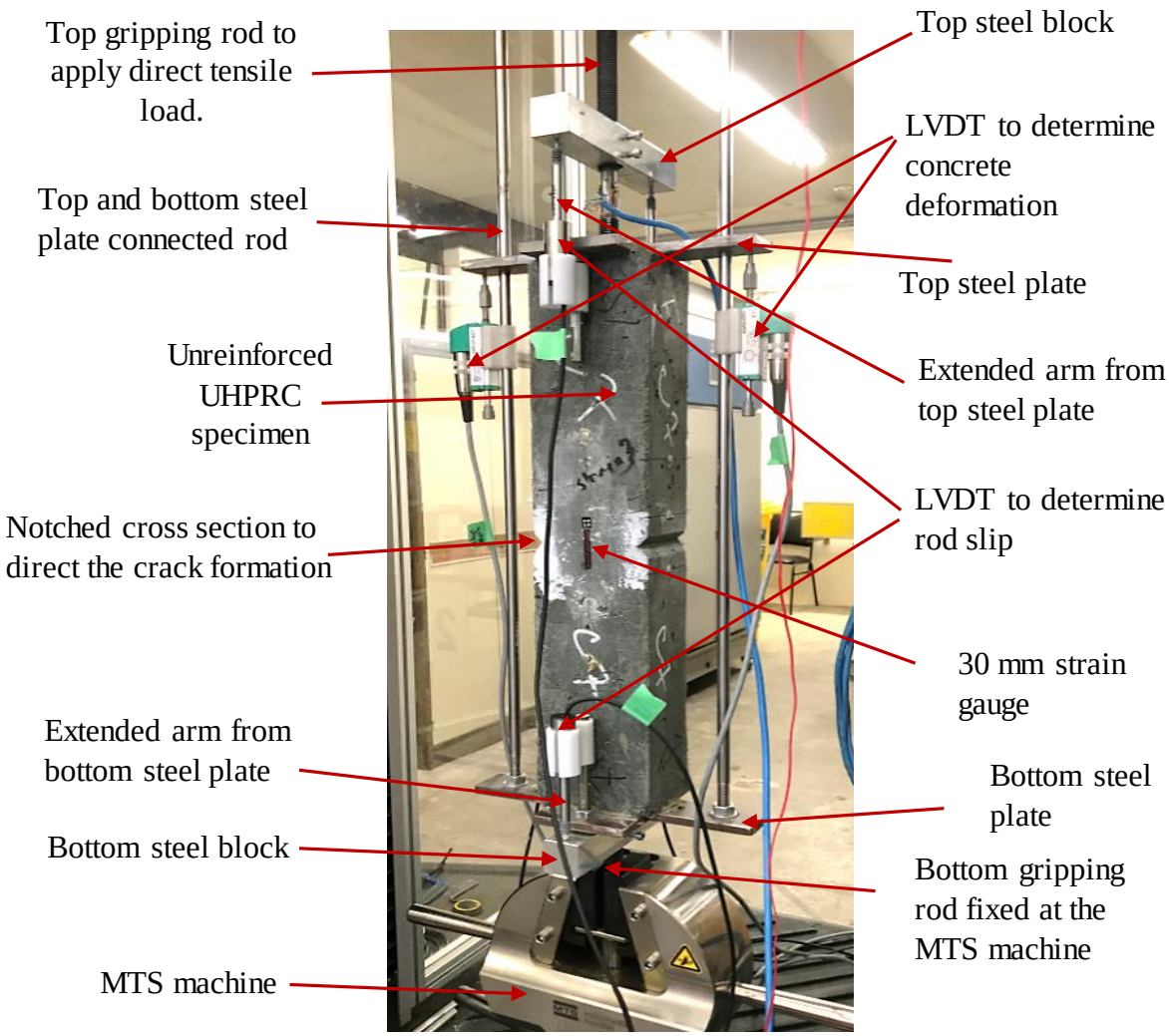

Fig. 3.13 Direct tension test set up for unreinforced UHPFRC specimen.

Steel plates were glued with an adhesive at top and bottom edge of the specimen to position the linear variable differential transformers (LVDTs). After the lapse of two hours, two steel blocks were screwed in fixed position to both top and bottom gripping rods. Later, the entire rig (including the specimen) was moved and mounted in to the MTS machine as shown in Fig. 3.13. The bottom gripping rod was fixed inside the bottom base of MTS machine and the top gripping rod was adjusted with the MTS machine to apply the direct tensile loads. Two identical LVDTs were attached to both rods of the rig shown in Fig. 3.13 to determine

the total concrete deformation. The end of each LVDT was attached to the top steel plate where the deformations were recorded by capturing the movement of the top steel plates. To determine the rod slip, four LVDTs (two LVDTs -at the top and another two LVDTs – at the bottom) were attached to the extended arms from top and bottom steel plates as shown in Fig. 3.13. The other end of these LVDTs were attached to the top and bottom steel blocks and the deformations were recorded with the movement of these steel blocks. Finally, all the LVDTs and strain gauges were connected to the data logger to record the measurements continuously.

3.6.2 Test Procedure

After completing the installation, the axial tensile loads were applied at a steady rate of 0.18 kN/min. While applying the tensile load, the pace rate for instantaneous tensile loading was kept at 0.18 kN/min. The application of the axial tensile load was continued even after the crack formation to measure the crack opening widths with increased load.

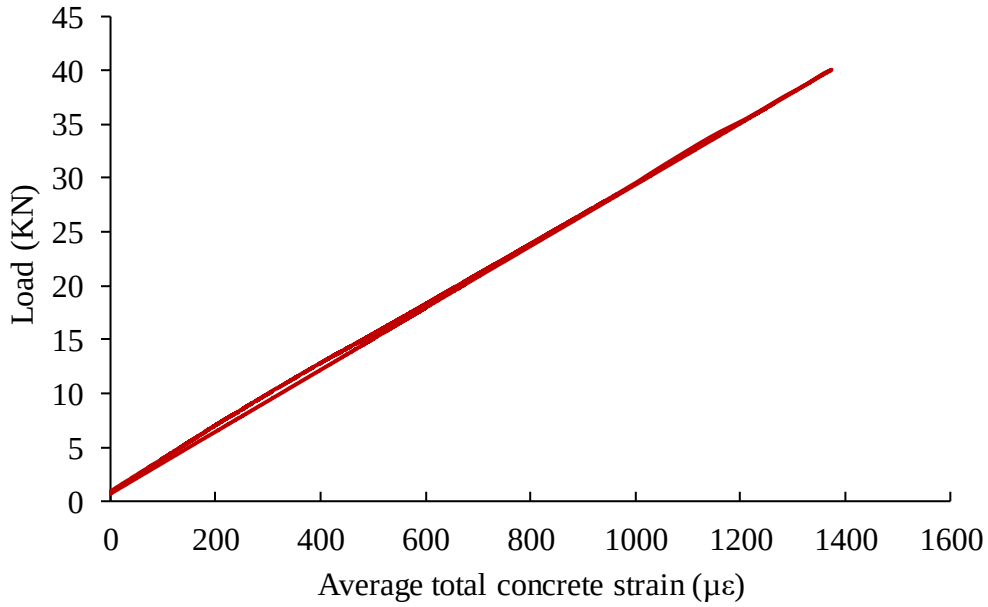

Fig. 3.14 Load vs average total concrete strain relationship of unreinforced UHPFRC specimen under direct tensile load at 28th day.

Two identical specimens were tested for direct tension test at 28-day and the average cracking load was determined. The evaluated cracking load was 40 kN and the associated average total concrete strain was 1374 με as shown in Fig. 3.14. The average total concrete strain for 50% and 75% of cracking loads were found to be of 687 με and 1080 με, respectively.

3.7 TENSILE CREEP TEST

3.7.1 Instrumentation

A steel frame was designed and built to perform the tensile creep test as shown in Fig. 3.15 and Fig. 3.16. The rig consisted of two C-section at top and bottom which were supported by rectangular hollow column.

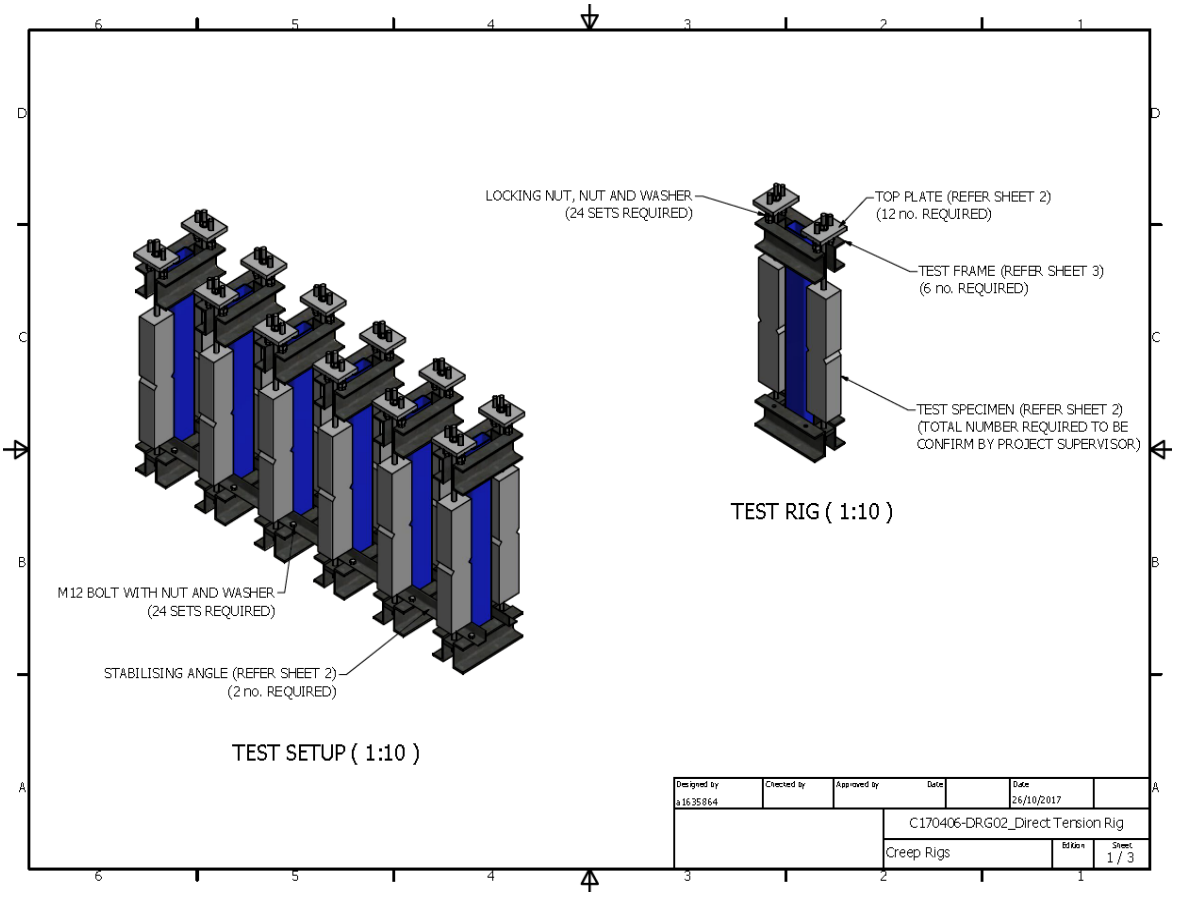

Fig. 3.15 Rig design for tensile creep test specimen (Courtesy: Kevin Farries, Senior Engineer, The University of Adelaide).

The rig was designed to carry the maximum tensile load of 150 kN. The rig was built in a way that 12 specimens could be installed in to the system simultaneously where the specimens can be kept under different sustained tensile load levels. Considering the feasibility and aims of this study, six unreinforced specimens were also used and installed in to the rig to obtain the tensile creep values of UHPFRC.

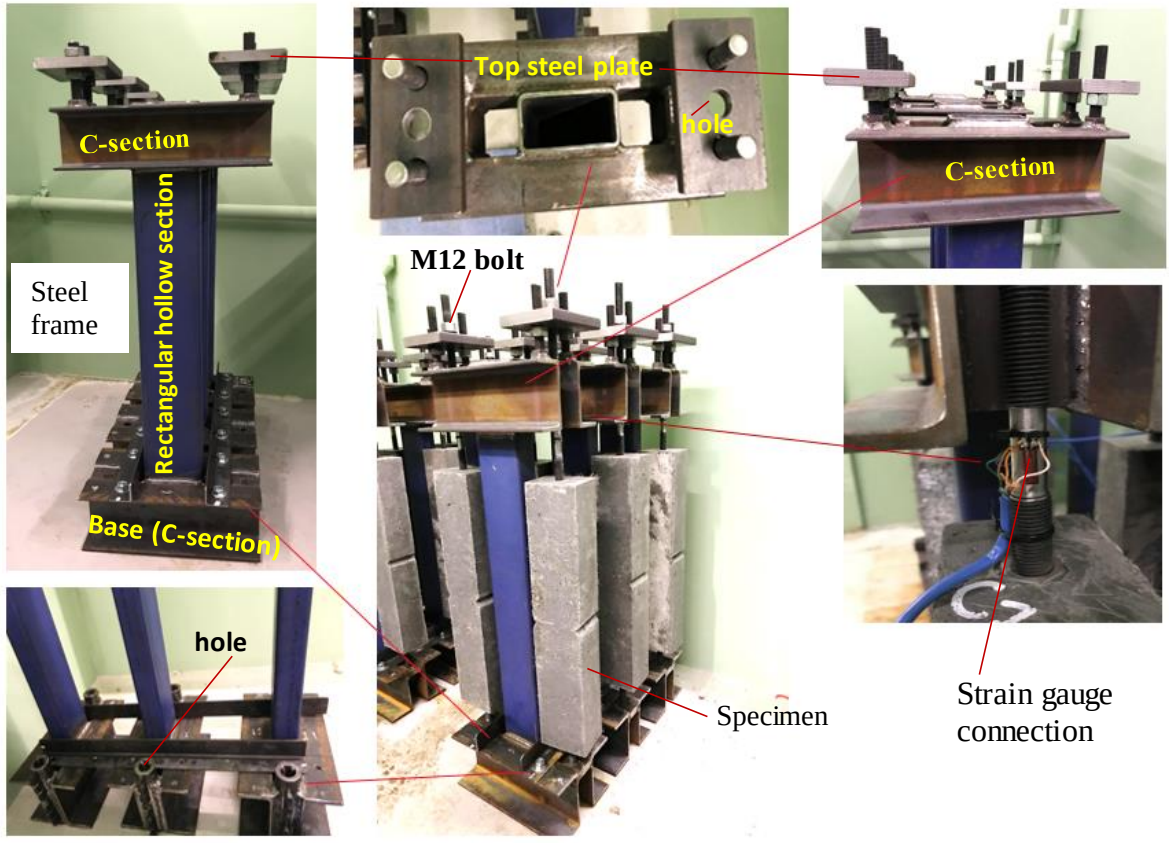

Fig. 3.16 Test set up for tensile creep experiment.

The specimens were prepared according to the requirements of tensile creep test shown in Fig. *3.6* prior to the installation. Afterwards, all the specimens were moved in to the rig and the bottom gripping rod of each specimen was inserted in to the hole (30 mm diameter) to fix at the base (C-section) of the rig. Three bolts were used and screwed to fix the bottom

gripping rod of each specimen. Then, the top gripping rod of each specimen was passed through the hole of top steel plate whilst the top steel plate was fixed, resting above the top C-section. A bolt of size 12 mm (M12) was inserted along the top gripping rod for screwing.

3.7.2 Test Procedure

Two of different sustained tensile loads were considered i.e. 50% and 75% of cracking load of unreinforced UHPFRC specimen from 28th day direct tension test (refer to the section 3.7). For each sustained loading two specimens were used, and each set of loaded specimens were installed along the same row of the rig as shown in Fig. 3.15. The strain gauges on threaded rods were connected to the multiplexer before applying the tensile loads. Then the instantaneous tensile load was applied to each specimen by screwing the M12 bolts reaching to the top plate. While applying the load, the strain of the rod was monitored from the multiplexer and the screwing was once stopped at desired strain of 687 με (corresponding to 50% of cracking load) and 1080 με (corresponding to 75% of cracking load). Thus, the sustained tensile load was applied to the specimens and while applying the tensile loads, special precautions were taken to keep the specimen under undisturbed and stable conditions. As soon as the loads were applied the demec readings were taken to determine the instantaneous strain of the specimen. During the entire test period, the strain was monitored regularly to maintain the constant tensile load up to 175 days of concrete age. Initially, the program was set to record the data of reinforcement strain automatically at intervals of 1 min for first week and later on after every 10 min. The demec readings were taken once every day for the first week and later on twice in every week. All the test specimens were kept in the fog room with a temperature of 23 ± 2^0 C and relative humidity of 50 ± 5% throughout the whole testing period.

After loading of sustained tensile loads at 175th day, the M12 bolts were unscrewed and the sustained tensile loads were released for complete relaxation. The demec readings were taken immediately after releasing the sustained loads and the demec readings were continuously taken until the full relaxation of the specimen was achieved. Afterwards, all the relaxed specimens including the specimens without any external load were tested for direct tension test at 180th day following the similar test procedure described in section 3.6 where the applied direct tensile loading rate was 0.18 kN/min.

3.8 TENSION STIFFENING TEST

3.8.1 For specimen under direct tensile loads

3.8.1.1 Instrumentation

The specimens were prepared according to the requirement of tension stiffening test shown in Fig. 3.7. The reinforced UHPFRC specimen was installed inside the MTS machine using the similar rig (Fig. 3.12) for unreinforced UHPFRC specimen used for direct tension test. The excessive length (150 mm) of top gripping rod was cut to fit in to the MTS machine. The steel plates of the rig were glued with adhesive to top and bottom edges of the specimen. Meanwhile, two steel blocks were screwed to fix the top and bottom gripping rods. As soon as the adhesive was hard enough, the entire rig set up was ready to be moved and installed inside the MTS machine. Fig. 3.17 shows the installation of the reinforced specimen inside the MTS machine. The bottom gripping rod of the specimen was fixed to the MTS machine whilst the direct tensile loads were applied from the top gripping rod. After installing the rig in to the MTS machine heads, two LVDTs were attached to the rod (top and bottom steel plate connected rod) of the rig to determine the total concrete deformation under direct tensile

load. The other end of these two LVDTs were attached to the top steel plate and the deformations were recorded continuously with the movement of the steel plates. Four LVDTs were also attached to the extended arms to the steel plate (two at the top edge of the specimen and two at the bottom edge of the specimen) and the end of these four LVDTs were attached to the top and bottom steel blocks, respectively. The slip of the rod was determined by recording the movement of these two steel blocks. Finally, all the LVDTs and strain gauges were connected to the multiplexer to record the measurements continuously.

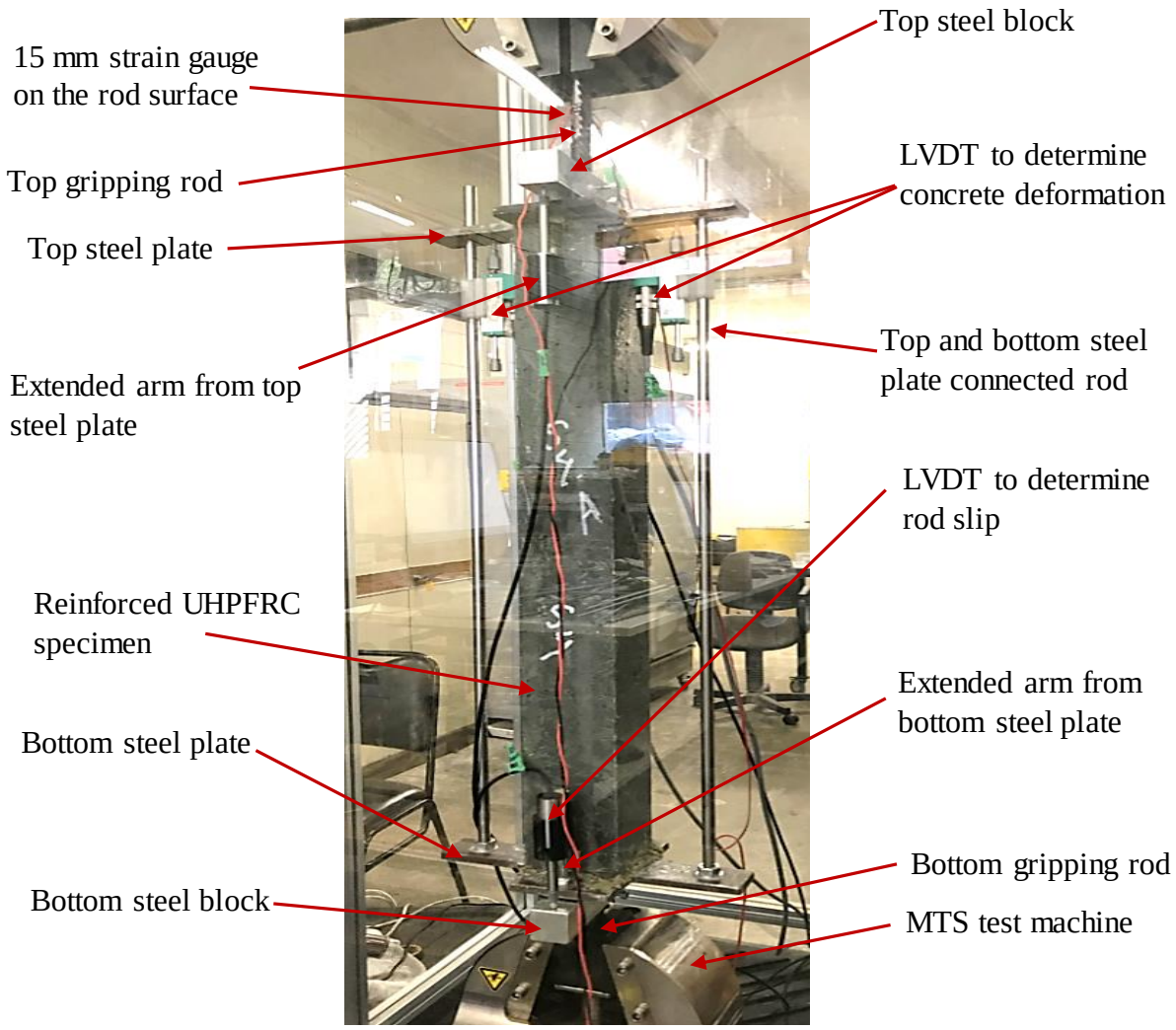

Fig. 3.17 Direct tensile test set up for reinforced concrete specimen.

3.8.1.2 Test Procedure

After completing the installation, the instantaneous loads were applied at a steady rate of 0.18 kN/min where the LVDT readings were also recorded continuously and the maximum applied load was 120 kN. At every 20 kN interval, the application of the load was paused and both crack width and crack spacing were measured manually using the electronic microscopic camera.

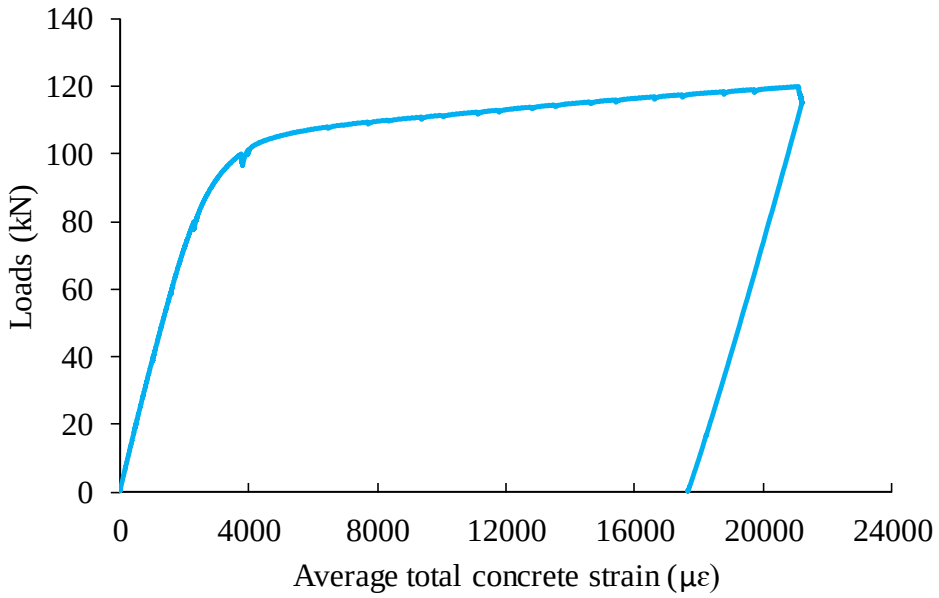

Fig. 3.18 Load vs average total concrete strain relationship of reinforced UHPFRC specimen under direct tensile load at 28th day from tension stiffening test.

The first cracking load was determined from the tension stiffening test of reinforced UHPFRC specimen at 28th day. The resultant cacking load was 40 kN for reinforced concrete specimen and the average total concrete strain was 1023 με as shown in Fig. 3.18. Different percentages of sustained tensile loads such as 50%, 75%, 100%, 150% and 200% of the cracking load were applied to investigate the time dependent tension stiffening effect of UHPFRC specimens. The associated average total concrete strain readings were 423 με, 685

με, 1023 με, 1585 με and 2023 με corresponding to sustained tensile loads of 20 kN, 40 kN, 60 kN and 80 kN, respectively.

3.8.2 For specimen under sustained tensile loads

3.8.2.1 Instrumentation

A rig was developed to conduct the tension stiffening test under sustained tensile loads for long term (175 days) as shown in Fig. 3.19 and Fig. 3.20. The rig was built in a way to install 12 specimens simultaneously where a range of sustained tensile loads could be applied

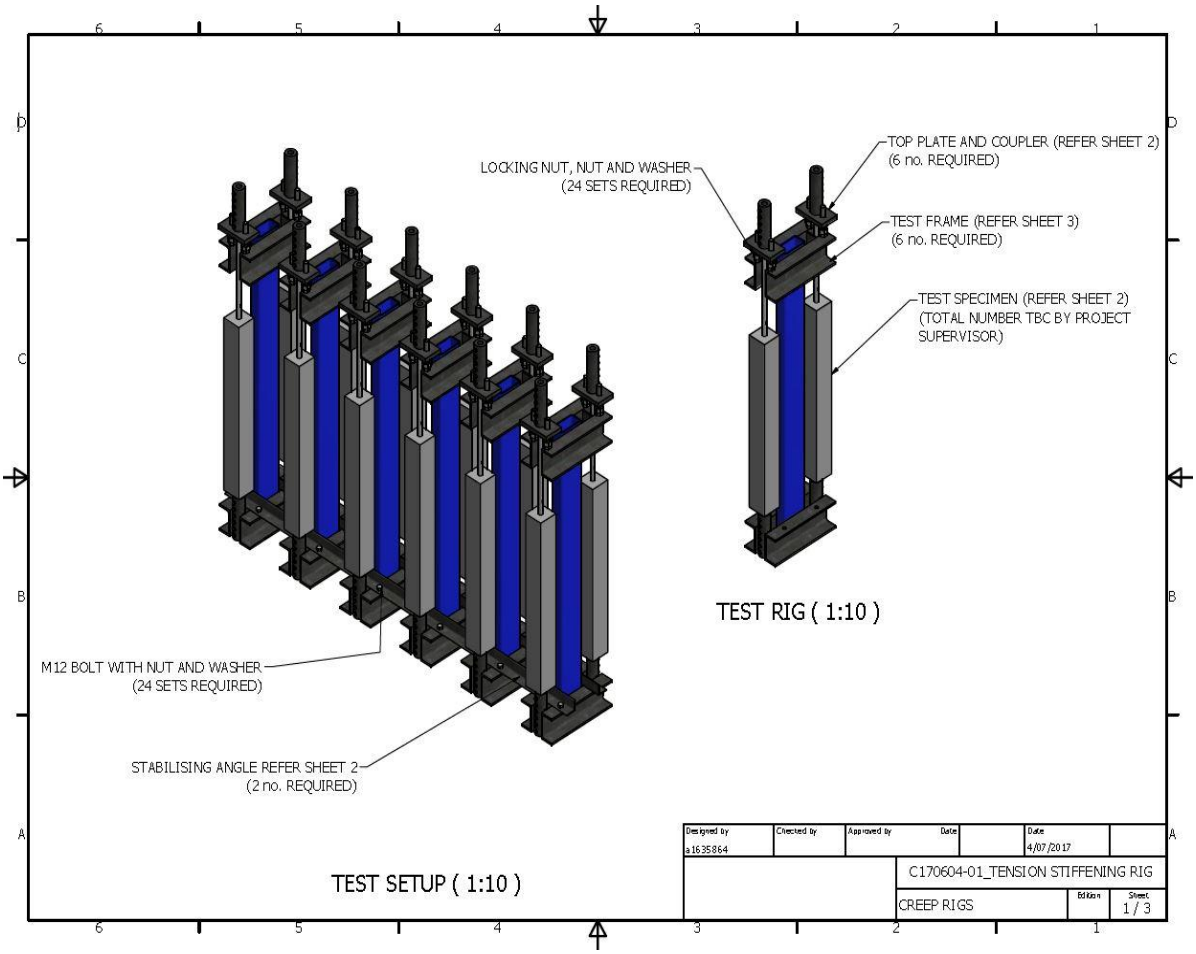

Fig. 3.19 Rig design for tension stiffening specimen (Courtesy: Kevin Farries, Senior Engineer, The University of Adelaide).

and the maximum tensile load capacity for the rig was 150 kN. The specimens were prepared following the design of tension stiffening test under sustained tensile loads as shown in Fig. 3.9.

In this rig, there were two C-sections at top and bottom which were supported by the rectangular hollow section. The base (bottom C-section) was drilled with holes to insert the bottom gripping rod of the specimen and each hole was provided with three bolts to fix the

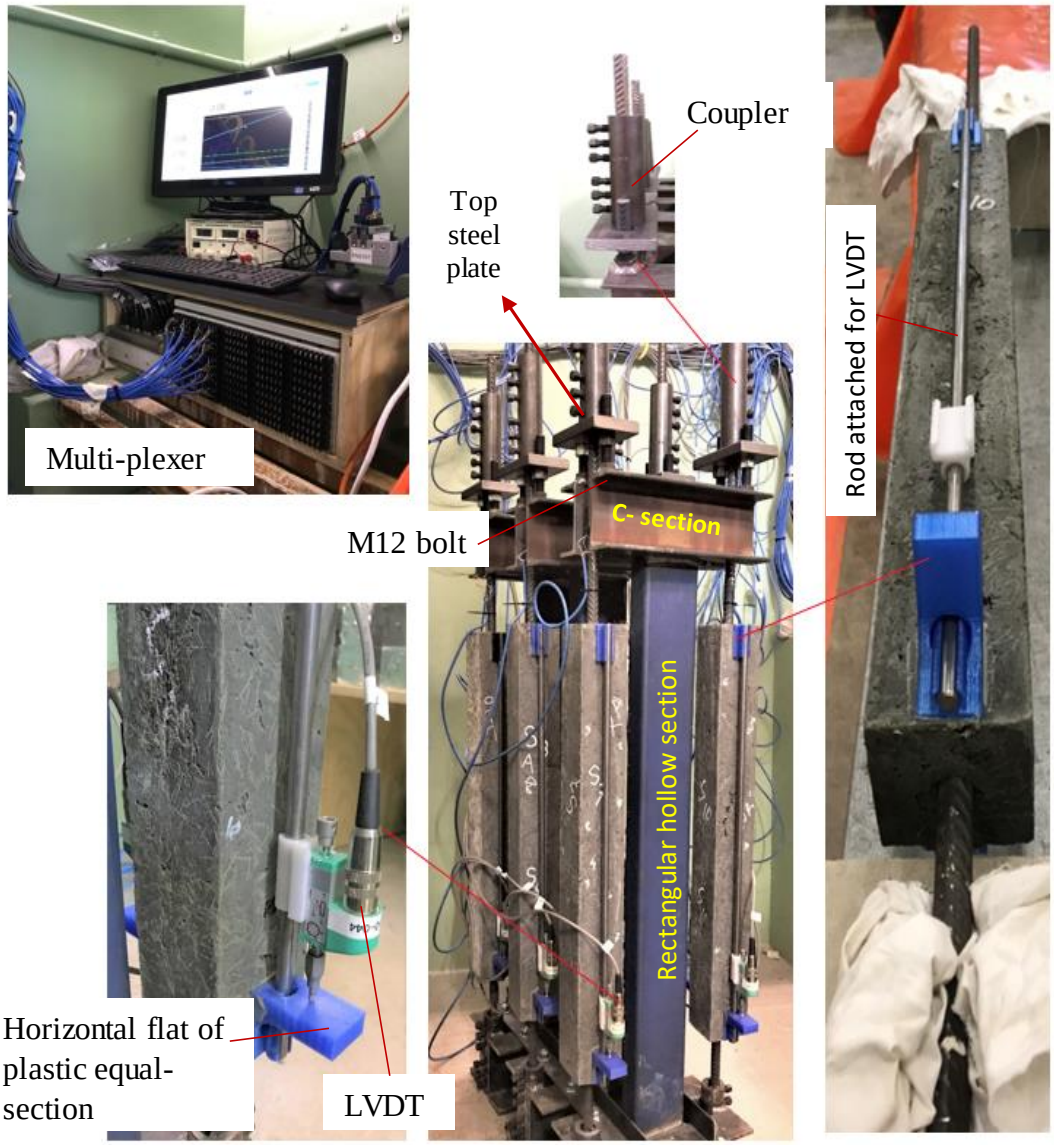

Fig. 3.20 Test set up for tension stiffening specimen.

bottom gripping rod of the specimen. After positioning the bottom gripping rod of each specimen, the top gripping rod was passed through the centre hole of top steel plate. The top steel plate was attached horizontally to the top C-section by two vertical threaded rods. Two M12 bolts were used beneath the top steel plate to hold on the vertical threaded rods laterally whereas the vertical threaded rods were welded to the top C-section. The tensile loads were applied to the specimen by tightening the M12 bolts beneath the steel plate and to sustain the applied tensile loads couplers were introduced. These couplers were attached to the top steel plate to hold the top gripping rod of the specimen which is shown in Fig. 3.20. Two LVDTs were attached to adjacent rod of each specimen. These two LVDTs were touched to the flat horizontal portion of the plastic L section of equal angles. The LVDTs and the electrical strain gauges on the reinforcement were connected to the multiplexer to record the test data continuously.

3.8.2.2 Test Procedure

The specimens were moved carefully in to the rig and the bottom gripping rod of each specimen was inserted to the base hole and then fixed by screwing all three bolts. The top gripping rod was passed through the centre hole of the steel plate and two M12 bolts beneath the top steel plate were screwed to apply the tensile loads. While applying the sustained tensile loads (20 kN, 40 kN, 60 kN and 80 kN to the designated labelled specimen, the associated strains were monitored in multiplexer so as to attain the desired sustain tensile loads. Two specimens were used for each type of loading and same loading specimens were installed in the same row of the rig. The loads were applied carefully to keep or maintain the specimen and LVDTs to their initial undisturbed conditions. Couplers were passed through the top gripping rods and supported by the top steel plate. The bolts of the coupler were

screwed and tightened to grip the top gripping rod of the specimen i.e. to maintain the sustained tensile loads.

Throughout the test period, the strain of the reinforcement was monitored to maintain sustain loading condition up to 175 days. Initially, the program was set to record the data at an interval of 1 min for first week and later it was increased to 10 min. The progress of the crack width and crack spacing were measured regularly over the entire test period. Electronic microscopic camera was used to measure the crack width of reinforced UHPFRC specimen. All the test specimens were kept in the fog room with ambient condition of 23 ± 2^0 C and 50 ± 5% relative humidity throughout the entire testing period.

At 175^{th} day, the M12 bolts beneath the top steel plate were unscrewed as well as the couplers bolt and the specimens were unloaded for completing the relaxation. As soon as the loads were released, the crack width and crack spacing for each specimen were measured using the electro microscopic camera. After the complete relaxation of all specimen, all the specimen including the non-loaded specimen were used for tension stiffening test under direct tensile loads at 180^{th} day.

3.9 CONCLUDING REMARKS

The experimental program of UHPFRC shrinkage and time dependent tensile behaviour i.e. tensile creep and tension stiffening mechanism has been presented in this chapter. The test specimen design such as specimen preparation in accordance with the related test requirement was achieved. The mix design of UHPFRC was presented and the casting of the concrete was performed for various test purposes. The experimental program for measuring the UHPFRC material properties such as the compressive strength, indirect splitting tensile strength, modulus of elasticity and direct tensile strength were obtained successfully.

The specimen size for the shrinkage test was modified to a larger prism size similar to the specimen size used for tension stiffening test in quest of determining the precise shrinkage induced shortening effect. The autogenous shrinkage test was conducted as well as the total shrinkage of the specimen, assisted in estimating the drying shrinkage strain values. The experimental program for shrinkage was considered significantly in determining the cracking strength and member length of UHPFRC specimen precisely. The minimum required number of shrinkage specimens were achieved for the tensile creep and tension stiffening tests.

The experimental program for the direct tensile strength of UHPFRC specimen was designed and the direct tensile strength at 28^{th} day and 180^{th} day was achieved for non-loaded specimen as well as for the sustained tensile loaded specimens at 180^{th} day. The post cracking behaviour of the unreinforced UHPFRC specimen was also achieved whereas the direct tensile load was applied even after the formation of cracks. This will contribute in determining crack opening width and understanding the tensile behaviour of UHPFRC.

The instrumentation and test procedure for tensile creep test were formulated and a rig was built to conduct the tests for applying sustained tensile loads. The time dependent average total concrete deformation was obtained for unreinforced UHPFRC specimens for different magnitudes of sustained tensile loads which will significantly contribute in understanding the tensile creep mechanism.

The experimental program for tension stiffening behaviour was formulated both for instantaneous loading and sustained tensile loaded specimens. A rig was fabricated for conducting the long-term tension stiffening test for UHPFRC specimens. The crack width, crack spacing, average total concrete deformation and reinforcement strains were measured throughout the intensive testing regime which will assist in analysing the tension stiffening effect of UHPFRC specimen both for short and long-term loading conditions.

CHAPTER 4 – RESULTS AND DISCUSSIONS

4.1 GENERAL

In this chapter, a detailed study is undertaken to describe the material mechanical properties, instantaneous properties and time-dependent tensile behaviour of UHPFRC, i.e. the tensile creep and tension stiffening mechanisms. The influence of shrinkage is considered and its influence on tensile creep and the tension stiffening mechanism are discussed. The response obtained from the tension stiffening test results is discussed in terms of load versus average concrete strain, crack width and crack spacing.

4.2 MATERIAL MECHANICAL PROPERTIES

4.2.1 Compressive strength, splitting tensile strength and modulus of elasticity

Compressive strength tests were conducted at 7^{th}, 21^{th}, 28^{th}, 56^{th} and 120^{th} days for UHPFRC and three specimens were used for each day of testing. The compressive strength test results are shown in Fig. 4.1(a), where the maximum compressive strength was 134 MPa, obtained at 120^{th} day, and the early age compressive strength was 76 MPa at 7^{th} day. In the case of UHPFRC, a lower water to binder ratio (w/b) is adopted to achieve higher strength, whereas the hydration rate in cementitious particles and porosity is comparatively low. Predominantly, these characteristics assisted in maintaining the water to binder ratio (w/b) low to produce a very high strength of UHPFRC, this correspondingly results in accelerating the attainment of greater compressive strength. After 28 days, the increasing rate of compressive strength was

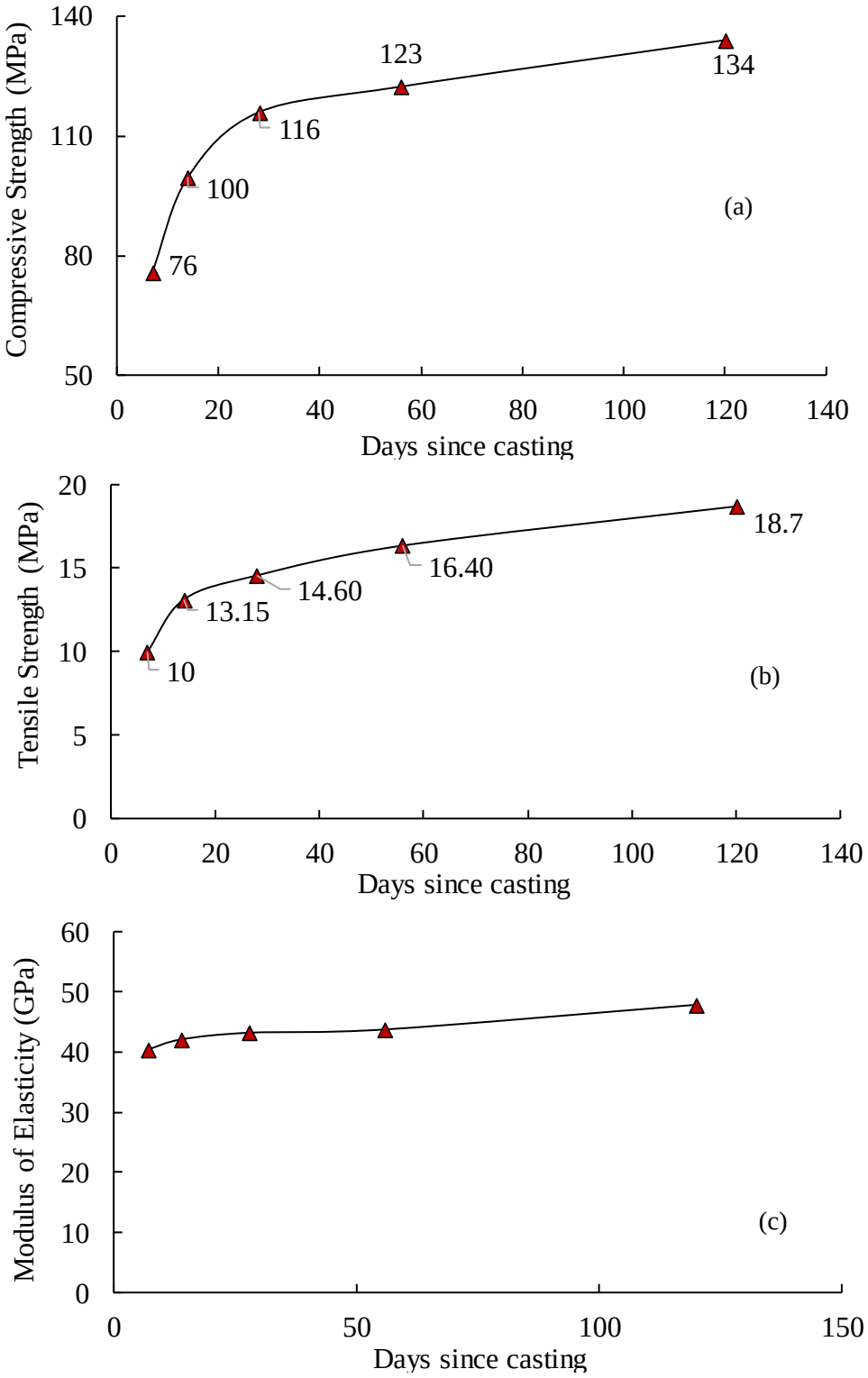

Fig. 4.1 Material mechanical properties – (a) compressive strength, (b) splitting tensile strength and (c) modulus of elasticity of UHPFRC at different ages.

comparatively slower than that of early age (first 28 days). This was due to the depercolation of the capillary pores, which reduced the moisture transfer between the cores of the specimen and its surrounding atmosphere, which subsequently slowed down the rate of increasing compressive strength. Generally, UHPFRC exhibits very high compressive strength, ranging from 100 MPa to 150 MPa (Le, 2008) at 28th day of testing, along with the developed ductile characteristics. In this study, the compressive strength was obtained within the expected range of 28th day.

Fig. 4.1(b) shows the indirect tensile strength of UHPFRC at 7th, 21th, 28th, 56th and 120th days. The maximum splitting cylindrical tensile strength was 18.7 MPa at 120th day and, at an early age of 7 days, the indirect tensile strength was 46.7% lower than the peak value. The splitting tensile strength was found to increase over the time period, where the strength values were 13.12 MPa, 14.56 MPa and 16.35 MPa at 21th, 28th and 56th days respectively. The indirect tensile strength of UHPFRC exhibits improved values over conventional concrete because of its incorporation with steel fibers. This is similar to what was observed by other investigations, such as Denarié et al. (2011) where the strength ranged similarly. Moreover, the loading configuration of splitting the tensile strength of UHPFRC exerts the stress of a biaxial state, which also significantly increases the fiber pull-out strength. However, the split cylindrical tensile strength is not the actual representation of the tensile strength of UHPFRC, both before and after cracking (Graybeal and Hartmann, 2003).

The modulus of elasticity (MOE) test was performed at different concrete age such as 7th, 21th, 28th, 56th and 120th days. The MOE test results were obtained from both the strain gauge readings shown in Fig. 4.1(c). The maximum MOE test value was 47.85 GPa at 120th day. It gradually increased from 40.4 GPa at 7th day to 47.8 GPa at 56th day. Similar findings were also reported where the estimated MOE for UHPFRC were 47.5 GPa (Máca et al., 2013) and

41.9 GPa (Graybeal, 2007) at 28th day, closer to the obtained MOE value of 43.20 GPa in this study.

4.2.2 Direct tensile strength

The direct tension test was conducted in two phases; firstly, it was done to determine the ultimate tensile strength under instantaneous tensile loads and secondly, after evaluating the pre-crack characteristics, the post cracking stage was analysed to determine the crack opening width.

The ultimate direct tensile strength was determined from the stress-strain relationship recorded under direct tension, as shown in Fig. 4.2. The specimen failure process was initiated close to the notch tip and, later, instantly covering most of the specimen width. The peak stress at crack initiation was considered as the maximum tensile stress i.e. the cracking strength. Table 4 shows the direct tensile strength of UHPFRC at different concrete ages.

Table 4 Direct tensile strength of UHPFRC.

Age of concrete (days)	Specimen type	Shrinkage strain (με)	Tensile strength (MPa)
28	Non-loaded specimen	335	6.7
180	Non-loaded specimen	563	9.5
180	C50	563	9.4
180	C75	563	8.4

Fig. 4.2 Direct tensile strength test at the laboratory.

The direct tension test was performed at 28th day for two non-loaded replicate specimens and the average direct tensile strength was 6.7 MPa. Later, the direct tensile strength was found to be 9.5 MPa for the non-loaded specimen at 180th day which was about 30% higher than the 28th-day direct tensile strength. This could be due to the hydration process, which strengthens the bond between the fibers and the cement matrix of UHPFRC and facilitates the denser inter facial transition zone. This contributed to achieving a higher resistance under tension over the time period, increasing the tensile strength. Similar findings were also reported by Kusumawardaningsih et al. (2015), where the direct tensile strength ranged from 7 to 15 MPa.

The specimens subjected to sustained tensile loads, i.e. the specimens with sustained tensile loads of 30 kN (C75) and 20 kN (C50), were brought under direct tensile strength at 180th day (after complete relaxation) to determine the effect of sustained tensile loads on direct tensile strength. The direct tensile strength for these two sustained loaded specimens of 20 kN and 30 kN were 9.4 MPa and 8.4 MPa, respectively. It was found that the direct tensile strength of sustained loaded specimens was lower than the corresponding non-loaded specimens at 180th day. It could be because of the disturbed microstructures in the UHPFRC, caused by the sustained tensile loads over the long-term. The UHPFRC has been produced with developed pseudo ductile properties and with increased tensile strain capacity because of the steel fibers. Nevertheless, UHPFRC specimens under sustained tensile loads may have a deterioration of the bond between the fibers and the cement matrix and reduce the resistance to tension while the specimen is under sustained tensile loads, long-term. It was also reported that the microstructure in the concrete material could modify under sustained loads in tension (Al-Kubaisy and Young, 1975), consequently affecting the strength magnitude. Therefore, the strength of UHPFRC could change during sustained loading conditions.

4.2.3 Crack opening width

The post cracking material properties under direct tension were evaluated from the relationship between the stress and the crack opening width, determined from the LVDT readings, as shown in Fig. 4.3. In Fig. 4.3, the initial elastic liner stress vs strain curve was neglected, as the focus is to analyze the post-cracking phase. However, the tensile strength failure curve was idealized as having two primary response mechanisms. The first mechanism was a sharp drop down from the maximum tensile stress and the second mechanism was softening (Roth et al., 2010). The sudden drop in strength was believed to be the consequence

of localized damage, formed within the cement matrix and the weakest section along the specimen width of the V notch section.

When the steel fibers were engaged, they decelerated the failure process related to brittle fracture along the inter-facial transition zone and developed some pseudo-ductile properties in the material. The activated steel fibers started to bridge the cracks, improve the load carrying capability to the crack opening and so commence crack widening.

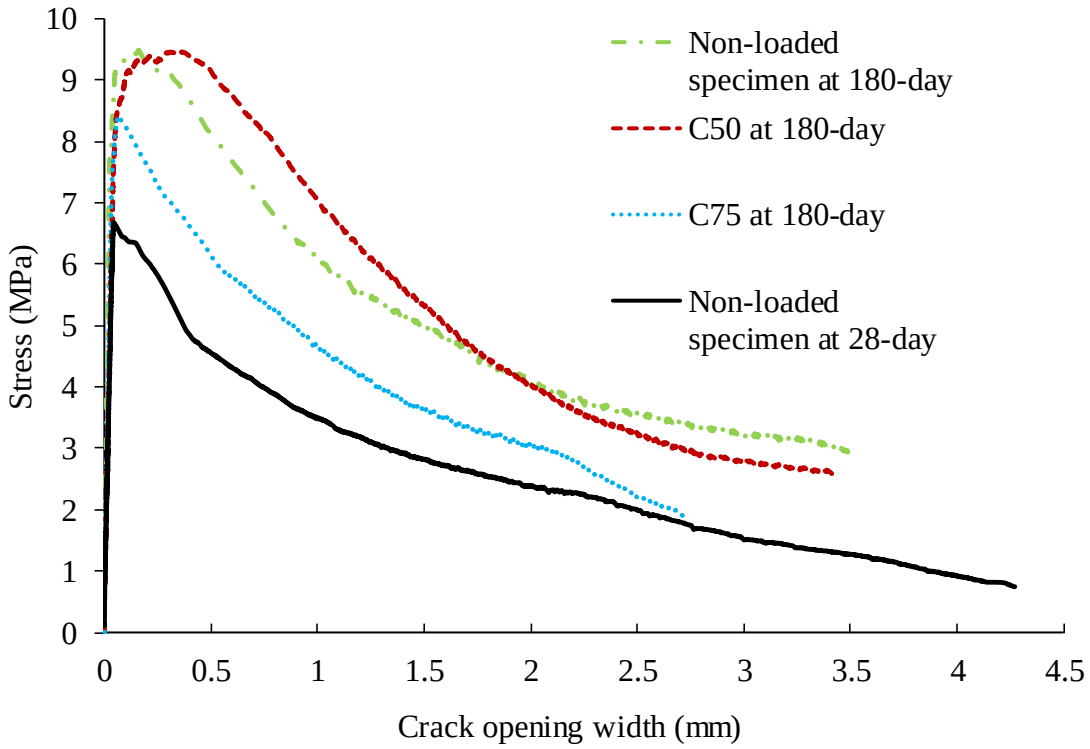

Fig. 4.3 Progress of crack opening width under direct tensile loads.

It is worth noting that the area of the v-notched cross-sections was used to determine the applied tensile stress. The crack opening width was determined from the average displacement of the LVDT readings. This was adopted assuming that the ultimate material strength had been reached for all displacement localized at the notched section. It was found

that the average crack opening width of a non-loaded specimen was 4.14 mm at 28th day, with the tensile stress dropping from a peak of 4.90 MPa to 1 MPa. After 180 days, the crack opening width for a non-loaded specimen was 3.43 mm, with the tensile stress ranging from 9 MPa to 3 MPa. It was observed that the crack opening width reduced with the increase of tensile strength. This was due to the improved higher resistance capacity of the concrete against tensile loads, leading to the lower crack opening widths.

For the specimen with sustained tensile loads of 20 kN (C50) and 30 kN (C75), the crack opening widths were 3.40 mm and 2.7 mm, respectively, at 180th day. The tensile stresses were ranged from 9 MPa to 3 MPa and 7.6 MPa to 1.9 MPa for specimens C50 and C75, respectively. As discussed before, the higher the tensile strength, the lower the crack opening width; nonetheless, under sustained loads, the response of the specimen was different. The ultimate tensile strength for both sustained tensile loaded specimens was lower than that of the non-loaded specimen at 180th day and their crack opening width was also reduced. This was due to the deterioration occurring because of the sustained tensile loads among the cement matrix and steel fibers in the UHPFRC correspondingly affecting the tensile strain and strength properties.

After complete relaxation (unloading), the sustained loaded specimen length was lower than the non-loaded specimen at 180th day. As the sustained loaded specimens were exposed to ambient conditions, shrinkage occurred during the test period, contributing to the shortened lengths. It has been reported that the shortening of the specimens could affect the cracking strength, as well as the tensile strain (Bischoff, 2003).

4.3 SHRINKAGE

The total shrinkage, drying shrinkage and autogenous shrinkage strain variation with the number of days since the casting of all the UHPFRC specimens are presented in Fig. 4.4. Please note that these specimens were kept under ambient conditions throughout the test period. The average shrinkage strain values of each type of shrinkage (total shrinkage and autogenous shrinkage) were obtained from two prismatic specimens. The drying shrinkage was calculated by deducting the autogenous shrinkage from the total shrinkage of the designated specimen. The drying shrinkage strain was -171 με for UHPFRC at 180th day, whereas the autogenous shrinkage strain was -391 με. It was obvious that a significant amount of the total shrinkage strain (-561 με) was caused by autogenous shrinkage when compared with the drying shrinkage, whilst the autogenous shrinkage was approximately 58% higher than the drying shrinkage. This characteristic is dissimilar to the behaviour of conventional concrete, demonstrating significantly higher drying shrinkage than autogenous shrinkage (Zhang et al., 2003). This is due to having a lower water to binder ratio (w/b) in UHPFRC, where a very low quantity of water exists inside the pores in comparison with ordinary concrete, which consequently causes the decrease in drying shrinkage. Moreover, it is also well known that an increase in w/b causes the increase in drying shrinkage (Tam et al., 2012).

Additionally, the production of UHPFRC includes the use of higher fineness fillers and admixtures that contribute to the reduced size pores due to the densified microstructure. The self-desiccation of this pore water ensuing in capillary pressure is inversely proportional to the radius or size of the pores according to the Laplace law (Hua et al., 1995). Thus, capillary pores with a smaller size cause greater autogenous shrinkage of UHPFRC. Similar

characteristics were also reported by Yoo et al. (2018), where the autogenous shrinkage strain of UHPFRC was higher than the drying shrinkage.

It was found that the increasing rate of shrinkage was much higher at an early age where autogenous shrinkage, drying shrinkage and total shrinkage were -220 με, -115 με and -335

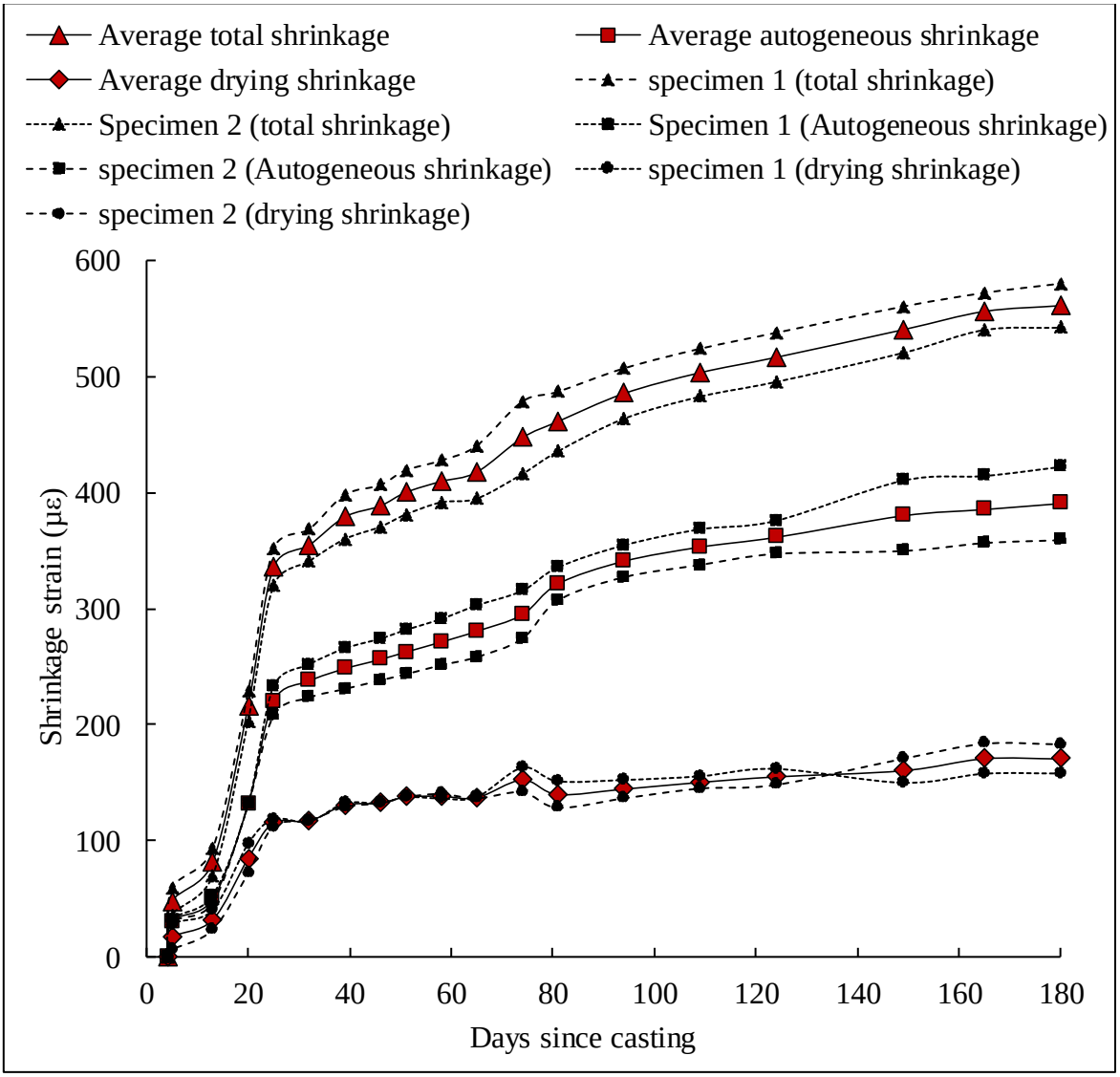

Fig. 4.4 Time dependent shrinkage strain of UHPFRC.

με respectively at 25th day. Later, the rate decelerated. A similar trend was also found in another study reported by Yoo et al. (2018), where the shrinkage strain was much steeper at the early age of 23 days and later the shrinkage progress was occurring moderately for

UHPFRC. This is due to the accelerated hydration process at an early age of the UHPFRC, leading to self-desiccation and causing the steeper shrinkage. Moreover, the cracks associated with shrinkage only occur at an early age for large scale thin UHPFRC structures.

The total, autogenous and drying shrinkage of UHPFRC were found to increase continuously up to 160 days and later the corresponding shrinkage strains exhibited minor increments. This is due to the quick evaporation of pore water from UHPFRC under ambient conditions at an early age, since the pore water content in UHPFRC was higher than for the surrounding atmosphere. After 160 days, the amount of pore water reduced significantly, and the shrinkage increment rate decelerated. It is important to consider shrinkage before applying load to any concrete member, as shrinkage strains cause the change in concrete member lengths and the cracking load of the member, which is termed shortening. Neglecting to account for the primary shortening of a concrete member may lead to inappropriate measurements of the post cracking strength of the member, becoming gradually worse as the shrinkage strain enhances in the long-term. For these reasons, shrinkage of UHPFRC specimens needs to be accounted for before applying loads to avoid any unexpected errors during the design process.

4.5 TENSILE CREEP STRAIN

The objective of these tests is to evaluate the effect of sustained tensile loads on unreinforced UHPFRC, i.e. tensile creep. The applied sustained tensile loads, such as 50% and 75% of the cracking loads, were chosen to maintain the mechanical linear behavior within the elastic range. As was reported by Ranaivomanana et al. (2013), sustained loads beyond the elastic limit might affect the precise values of tensile creep strain because of they possess larger unpredictable characteristics when illustrating the tensile strength of concrete. Furthermore,

sustained loading could impact on the material's microstructure, eventually affecting the time dependent actual stress and the material strength.

The tensile creep strain is presented in Fig. 4.5 under two different sustained tensile loads. The tensile creep strain value is supposed to be small, as was previously reported by Reviron et al. (2008) and Rossi et al. (2012): approximately a similar magnitude to that of the shrinkage strain. When investigating such results, the shrinkage was measured from the load

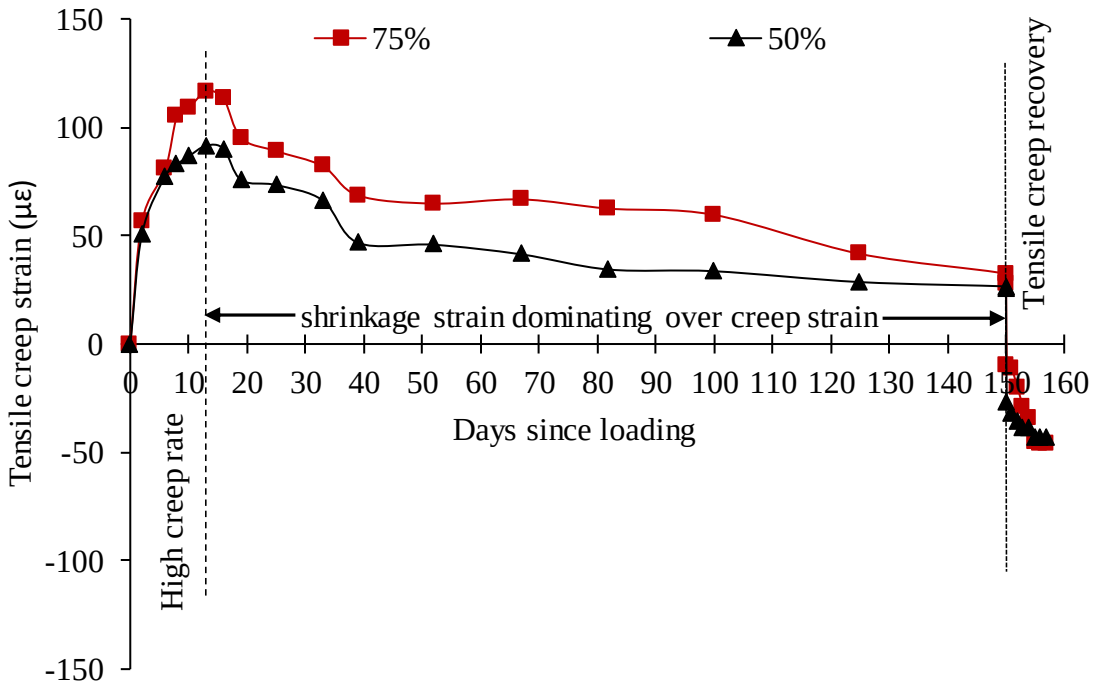

Fig. 4.5 Tensile creep strain of UHPFRC under varying sustained tensile loads.

free specimens with the same curing conditions as the tensile creep specimen. Furthermore, the shrinkage specimens had the same shape, size and ambient conditions as the tensile creep specimens from the same batch of concrete mix, to minimize the scatter in results obtained under sustained tensile loads. The total shrinkage strain was the average magnitude of two controlled prismatic specimens. This approach, layering the shrinkage and creep, is common

practice, whilst the shrinkage strain of an unloaded specimen is assumed to be equivalent to the loaded specimen shrinkage, as reported by Denarié et al. (2006) and Rossi et al. (1994).

Initially, the loads were applied gradually to avoid the dynamic effects in the specimen and the apparatus at the very beginning of the tensile creep test, as shown in Fig. 4.6. The UHPFRC specimens suffered elastic (instantaneous) strain immediately after applying the tensile loads. This instantaneous strain was not considered a part of the tensile creep and it was subtracted from the total strain (shrinkage strain + tensile creep). Fig. 4.5 shows the tensile creep strain rate was higher during the first 13 days, where the tensile creep strains were 117 με and 92 με for the specimen with 20 kN and 30 kN sustained tensile loads, respectively. A similar trend was reported by Garas et al. (2010), where tensile creep strain showed a higher creep rate up to the first 13 days for UHPFRC, whilst the tensile creep strain was 100 με at 10 days. Nevertheless, after 13 days, the tensile creep strain was dominated by the shrinkage strain and the tensile creep strain values dropped progressively. This was due to low strain progress under tensile loads, while the dispersion of the shrinkage strain was occurring at a higher rate. Initially, the steel fibers of UHPFRC increased the pathways for the water inside the UHPFRC. Furthermore, the loading of the UHPFRC specimens triggered the exudation and transportation of adsorbed gel water. This accelerates the high creep rate at an earlier age than for conventional concrete. After 13 days, the quantity of water inside the UHPFRC reduced due to evaporation, which decelerated the progress of the tensile creep strain. This surprising behaviour was also observed by Kovler (1999); Reinhardt and Rinder (2006) and Ranaivomanana et al. (2013), where the tensile creep strain was found to reduce whilst exhibiting negative magnitudes.

A tensile creep specimen with 30 kN sustained tensile loads (C75) showed 21.70% higher tensile creep strain value than that of a 20 kN sustained tensile load (C50) specimen at 13th

day. It was observed that the higher the sustained stress, the higher the tensile creep strain was achieved at early age. This is because the applied sustained tensile loads were within the elastic range, exhibiting the linear stress-strain relationship. After 150 days of loading, the tensile creep strain of C75 was 7.04% higher than the tensile creep of C50, as the difference between these two tensile creep specimens was reduced over the time period. This is because sustained tensile loads were applied over the long-term, which affected the microstructure of the UHPFRC and its strength, leading to the scattered values of tensile creep strain.

Fig. 4.6 Tensile creep test set up at the laboratory.

The magnitudes of tensile creep strain recovery are also shown in Fig. 4.5 where, after releasing the loads, the specimens underwent relaxation. The recovery in tensile creep strain was recorded until complete relaxation. The final average tensile creep strain recovery was 45.8 με and -43.1 με at 180th day for specimens C75 and C50, respectively.

4.6 TENSION STIFFENING

4.6.1 Load versus average strain

Fig. 4.8 shows the load versus average concrete strain at 28th day, for two identical specimens (Specimen 1 and Specimen 2), with similar sizes and shapes. The average concrete strain was estimated by dividing the average displacement values, determined from LVDT readings and the initial specimen length. The shrinkage strain was considered prior to the load application at 28th day to avoid the shortening effect. Therefore, the elongation of the specimen was negative due to shrinkage prior to the load application and this factor was accounted for while calculating the average concrete strain value. Before cracking occurred in the concrete specimen, the concrete strain increased linearly with the increase in applied load. Specimens 1 and 2 exhibited a linear trend up to a strain of 5.82×10^{-5} ε and 3.5×10^{-5} ε respectively, while the corresponding first cracking strengths were 1.87 MPa and 1.61. Later, with the increase in applied tensile load, there was a rapid formation of cracks, as shown in Fig. 4.7, and this led to the drop in the tensile loads in the concrete, due to the drop in tensile strength.

The UHPFRC specimens were capable of carrying loads larger than the yielding load of the reinforcing steel bar. This can be attributed to the improved bond strength between the reinforcement and the concrete as a result of the steel fibers, which increased the tensile strength in the concrete. When the transverse cracks were formed, the loads were transferred to the steel reinforcement, inducing greater strain differences and causing the reinforcement to slip.

During this period, the deformed bar exerted a radial pressure onto the cement matrix as the steel reinforcement slipped. This pressure was carried by the steel fibers through the crack bridging effect and assisted in transferring the tension across the cracks. Thus, a

comparatively lower load was transferred to the reinforcement with the crack initiation, inducing inferior strain differences between the cement matrix and the reinforcing bar. Principally, these multiple crack developments are controlled by the ability of the steel fibers

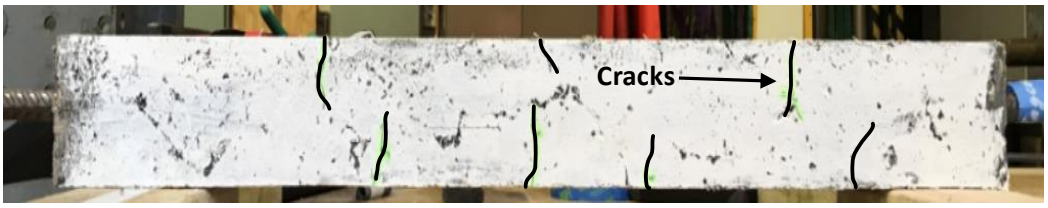

Fig. 4.7 The formation of cracks from tension stiffening test at 28th day.

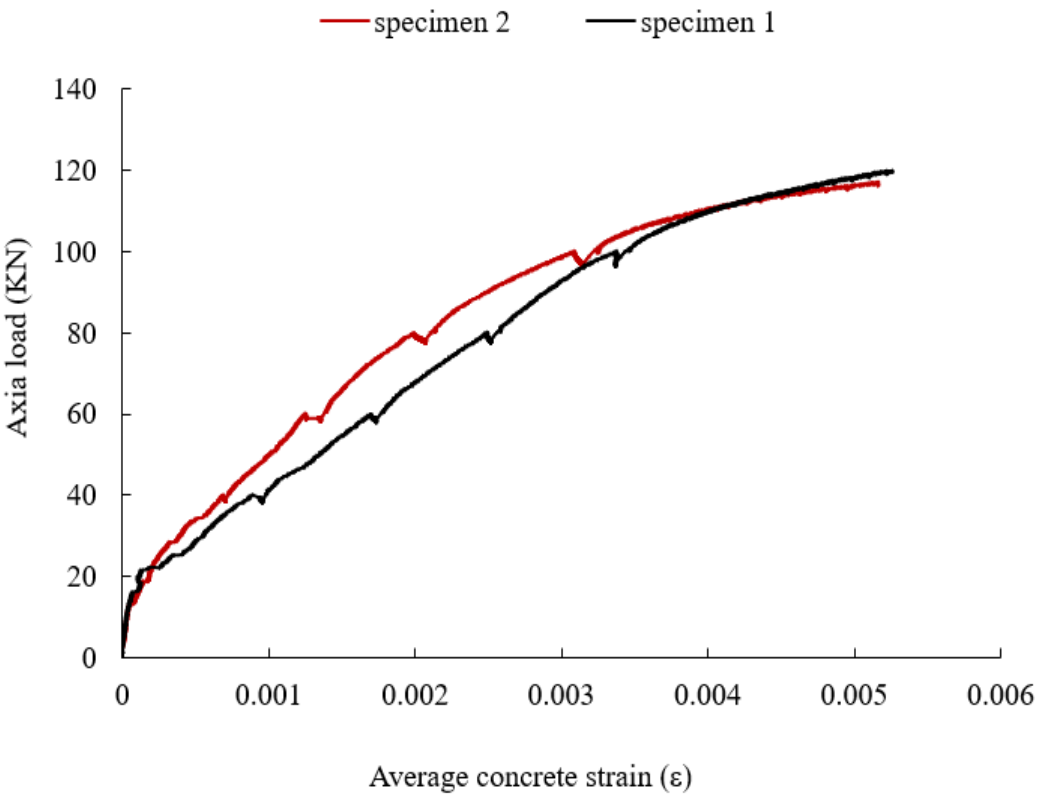

Fig. 4.8 Average concrete strain from tension stiffening test at 28th day.

Fig. 4.9 Electro microscopic images for the bridging of cracks through steel fibers.

to transfer loads across the cracks, allowing the surrounding concrete to carry the load continuously with the reinforcement, after the initiation of multiple cracks. Hence, the strain hardening phenomenon has been observed for the UHPFRC specimen at higher stress levels. The strain hardening for both Specimens 1 and 2 was observed up to 99.7 kN and 100 kN, respectively, where the fibers were active at their maximum levels. The strain hardening ranged from 59 με to 3500 με and 33 με to 3200 με for Specimens 1 and 2, respectively. However, it has been observed that specimens can reach a higher strain magnitude during the crack localization stage. The formation of multiple transverse cracks was found in the concrete specimens up to the yielding of the longitudinal bar shown in Fig. 4.10. There were approximately 5 to 12 transverse cracks in both Specimens 1 and 2 prior to the localization of the cracks. The softening of the UHPFRC specimens was observed beyond the yielding point, reaching to a maximum strain of 5300 με and 5200 με at 120 kN and 117 kN, respectively. Meanwhile, the fibers did not transfer any further loads along the cracks, as the

fibers were not connected to the adjacent side of the crack opening. The fibers were pulled out for investigation and no breakage of fibers was observed.

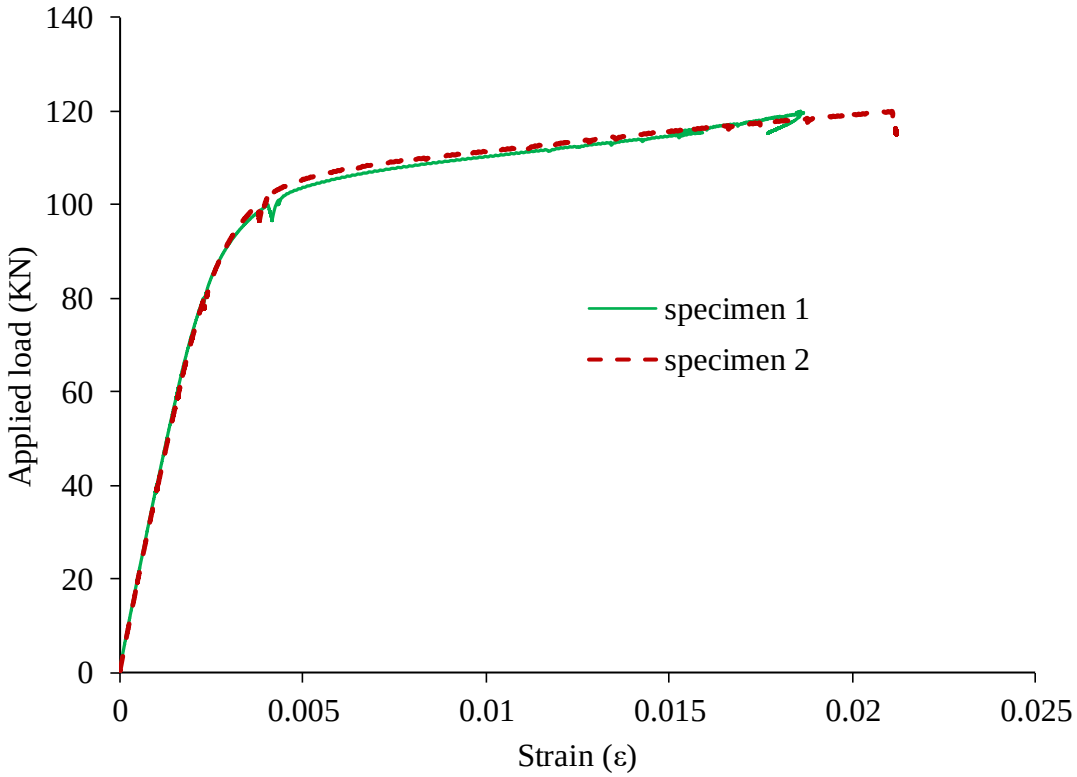

Fig. 4.10 Load vs steel strain relationship from tension stiffening test at 28th day.

4.6.2 Effect of sustained tensile loads

From the 28th day tension stiffening test results, the steel strain was measured for the associated cracking strength to determine the desired sustained tensile loads at 20 kN, 40 kN, 60 kN and 80 kN. The sustained tensile loads were applied to the UHPFRC specimens and two specimens were used for each sustained tensile load. Immediately after applying the sustained tensile loads, the instantaneous strains were measured to determine the tension stiffening effect precisely. The average concrete strain was determined from two LVDT readings.

Immediately after applying the load, the average concrete strain reached 1160 με, 670 με, 400 με and 170 με for varying sustained tensile loads of 80 kN, 60 kN, 40 kN and 20 kN, respectively, as shown in Fig. 4.12. It is worth mentioning that immediately after applying the sustained tensile loads, the specimens with sustained tensile loads of 20 kN (T20) and 40 kN (T40) showed no cracks. This is due to the lower (20 kN) or equal (40kN) applied loads,

Fig. 4.11 Specimens under varying sustained tensile loads.

when compared with the first cracking load of 40 kN from the 28th day tension stiffening test results. The LVDT readings were recorded continuously using the multiplexer to determine the deformation rate with time. Meanwhile, the formation of new cracks was traced and measured. The first crack was visible after23 hours for the 40 kN loaded specimen. After 52 hours another two new cracks were traced. Again, for the 20 kN loaded specimen, the first crack was traced after 7 days of loading at which point a total of four cracks were identified. It was surprising to note that the stress of the UHPFRC specimen might decay under sustained

loads even when the applied tensile loads were within the elastic limit. It was observed that the higher load, the less time is needed for the decay to occur. The decay was due to defects

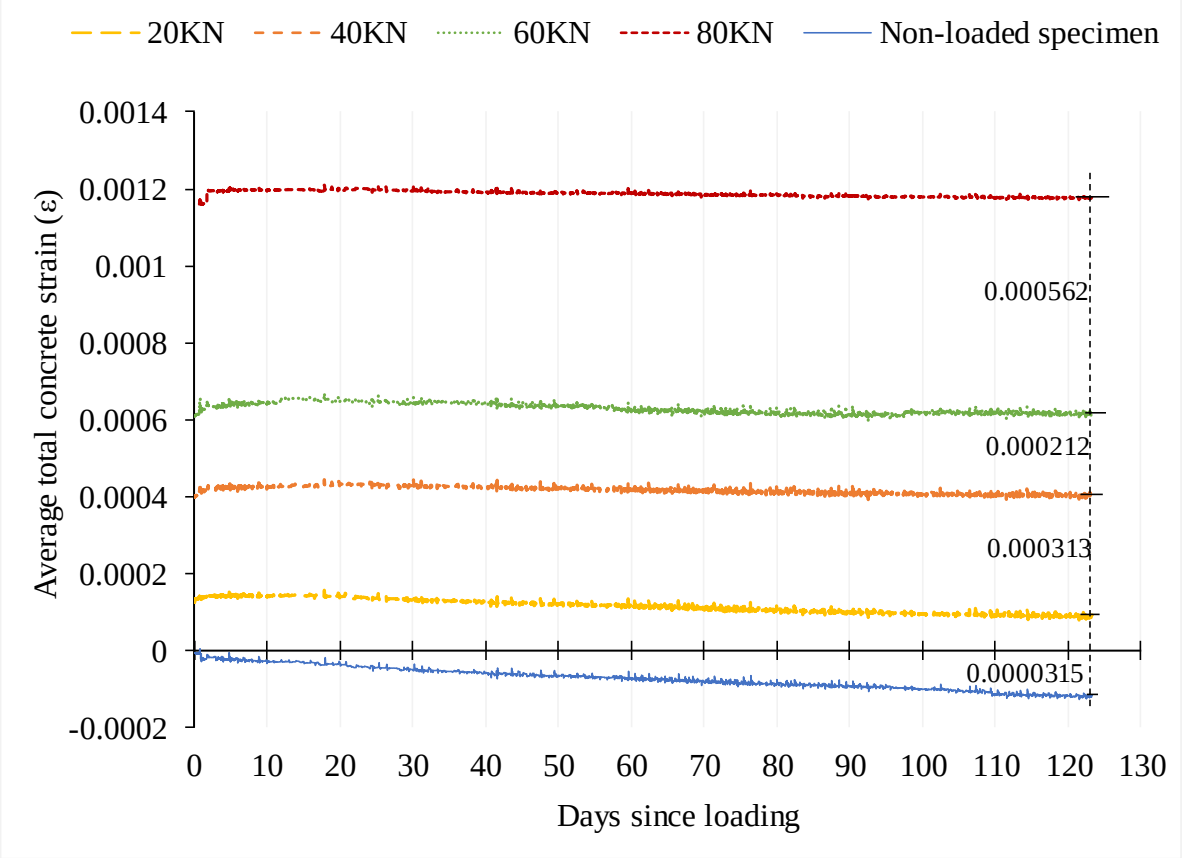

Fig. 4.12 Time dependent average total concrete strain under varying sustained tensile loads.

in the microstructure of the UHPFRC under sustained tensile loads, such as the deterioration of the bond strength between the cement matrix and the steel fibers and also between the interfacial transition zone of the cement matrix and the reinforcing bar. However, the specimens with sustained tensile loads of 80 kN (T80) and 60 kN (T60) reached the strain hardening phase immediately after applying the loads, exhibiting a total number of four and two cracks, respectively. Later, it was observed that the formation of new cracks for both of these specimens was greater at an early age, where the maximum number of the cracks appeared within the first 25 days. Specimen T80 showed a total of 12 cracks, whereas the 60

kN loaded specimen showed a total of 9 cracks during the entire test period. It is important to mention that the total number of transverse cracks was dependent on the magnitude of the sustained tensile loads i.e. the higher the sustained tensile loads, the higher the number of transverse cracks would form.

4.6.3 Effect of shrinkage

The time-dependent total average concrete strain was measured for different sustained tensile loads, as shown in Fig. 4.12. It was observed that the average concrete strain of specimen T20 increased from 125 με to 142 με for first 7 days following the elastic characteristics and reached a strain of 148 με with the formation of the first crack. The average concrete strain was found to decrease over time, unless a new crack formed. The maximum average concrete strain of 148 με was found with the formation of the final crack at 26^{th} day and 17 hours. Later the strain decreased as time progressed. Specimen T40 showed a similar trend, increasing the average concrete strain from 419 με following the elastic behaviour and abruptly stepping up to 435 με with the formation of the first crack. The peak average concrete strain was 448 με at 38^{th} day with the formation of the final cracks. Afterwards, the average concrete strain descended. This change could be attributed to the shrinkage effect, as the test specimens were exposed to ambient conditions and the drying of the specimen was still happening. Initially, the tensile strain was higher than the shrinkage strain as the specimen was under the impact of applied loads. With the formation of new cracks, a sudden increase in the concrete strain was observed consistently as the existing cracks were widening and later, this slowed down to settle the impact. Consequently, with the formation of the final cracks, the progress of the tensile strain was too slow, so the shrinkage strain dominated the final average total concrete strain. The average concrete strain for both Specimens, T80 and T60, exhibited lower fluctuation, as the maximum number of transverse cracks was formed

at an early age of sustained loading. The average concrete strain did not suddenly jump to the higher strain because of the formation of several cracks simultaneously after immediate load application. These specimens settled down rapidly from the impact of crack formation, leading to the slow progress of tensile strain. Later, the total average concrete strain decreased over the time period because of the shrinkage. The non-loaded specimen was included to determine the shrinkage effect on a non-loaded specimen. It was observed that when the specimen was free of the applied loads, the average total concrete strain was due to shrinkage alone. The final average concrete strain for the non-loaded specimen was -0.0001194 με. Considering the effect of shrinkage strain, the final average concrete strain would be 1294 με, 732 με, 520 με and 207 με due to the sustained tensile loads of 80 kN, 60 kN, 40 kN and 20 kN, respectively.

4.6.4 Tension stiffening test under direct tensile loads for sustained loaded specimens

The sustained tensile loaded specimens were unloaded at 175th day and the tension stiffening test under direct tension was performed at 180th day, after complete relaxation of the specimens, as shown in Fig. 4.13. As soon as the specimens were unloaded, the strains were measured until complete relaxation had occurred. Specimen T20 followed the expected elastic behaviour and, after complete relaxation, it almost recovered to the original levels of an on-loaded specimen at 180th day. However, Specimen T40 did not show much of the expected elastic behaviour and was unable to return to the original position when compared with the non-loaded specimen.

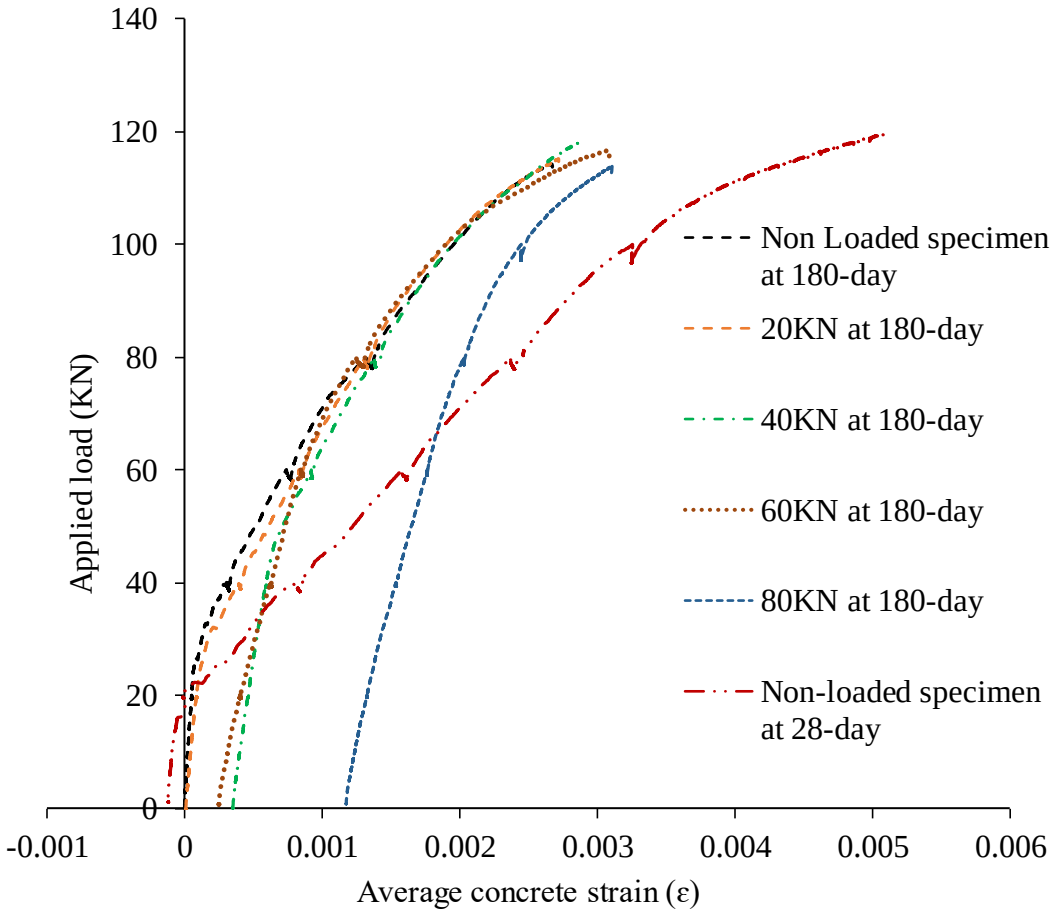

Fig. 4.13 Average concrete strain of different sustained loaded specimens for tension stiffening at 180th day.

This is due to the disturbed microstructure, caused by the sustained tensile loads for the long-term, as discussed earlier. Similarly, Specimens T80 and T60 exhibited permanent deformation when compared with the non-loaded specimens after complete relaxation, as expected. The specimens elongated just after unloading and after complete relaxation, so that the lengths of the specimens were higher prior to the unloading. This could be attributed to the effect of strain hardening, related to the elasticity of the reinforcing bar. As soon as the loads were released, the reinforcing bar returned to its original shape, following the linear

stress-strain curve, whilst the existing cracks did not maintain their elastic properties, contributing to the total elongation of the specimens.

Table 5 Cracking strength and strain details of UHPFRC for tension stiffening test under direct tension.

Specimen type (age in days)	Cracking strength (MPa)	Peak elastic strain (με)	Strain hardening range (με)	Final concrete strain (με)
T0 (28)	1.73	58	59 to 3500	500
T0 (180)	2.69	55	56 to 1400	2600
T20 (180)	2.61	74	75 to 1300	2700
T40 (180)	2.55	200	200 to 2200	2800
T60 (180)	2.54	140	140 to 1900	3100
T80 (180)	2.62	160	160 to 800	3500

The elastic strain and associated cracking strength are given in Table 5, where the maximum cracking strength was estimated for all the specimens at 180th day. This was due to keeping the non-loaded specimen undisturbed, which assisted in achieving stronger bond strengths when compared with the sustained tensile loaded specimens. With the increase in applied tensile loads, the specimens were forced into the strain hardening phase. It was observed that the progress rate of tensile strain for the sustained tensile loaded specimens was lower than that for the non-loaded specimens. This was due to the cracks already present in the sustained loaded specimens, prior to the tension stiffening test under direct tensile loads. When applying the tensile loads, the crack openings were sufficiently matured that they could not react as much as the non-loaded specimens to exhibit the higher tensile strain rate. However, the final total strain values of all the sustained loaded specimens were higher than for the T0-180 specimen. The non-loaded specimen (T0-28) at 28th day was included for comparison with the results obtained from the specimens in long term. The first cracking strength for Specimen T0-28 was 1.73 MPa, whilst the final average concrete strain value was 500 με. It

was observed that the final average concrete strain of T0-28 was approximately 52% greater than that of Specimen T0-180 and it was also greater than any of the sustained tensile loaded specimens. This is attributed to its lower tensile strength, which ultimately resulted in the highest concrete strain.

4.6.5 Crack width

Fig. 4.14 shows the crack width for different sustained tensile loaded and non-loaded specimens under direct tensile loads at an applied loading rate of 0.18 kN/min. The maximum average crack width for non-loaded specimens was 0.23 mm at 28^{th} day, where the first crack appeared at 37.50 kN. However, for the non-loaded specimens at 180^{th} day, the first crack was observed at 20 kN: when the crack width was 0.01 mm and the load was 40 kN, the corresponding crack width was 0.017 mm. It is worth mentioning that the first crack width for the non-loaded specimen at 180^{th} day was lower than that observed at 28^{th} day. This was

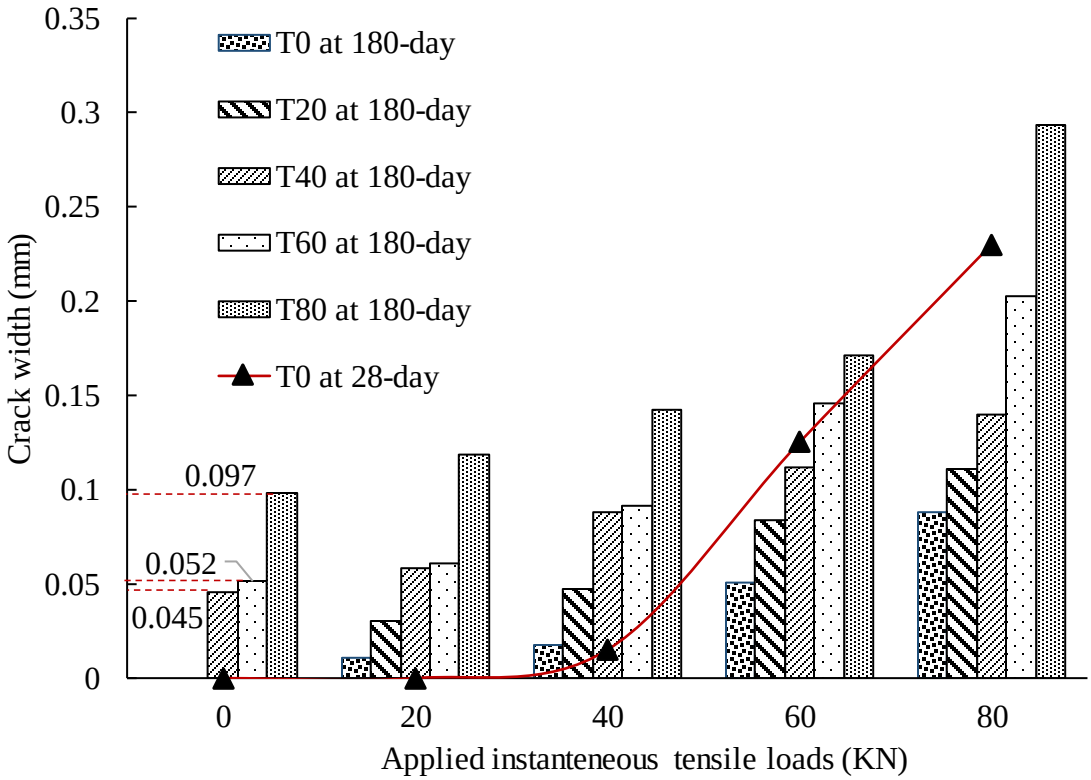

Fig. 4.14 Crack width for different sustained tensile loaded (80 kN, 60 kN, 40 kN and 20 kN) and non-loaded specimens under instantaneous tensile load.

due to the shrinkage effect on the reinforced UHPFRC specimen, which reduces the cracking strength in the long-term. Similar phenomena were also reported by Bischoff (2003), where the shrinkage strain in the long-term changed the effective length of the specimen, as well as the cracking strength. It was observed that the crack width magnitude for both the short-term (28 days) and the long-term (180 days) for the non-loaded specimens at an applied tensile load of 40 kN was almost same. With the increased loads, i.e. at 60 kN and 80 kN, the crack width over the long-term was significantly reduced, by 150% and 187% than the crack width of short-term. The change is due to the increased tensile strength in the UHPFRC and the stronger bond between the cement matrix and the steel fibers resisting any fiber pull-out while bridging the cracks. The average maximum crack widths were 0.11 mm, 0.13 mm, 0.20 mm and 0.30 mm for 20 kN, 40 kN, 60 kN and 80 kN sustained loaded specimens, respectively,

when subjected to instantaneous tensile loads, as shown in Fig. 4.14. The existing average crack widths (after complete relaxation) of 0.04, 0.05, 0.09 mm for Specimens T40, T60 and T80, respectively, were recorded prior to the instantaneous loading. The ultimate average crack width for the sustained loaded specimens was much higher than for the non-loaded specimens in the long-term. This could be attributed to the weakening bond between the cement matrix and the steel fibers for sustained tensile loaded specimens, whilst the bridging mechanism of the steel fibers across the cracks was disturbed. Subsequently, this reduced the resisting capacity of the steel fibers across the cracks and it further accelerated the progress of the cracks widening at a higher rate, while subjecting them to instantaneous tensile loads. Therefore, the higher the sustained tensile loads the greater were the crack widths observed under instantaneous loads.

Fig. 4.15 shows the time-dependent crack widths under sustained tensile loads for reinforced UHPFRC specimens. The maximum crack width of 0.36 mm was observed at an applied sustained tensile load of 20 kN, where the crack width was progressing rapidly at a higher rate. This was due to the formation of all 4 cracks simultaneously at 30^{th} day and correspondingly contributed to the increase in the average crack width. However, for the rest

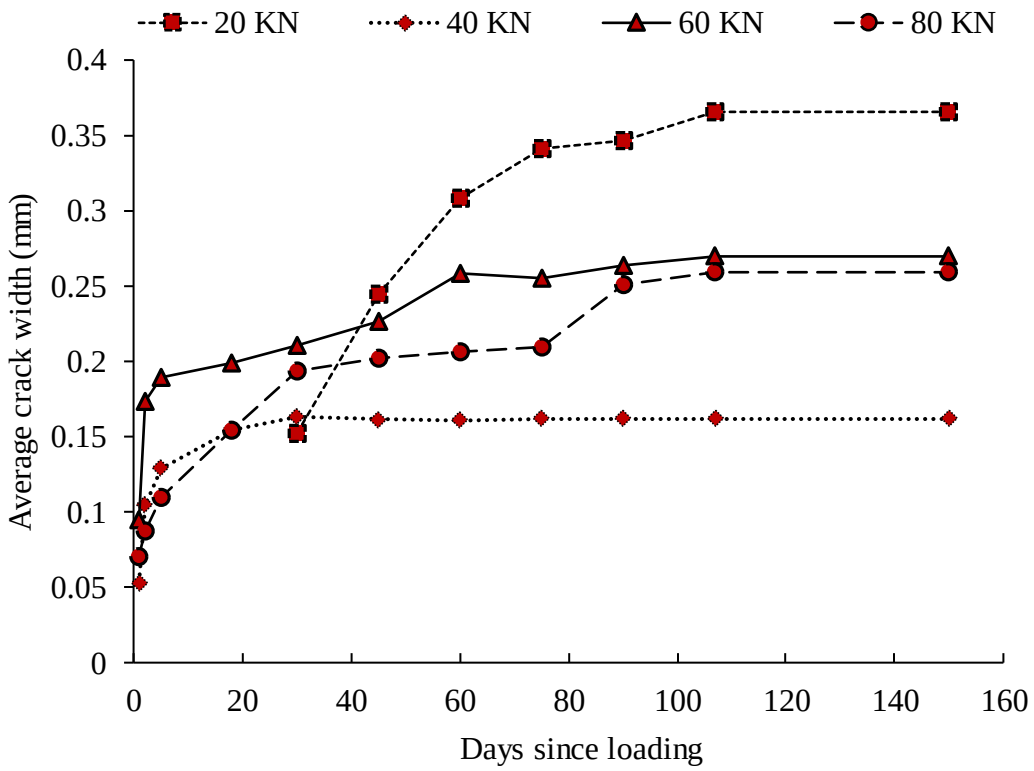

Fig. 4.15 Time dependent crack width (mm) under different sustained tensile loads.

of the sustained tensile loads (40 kN, 60 kN and 80 kN) the crack width was found to progress slowly, and several cracks were observed immediately after applying the loads. With the progress of time, new transverse cracks were observed along the member lengths. Simultaneously, reductions in the crack widths of previously formed cracks were also observed. Thus, the average crack widths are found to decelerate with the increased number of cracks. It should be noted that the higher number of transverse cracks in UHPFRC contributes in controlling the crack widths over the long-term.

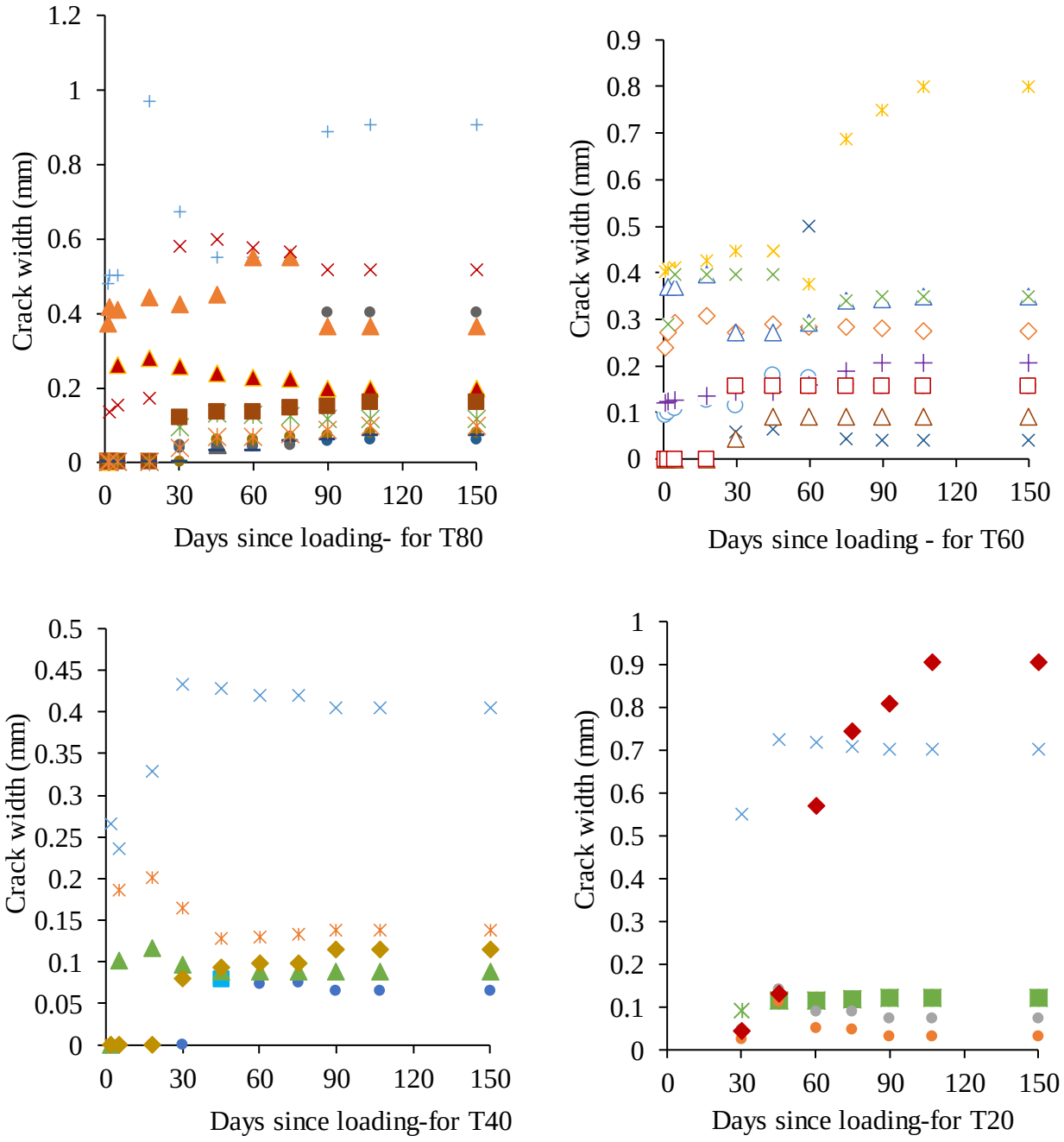

Fig. 4.16 Progress of crack width under varying sustained tensile loads (80 kN, 60 kN, 40 kN and 20 kN).

4.6.6 Crack spacing

Fig. 4.17 and Table 6 show the average crack spacing for reinforced UHPFRC specimens under instantaneous and sustained tensile loads. At 28th day, the average crack spacing for

non-loaded specimens was 110 mm, where a total of 12 cracks were traced under instantaneous loading. Again, the average crack spacing for non-loaded specimens was 86.4 mm, associated with the formation of 15 transverse cracks at 180th day. It is worth mentioning that the crack spacing decreased with the increase in crack numbers in the UHPFRC over the long-term.

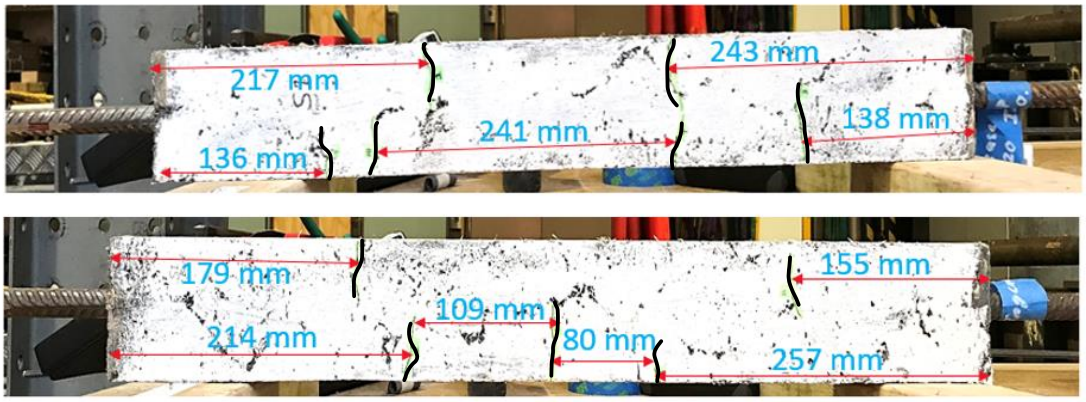

Fig. 4.17 Average crack spacing of reinforced UHPFRC specimen under instantaneous load at 28th-day.

Table 6 Average crack spacing of reinforced UHPFRC specimen.

Specimen type (age of concrete)	Total number of cracks prior to the application of instantaneous load at 175th day	Total number of cracks after applying instantaneous load at 180th day	Average crack spacing (mm) under sustained tensile loads up to 175-days	Average crack spacing (mm) under instantaneous load at 180th day
T0 (180)	0	15	0	86.4
T20 (180)	6	19	220	69
T40 (180)	7	16	188.57	82.5
T60 (180)	8	12	165	129.6
T80 (180)	11	13	120	101.53

The average crack spacings for Specimens T20, T40, T60 and T80 were 220 mm, 188.60 mm, 165 mm and 120 mm, respectively, at 175th day. The time-dependent progress of the crack spacing is presented in Fig. 4.18, where, with the formation of each new crack, the

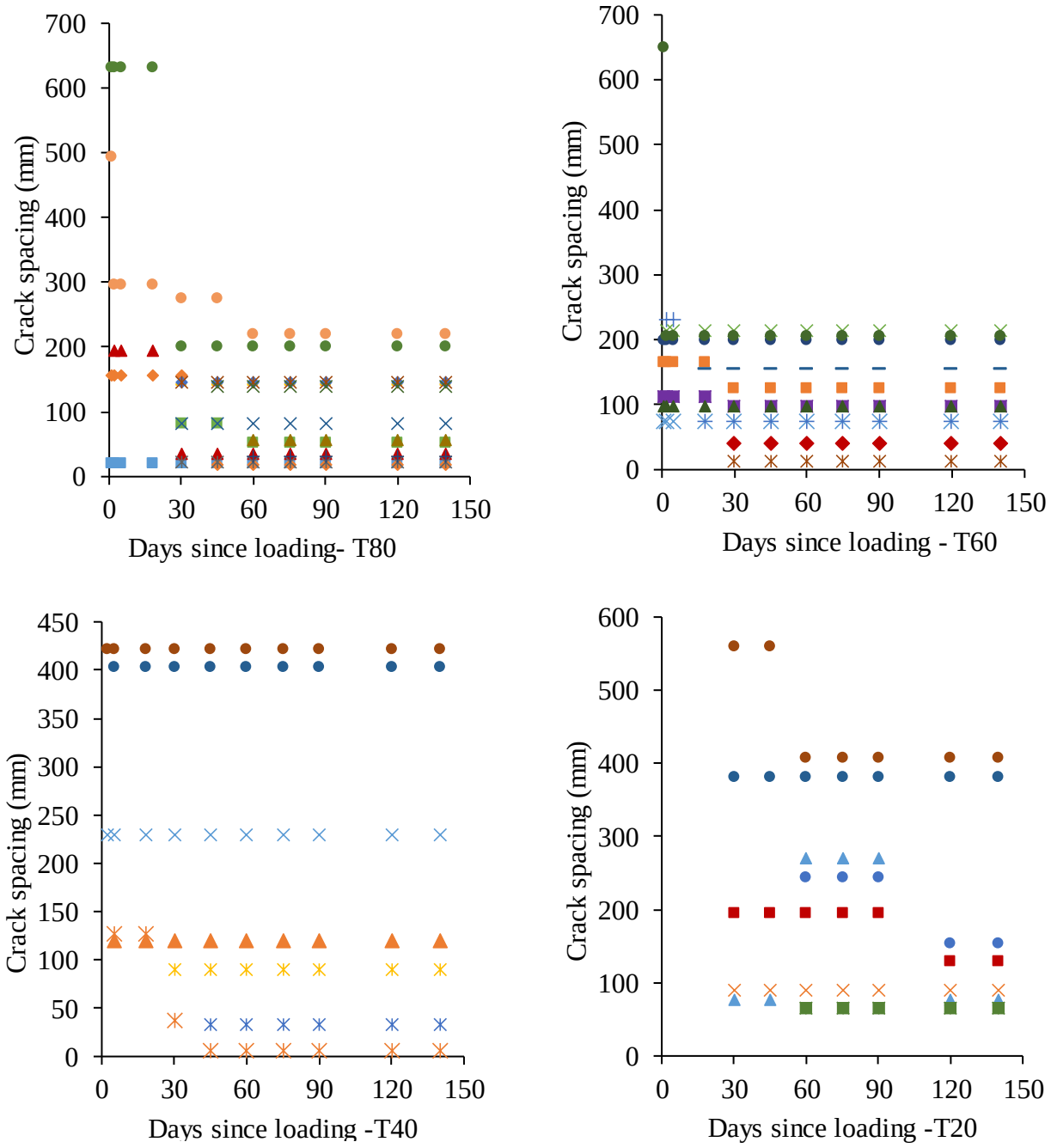

Fig. 4.18 Progress of crack spacing for various cracks under varying sustained tensile loads (80 kN, 60 kN, 40 kN and 20 kN).

crack spacing decreased. The higher the sustained tensile loads, the greater the number of cracks that were measured prior to the application of instantaneous tensile loads. It was interesting to observe that after applying instantaneous tensile loads to the higher sustained

tensile loaded specimens i.e. T60 and T80, the crack numbers stabilised and did not increase as much in comparison to the lower sustained tensile loaded specimens, T20 and T40, as given in Table 6. This was due to the pre-existing cracks in the greater sustained tensile loaded specimens (60 kN and 80 kN) resisting the formation of new cracks rather than merely increasing the crack width, which would increase the crack spacing correspondingly. However, the specimens with 20 kN and 40 kN sustained tensile loads exert a significant increase in crack numbers under instantaneous loads, contributing to a decrease in crack spacing. This is attributed to the formation of new cracks beyond the elastic stress, while applying instantaneous tensile loads.

4.7 SUMMARY

The experimental results of the time-dependent tensile behaviour tests of UHPFRC have been presented and the major findings are discussed in this chapter.

In this study, material mechanical properties, such as compressive strength, indirect splitting tensile strength and modulus of elasticity test results have been presented at different curing ages. The compressive strength of UHPFRC was found to increase with the increase of time. The maximum strength for UHPFRC was 134 MPa at 120th day. The obtained splitting tensile strength and modulus of elasticity magnitudes were found to increase with the progress of time, whilst both of these test results were within the range of expected standard magnitudes for UHPFRC.

It has been demonstrated that shrinkage has a profound influence on unreinforced and reinforced UHPFRC specimens, especially on the cracking strength and member length. A significant amount of the total shrinkage strain was caused by autogenous shrinkage, whilst the drying shrinkage strain was lower than that of the autogenous shrinkage. The shrinkage

strain influenced the load versus average concrete strain relationship both before and after applying sustained tensile loads. It is worth noting that shrinkage has a minor effect on UHPFRC when the cracks are stabilized for reinforced UHPFRC specimens subjected to sustained tensile loads in the long-term.

The direct tensile strength for UHPFRC specimens was 6.7 MPa at 28th day, whilst the direct tensile strength was found to increase with an increased curing period. The obtained direct tensile strength of the sustained tensile loaded specimens was lower than that of the non-loaded specimens over the long-term. It is worth noting that the higher the sustained tensile loads, the lower the direct tensile strength can be obtained. The crack opening width was found to reduce with the increase of tensile strength in UHPFRC.

The tensile creep specimens were installed inside the newly designed rig in such a way that varying sustained tensile loads could be adopted simultaneously for similar specimen sizes and shapes. In this study, two varying sustained tensile loads were chosen: 75% (40 kN) and 50% (i.e. 30kN and 20 kN) of the cracking load. The tensile creep strain increased at a higher rate for the first 13th day. Afterwards it decelerated because of the shrinkage effect.

The tension stiffening test was conducted for instantaneous tensile loading and sustained tensile loading. In the case of instantaneous tensile loading, the reinforced UHPFRC specimens exhibited transverse cracks after reaching the strain hardening stage prior to the localization of cracks. Softening of the UHPFRC was observed when the steel fibers were not transferring any further loads along the cracks, as the fibers were not connected to the adjacent side of the crack opening. The fibers were pulled out and no breakage of the fibers was noted. Reinforced UHPFRC specimens subjected to higher sustained tensile loads ($\geq$ 60 kN) exhibited transverse cracks in the long-term, whereas lower sustained tensile loads ($\leq$ 40 kN) were observed with no transverse cracks at early ages. The ultimate average crack width

for the sustained loaded specimens was much higher than for the non-loaded specimens over the long-term. The crack spacing for sustained tensile loaded specimens was found to decrease with any increase in the numbers of cracks.

CHAPTER 5 : CONCLUSIONS AND RECOMMENDATIONS

5.1 GENERAL REMARKS

To investigate the long-term tensile creep behaviour of UHPFRC, four phases of research were conducted. These were a deep literature review, development of a tension stiffening and tensile creep rig to apply sustained loads, an experimental campaign, and analysis of the test results.

The key outcomes of this study are (i) the evaluation of the UHPFRC material properties, including compressive strength, modulus of elasticity, splitting tensile strength, and direct tensile strength; (ii) evaluation of UHPFRC creep behaviour under different sustained tensile loads (iii) investigation of reinforced UHPFRC tension stiffening prisms under instantaneous direct tensile loads; and (iv) investigation into time-dependent behaviour of tension stiffening prisms when subjected to a range of sustained tensile loads.

From the outcomes of this work, the following specific conclusions can be drawn:

5.2 MATERIAL PROPERTIES

1. The compressive strength of UHPFRC was found to increase with any increase in time. The maximum strength for UHPFRC was 134 MPa at 120^{th} day. At 28^{th} day, the compressive strength for UHPFRC was 116 MPa, which was about 13.43% lower than the optimum strength achieved by UHPFRC at 120^{th} day. It was observed that the increasing rate of compressive strength after 28 days was lower than that at 7^{th} day to 28^{th} day. This could be due to the elevated hydration process of the UHPFRC specimen at an early age. After 28 days, because of the lower water to binder ratio of

0.12 and evaporation of the water from the surface of the concrete, the hydration process slows, and this affects the rate of compressive strength gain.

2. The maximum splitting tensile strength for UHPFRC was 18.7 MPa at 120th day, which was 28.4% higher than at 28th day. The obtained splitting tensile strength of UHPFRC ranged from 10 MPa to 18.7 MPa between 7th day and 120th day, which was similar to the standard magnitudes of splitting tensile strength ranging from 7 MPa to 15 MPa.
3. The modulus of elasticity (MOE) test was performed for UHPFRC cylindrical specimens. It was found that the MOE ranged between 40.4 GPa at 7th day to 47.85 GPa at 120th day. The MOE values were comparatively closer to the previously reported MOE values of 41 GPa to 47 GPa for UHPFRC.

5.3 SHRINKAGE

A significant portion of the measured total shrinkage was caused by autogenous shrinkage rather than drying shrinkage, and this is unlike the behaviour observed in conventional concrete. The ultimate autogenous shrinkage strain was -380.65 με, whereas the drying shrinkage strain was -159.6 με for a total shrinkage strain of -560 με at 180th day. It was observed that the shrinkage strains developed rapidly in the first 25 days, with the recorded autogenous shrinkage, drying shrinkage and total shrinkage strains measured being -220 με, -115 με and -335 με. Later, the shrinkage strain rate decelerated and, after 150 days, the progress of shrinkage strain was found to slow to a negligible rate.

5.4 DIRECT TENSION TEST

1. The direct tensile strength for the UHPFRC specimens was 6.7 MPa at 28th day, where the first cracking strength was 40 kN. A similar test was repeated at 180th day for a load free specimen under the same curing requirements in specific ambient conditions. The measured tensile strength for the UHPFRC specimen was 9.5 MPa, which was approximately 29.5% higher than for the direct tensile strength at 28th day. The direct tensile strength was found to increase with the increased curing period.
2. The direct tensile strength of sustained tensile loaded specimens was lower than for non-loaded specimens. This was due to the sustained tensile loads, which caused the deterioration of the microstructure in the UHPFRC and affected the strength. This phenomenon was more clearly observed when the direct tensile strength of the 75% sustained tensile specimen was lower than the 50% sustained tensile loaded specimen. It was observed that the higher the sustained tensile loads, the lower the direct tensile strength of the UHPFRC.
3. The crack opening width was found to reduce with an increase in tensile strength for non-loaded specimens. The crack openings for 75% and 50% sustained tensile loaded specimens were 2.70 mm and 3.40 mm respectively at 180th day. It was observed that the tensile stress dropped from 7.6 MPa for 75% sustained loaded specimens, whereas for 50% sustained loaded specimens, it dropped from 9 MPa.

5.5 TENSILE CREEP

1. In this research, two varying sustained tensile loads were chosen to conduct the tensile creep test. One was 75% of the cracking load (40 kN) and another one was 50% of the cracking load (40kN) i.e. 30kN and 20 kN, respectively.

2. The tensile creep increased at a higher rate for the first 13 days, obtaining tensile creep strains of 117 με and 92 με for the specimen with 30 kN and 20 kN sustained tensile loads, respectively. It was observed that the higher the sustained stress, the higher the tensile creep strain was achieved by the tensile creep specimen at an early age.
3. After 13 days of sustained tensile loading, the tensile creep strain was found to decelerate and the tensile creep strain showed descending characteristics up to 150 days. This was due to the shrinkage strain, which dominated the tensile strain. It was observed that shrinkage had a vital role in controlling the overall time-dependent deformations. The final tensile creep strain was 27.36 με and 25.65 με for specimens with 30 kN and 20 kN sustained tensile loads, respectively. It was found that the tensile creep strain of the 30 kN specimen was 7.04% higher than the tensile creep of the 20 kN specimen at 150th day, whilst the difference between these two tensile creep specimens reduced over time.

5.6 TENSION STIFFENING

1. This research investigated the tension stiffening response of steel reinforced UHPFRC, using a tension stiffening prism under a direct tensile load. A rig was designed and produced to investigate the tension stiffening effect under varying sustained tensile loads for similar sizes and shapes of specimens.
2. Two replicates reinforced the UHPFRC specimens, numbered 1 and 2, and were used to determine the tension stiffening effect under direct tension. Before cracking occurs in a concrete specimen, the concrete strain and applied load exhibit a linear stress strain curve. Specimen 1 and Specimen 2 exhibited a linear strain of 5.82 × 10-5 ε

and 3.5 × 10-5 ε, respectively, whilst the first cracking strength was 1.87 MPa and 1.61 MPa for both specimens.

3. The strain hardening for both Specimens 1 and 2 was observed up to 99.7 kN and 100 kN, respectively, where the fibers were active at their maximum levels. The strain hardening ranged from 59 με to 3500 με and 33 με to 3200 με for Specimens 1 and 2, respectively. The transverse cracks were formed at the strain hardening phase and an approximate total of 5 to 12 transverse cracks were found prior to the localization of cracks for both specimens.
4. Softening of the UHPFRC specimens was observed beyond the yielding point, where the fibers were not transferring any further loads along the cracks as they were not connected to the adjacent side of the crack opening. The fibers were pulled out and no breakage of the fibers was observed.
5. Tension stiffening tests were conducted for two replicates under each sustained tensile load, commencing at 28th day. Immediately after applying the sustained tensile loads, the specimens with 80 kN and 60 kN sustained tensile loads showed several transverse cracks, after which strain hardening occurred. The majority of transverse cracks for these two specimens formed within the first 25 days. However, the first crack was visible after 23 hours for the 40 kN sustained loaded specimen and, after 52 hours, a further two new cracks were traced. For the 20 kN loaded specimen, the first crack was traced after 7 days of loading. Later, a total of four cracks were identified. It was found that the higher the sustained tensile loads, the higher the number of transverse cracks that would form.
6. Tension stiffening was significantly affected by shrinkage. When a new crack formed, a sudden increment in the total concrete strain was observed and later the total concrete strain was found to reduce until another new crack formed, especially for

specimens under sustained loads of 20 kN and 40 kN. This was due to the slower progress of strain under sustained tensile loads, compared with the shrinkage strain. It was found that for the specimens with higher sustained tensile loads, such as 80 kN and 60 kN, stepping to the strain hardening phase was independent of new crack formation to increase the total concrete strain. For these specimens, the total average concrete strain was found to decrease continuously over the long term.

7. The specimens under sustained tensile loads reacted differently for varying sustained tensile loads. It was observed that the specimens with 80 kN and 60 kN sustained tensile loads changed drastically and, even after releasing the sustained loads, the specimens were elongated compared with the load free steel reinforced UHPFRC specimens under same ambient conditions. However, the specimens with 20 kN sustained tensile loads showed elastic behaviour after releasing the load, whereas specimens with 40 kN sustained tensile loads failed to follow the elastic stress strain curve. It was observed that the progress rate of tensile strain for sustained tensile loaded specimens under direct tensile loads was lower than for the non-loaded specimens. It might be because of the cracks already presented in the sustained loaded specimens prior to the tension stiffening test. While applying the tensile loads, the crack openings matured sufficiently and so could not react as much as the non-loaded specimens to exhibit the higher tensile strain rate.
8. The maximum average crack width for non-loaded specimens was 0.23 mm at 28^{th} day where the first crack appeared at 37.50 kN. For the non-loaded specimens at 180^{th} day, the first crack was observed at 20 kN where the crack width was 0.01 mm. When the load was at 40 kN, the corresponding crack width was 0.017 mm. It is worth mentioning that the first crack width for the non-loaded specimens at 180^{th} day was lower than that observed at 28^{th} day. The ultimate average crack width for the

sustained loaded specimens was much higher than for the non-loaded specimens over the long-term.

9. Crack spacing decreased with the increase in crack numbers in UHPFRC over the long-term, when subjected to instantaneous tensile loading. The crack spacing for sustained tensile loaded specimens was found to decrease with any increase in crack numbers.

5.7 RECOMMENDATIONS FOR FUTURE WORKS

Although much research has been conducted for UHPFRC, we are yet to understand the tensile behaviour of UHPFRC fully, especially over the long-term. Following the experimental results of this research, the following recommendations are made:

1. Specific fiber contents were used to produce UHPFRC for this study; to maintain feasibility and to reach the objectives in time. It is recommended that later research should vary the steel fiber content and types to understand the influence of steel fiber on tensile creep over the long term.
2. The cracking path for the V notch prism of direct tension test specimens did not follow the directed V notch section. It is recommended that later researchers position the specimen in the MTR machine with extra care, prior to loading. The gripping arms of the MTR machine also require positioning at the centre line of the specimen to avoid any eccentricity.
3. The instantaneous strain for tensile creep specimens was determined immediately after applying the sustained tensile loads. It is suggested that future researchers should use LVDT instead of mechanical demec gauges to determine the instantaneous strain more precisely for tensile creep specimens.

4. The designed tensile creep rig needs to be modified for future research work, especially the load application method. It is recommended that, as a development of the load application method, the specimens should not be disturbed while applying the loads.

REFERENCES

Abrishami, H. H., & Mitchell, D. (1996). Influence of splitting cracks on tension stiffening. *Structural Journal, 93*(6), 703-710.

Al-Fayadh, S., Engström, B., & Magnusson, J. (2001). Cracking behaviour of reinforced concrete tensile members. *Tension of Reinforced Concrete Prisms-Round Robin Analysis and tests on Bond-Report of RILEM TC 147-FMB*, 1-1.

Al-Kubaisy, M., & Young, A. (1975). Failure of concrete under sustained tension. *Magazine of Concrete research, 27*(92), 171-178.

Al Madhoun, A. T. (2013). Mechanical Properties of Ultra High Performance Fiber Reinforced Self-CoMPacting Concrete. *Mechanical Properties of Ultra High Performance Fiber Reinforced Self-CoMPacting Concrete*.

Altoubat, S. A., & Lange, D. A. (2001). Tensile basic creep: measurements and behavior at early age. *ACI materials journal, 98*(5), 386-393.

Andreasen, A. H. M. (1930). Ueber die Beziehung zwischen Kornabstufung und Zwischenraum in Produkten aus losen Körnern (mit einigen Experimenten). *Kolloid-Zeitschrift, 50*(3), 217-228. doi:10.1007/bf01422986

Arafa, M., Shihada, S., & Karmout, M. (2010). Mechanical properties of ultra high performance concrete produced in the Gaza Strip. *Asian Journal of Materials Science, 2*(1), 1-12.

ACI 363R (1992). Report on High-Strength Concrete. American Concrete Institute, Farmington Hills, Mich., 55.

ASTM C512 (2002). Standard test method for creep of concrete in compression. Paper presented at the ASTM.

ASTM C496. (2011). Standard test method for splitting tensile strength of cylindrical concrete specimens.

ASTM C39 (2012). Standard test method for compressive strength of cylindrical concrete specimens.

ASTM C09 (2014). Standard Test Method for Static Modulus of Elasticity and Poisson's Ratio of Concrete in Compression1.

Ashby, M. F. (2011). Materials selection in mechanical design (Burlington, MA: Butterworth-Heinemann.

Atrushi, D. S. (2003). *Tensile and compressive creep of young concrete: Testing and modelling*: Fakultet for ingeniørvitenskap og teknologi.

Balazs, G. L. (1993). Cracking analysis based on slip and bond stresses. *ACI materials journal, 90*, 340-340.

Bandelt, M. J., & Billington, S. L. (2016). Bond behavior of steel reinforcement in high-performance fiber-reinforced cementitious composite flexural members. *Materials and Structures, 49*(1-2), 71-86.

Bažant, Z., & Najjar, L. (1972a). Nonlinear water diffusion in nonsaturated concrete. *Materials and Structures, 5*(1), 3-20.

Bažant, Z., & Najjar, L. (1972b). Nonlinear water diffusion in nonsaturated concrete. *Matériaux et Construction, 5*(1), 3-20.

Bažant, Z., & Wu, S. (1974). Rate-type creep law of aging concrete based on Maxwell chain. *Matériaux et Construction, 7*(1), 45-60.

Bazant, Z. P. (1988). *Mathematical modeling of creep and shrinkage of concrete*: A Wiley Publication, NewYork, 99-115.

Bažant, Z. P., & Baweja, S. (1995). Justification and refinements of model B3 for concrete creep and shrinkage 1. statistics and sensitivity. *Materials and Structures, 28*(7), 415-430.

Bažant, Z. P., & Prasannan, S. (1989a). Solidification theory for concrete creep. I: Formulation. *Journal of engineering mechanics, 115*(8), 1691-1703.

Bažant, Z. P., & Prasannan, S. (1989b). Solidification theory for concrete creep. II: Verification and application. *Journal of engineering mechanics, 115*(8), 1704-1725.

B Wittmann, F. H. (1982). Creep and shrinkage mechanisms. Creep and shrinkage in concrete structures, 129-161.

Bellander, U. (1976). *INSPECTION SYSTEMS FOR DOCUMENTATION OF CONCRETE STRENGTH-QUALITY CRITERIA AND TEST FREQUENCY.* Retrieved from

Bentz, D. P., & Garboczi, E. J. (1991). Percolation of phases in a three-dimensional cement paste microstructural model. *Cement and Concrete Research, 21*(2-3), 325-344.

béton, C. e.-i. d. (1993). *CEB-FIP model code 1990: Design code*: Telford.

Bielenberg, A., Kerlin, M., Oppenheim, J., & Roberts, M. (2016). Financing change: How to mobilize private-sector financing for sustainable infrastructure. *McKinsey Center for Business and Environment*.

Bischoff, P. H. (2001). Effects of shrinkage on tension stiffening and cracking in reinforced concrete. *Canadian Journal of Civil Engineering, 28*(3), 363-374.

Bischoff, P. H. (2003). Tension stiffening and cracking of steel fiber-reinforced concrete. *Journal of materials in civil engineering, 15*(2), 174-182.

Bissonnette, B., & Pigeon, M. (1995). Tensile creep at early ages of ordinary, silica fume and fiber reinforced concretes. *Cement and Concrete Research, 25*(5), 1075-1085.

Bjøntegaard, Ø. (1999). *Thermal dilation and autogenous deformation as driving forces to self-induced stresses in high performance concrete*: Norges Teknisk-Naturvitenskapelige Universitet.

Błyszko, J. (2017). CoMParative analysis of creep in standard and fibre reinforced concretes under different load conditions. *Procedia Engineering, 193*, 478-485.

Boltzmann, L. (1876). On the theory of the elastic aftereffect. *Poggendorff's Ann. Phys. Chem, 7*, 624-645.

Brooks, J., & Neville, A. (1977). A comparison of creep, elasticity and strength of concrete in tension and in compression. *Magazine of Concrete research, 29*(100), 131-141.

Byfors, J. (1980). *Plain concrete at early ages*: Cement-och betonginst.

Chao, S.-H., Naaman, A. E., & Parra-Montesinos, G. J. (2009). Bond behavior of reinforcing bars in tensile strain-hardening fiber-reinforced cement composites. *ACI Structural Journal, 106*(6), 897.

Charron, J.-P., Denarié, E., & Brühwiler, E. (2007). Permeability of ultra high performance fiber reinforced concretes (UHPFRC) under high stresses. *Materials and Structures, 40*(3), 269-277.

Clark, L., & Cranston, W. (1980). The influence of bar spacing on tension stiffening in reinforced concrete slabs *Advances in concrete slab technology* (pp. 118-128): Elsevier.

Concrete, A. I. C. C. o., & Aggregates, C. (2014). *Standard Test Method for Static Modulus of Elasticity and Poisson's Ratio of Concrete in Compression1*: ASTM International.

Cook, D. J. (1972). *Some aspects of the mechanism of tensile creep in concrete*. Paper presented at the Journal Proceedings.

Corinaldesi, V., & Moriconi, G. (2012). Mechanical and thermal evaluation of Ultra High Performance Fiber Reinforced Concretes for engineering applications. *Construction and Building Materials, 26*(1), 289-294.

Coutinho, A. S. (1977). A contribution to the mechanism of concrete creep. *Matériaux et Construction, 10*(1), 3-16.

Creep, S. S. T. M. f., & Shrinkage. (1998). Measurement of time-dependent strains of concrete. *Materials and Structures, 31*, 507-512.

Davis, R. E., Davis, H. E., & Brown, E. H. (1937). *Plastic flow and volume changes of concrete*. Paper presented at the Proceedings.

Denarié, E., & Brühwiler, E. (2011). Strain-hardening Ultra-high Performance Fibre Reinforced Concrete: Deformability versus Strength Optimization. *Restoration of Buildings and Monuments, 17*(6), 397-410.

Denarié, E., Cécot, C., & Huet, C. (2006). Characterization of creep and crack growth interactions in the fracture behavior of concrete. *Cement and Concrete Research, 36*(3), 571-575.

Ding, Y., Yu, J.-t., Yu, K.-Q., & Xu, S.-l. (2018). Basic mechanical properties of ultra-high ductility cementitious composites: From 40 MPa to 120 MPa. *Composite structures, 185*, 634-645.

Ebead, U., & Marzouk, H. (2005). Tension-stiffening model for FRP-strenghened RC concrete two-way slabs. *Materials and Structures, 38*(2), 193-200.

Economy, N. C. (2014). The global commission on the economy and climate. *Washington DC: World Resources Institute*.

Fehling, E., Schmidt, M., & Stürwald, S. (2008). *Ultra High Performance Concrete (UHPC): Proceedings of the Second International Symposium on Ultra High Performance Concrete, Kassel, Germany, March 05-07, 2008*: kassel university press GmbH.

Garas, V., Kurtis, K., & Kahn, L. (2012). Creep of UHPC in tension and compression: effect of thermal treatment. *Cement and Concrete Composites, 34*(4), 493-502.

Garas, V. Y., Kahn, L. F., & Kurtis, K. E. (2009). Short-term tensile creep and shrinkage of ultra-high performance concrete. *Cement and Concrete Composites, 31*(3), 147-152.

Garas, V. Y., Kahn, L. F., & Kurtis, K. E. (2010). Tensile creep test of fiber-reinforced ultra-high performance concrete. *Journal of testing and evaluation, 38*(6), 674-682.

Gettu, R., Zerbino, R., & Jose, S. (2017). Factors Influencing Creep of Cracked Fibre Reinforced Concrete: What We Think We Know & What We Do Not Know *Creep Behaviour in Cracked Sections of Fibre Reinforced Concrete* (pp. 3-12): Springer.

Gilbert, R. (2002). Creep and shrinkage models for high strength concrete–proposals for inclusion in AS3600. *Australian Journal of Structural Engineering, 4*(2), 95-106.

Gilbert, R., Bradford, M., Gholamhoseini, A., & Chang, Z.-T. (2012). Effects of shrinkage on the long-term stresses and deformations of composite concrete slabs. *Engineering Structures, 40*, 9-19.

Gilbert, R. I., & Ranzi, G. (2010). *Time-dependent behaviour of concrete structures*: CRC Press.

Goto, Y. (1971). *Cracks formed in concrete around deformed tension bars.* Paper presented at the Journal Proceedings.

Graybeal, B., & Davis, M. (2008). Cylinder or cube: strength testing of 80 to 200 MPa (11.6 to 29 ksi) ultra-high-performance fiber-reinforced concrete. *ACI materials journal, 105*(6), 603.

Graybeal, B. A. (2007). Compressive behavior of ultra-high-performance fiber-reinforced concrete. *ACI materials journal, 104*(2), 146.

Graybeal, B. A., & Hartmann, J. L. (2003). *Strength and durability of ultra-high performance concrete.* Paper presented at the Concrete Bridge Conference.

Gribniak, V., Kaklauskas, G., & Bacinskas, D. (2008). Shrinkage in reinforced concrete structures: a computational aspect. *Journal of Civil Engineering and Management, 14*(1), 49-60.

Habel, K., Viviani, M., Denarié, E., & Brühwiler, E. (2006). Development of the mechanical properties of an ultra-high performance fiber reinforced concrete (UHPFRC). *Cement and Concrete Research, 36*(7), 1362-1370.

Harajli, M. (2009). Bond stress–slip model for steel bars in unconfined or steel, FRC, or FRP confined concrete under cyclic loading. *Journal of structural engineering, 135*(5), 509-518.

Hassan, A., Jones, S., & Mahmud, G. (2012). Experimental test methods to determine the uniaxial tensile and compressive behaviour of ultra high performance fibre reinforced concrete (UHPFRC). *Construction and Building Materials, 37*, 874-882.

Hatt, W. (1907). *Notes on the effect of time element in loading reinforced concrete beams.* Paper presented at the Proc. ASTM.

Heilmann, H. (1969). Beziehungen zwischen Zug-und Druckfestigkeit des Betons. *beton, 19*(2), 68-70.

Hillerborg, A., Modéer, M., & Petersson, P.-E. (1976). Analysis of crack formation and crack growth in concrete by means of fracture mechanics and finite elements. *Cement and Concrete Research, 6*(6), 773-781.

Holt, E., & Leivo, M. (2004). Cracking risks associated with early age shrinkage. *Cement and Concrete Composites, 26*(5), 521-530.

Hua, C., Acker, P., & Ehrlacher, A. (1995). Analyses and models of the autogenous shrinkage of hardening cement paste: I. Modelling at macroscopic scale. *Cement and Concrete Research, 25*(7), 1457-1468.

Huet, C. (1980). Adaptation d'un algorithme de Bazant au calcul des multilames visco-élastiques vieillissants. *Matériaux et Construction, 13*(2), 91-98.

Hung, C.-C., Lee, H.-S., & Chan, S. N. (2019). Tension-stiffening effect in steel-reinforced UHPC composites: Constitutive model and effects of steel fibres, loading patterns, and rebar sizes. *Composites Part B: Engineering, 158*, 269-278.

Hüsken, G. (2010). A multifunctional design approach for sustainable concrete: with application to concrete mass products.

Ian Gilbert, R. (2007). Tension stiffening in lightly reinforced concrete slabs. *Journal of structural engineering, 133*(6), 899-903.

Illston, J. (1965). The creep of concrete under uniaxial tension. *Magazine of Concrete research, 17*(51), 77-84.

Illston, J. (1972). Long-term cracking in reinforced concrete beams. *Proc. Inston. Civ. Engrs, 53*, 445-459.

Jafarifar, N., Pilakoutas, K., & Bennett, T. (2014). Moisture transport and drying shrinkage properties of steel–fibre-reinforced-concrete. *Construction and building materials, 73*, 41-50.

Jayasinghe, M. (2011). Prediction of time-dependent deformations in post-tensioned concrete suspended beams and slabs in tall buildings.

Kamen, A. (2007). *Comportement au jeune âge et différé d'un BFUP écrouissant sous les effets thermomécaniques*. Retrieved from

Kamen, A., Denarié, E., Sadouki, H., & Brühwiler, E. (2009). UHPFRC tensile creep at early age. *Materials and Structures, 42*(1), 113.

Kanstad, T., Hammer, T., Bjøntegaard, Ø., & Sellevold, E. (1999). Mechanical properties of young concrete: Evaluation of test methods for tensile strength and modulus of elasticity. *Determination of model parameters, SINTEF-report no. STF22 A, 99762*.

Kasai, Y., Vokoyama, K., & Matsui, I. (1972). *Tensile properties of early-age concrete*. Paper presented at the Proceedings of Conference on Mechanical Behaviour of Materials.

Kasai, Y., Yokoyama, K., & Hiraga, T. (1961). *Initial Strength of Concrete*.

Khan, A. A., Cook, W. D., & Mitchell, D. (1996). Tensile strength of low, medium, and high-strength concretes at early ages. *Materials Journal, 93*(5), 487-493.

Kishek, M. A. (1984). *Tension stiffening and crack widths in reinforced concrete beam and slab elements*. University of Cambridge.

Kizhakommudom, H., Li, Z., & Schiff, S. D. (2014). Research Project No. 682 Development of High-Strength/High Performance Concrete/Grout Mixtures for.

Kolver, K., Igarashi, S., & Bentur, A. (1999). Tensile creep behavior of high strength concretes at early ages. *Materials and Structures, 32*(5), 383-387.

Kovler, K. (1994). Testing system for determining the mechanical behaviour of early age concrete under restrained and free uniaxial shrinkage. *Materials and Structures, 27*(6), 324.

Kovler, K. (1995). Interdependence of creep and shrinkage for concrete under tension. *Journal of materials in civil engineering, 7*(2), 96-101.

Kovler, K. (1999). A new look at the problem of drying creep of concrete under tension. *Journal of materials in civil engineering, 11*(1), 84-87.

Kristiawan, S. (2006). STRENGTH SHRINKAGE AND CREEP OF CONCRETE IN TENSION AND COMPRESSION. *Civil Engineering Dimension, 8*(2), 73-80.

Kusumawardaningsih, Y., Fehling, E., Ismail, M., & Aboubakr, A. A. M. (2015). Tensile strength behavior of UHPC and UHPFRC. *Procedia Engineering, 125*, 1081-1086.

Ladaoui, W. (2010). *Etude expérimentale du comportement Thermo-Hydro-Mécanique à long terme des BHP destinés aux ouvrages de stockage des déchets radioactifs*. Université de Toulouse, Université Toulouse III-Paul Sabatier.

Lagier, F., Massicotte, B., & Charron, J.-P. (2016). Experimental investigation of bond stress distribution and bond strength in unconfined UHPFRC lap splices under direct tension. *Cement and Concrete Composites, 74*, 26-38.

Lam, J.-P. (2002). Evaluation of concrete shrinkage and creep prediction models.

Laube, M. (1990). *Werkstoffmodell zur Berechnung von Temperaturspannungen in massigen Betonbauteilen im jungen Alter*. Retrieved from

Le, T. T. (2008). *Ultra high performance fibre reinforced concrete paving flags*. University of Liverpool.

Lee, Y., Kang, S.-T., & Kim, J.-K. (2010). Pullout behavior of inclined steel fiber in an ultra-high strength cementitious matrix. *Construction and building materials, 24*(10), 2030-2041.

Li, V. C., Wang, S., & Wu, C. (2001). Tensile strain-hardening behavior of polyvinyl alcohol engineered cementitious composite (PVA-ECC). *ACI Materials Journal-American Concrete Institute, 98*(6), 483-492.

Li, Y., Bao, J., & Guo, Y. (2010). The relationship between autogenous shrinkage and pore structure of cement paste with mineral admixtures. *Construction and Building Materials, 24*(10), 1855-1860.

Ma, J., Orgass, M., Dehn, F., Schmidt, D., & Tue, N. (2004). *CoMParative investigations on ultra-high performance concrete with and without coarse aggregates*. Paper presented at the Proceedings of international symposium on ultra high performance concrete, Germany.

Máca, P., Sovják, R., & Vavřiník, T. (2013). Experimental investigation of mechanical properties of UHPFRC. *Procedia Engineering, 65*, 14-19.

Martin, J., Stanton, J., Mitra, N., & Lowes, L. N. (2007). Experimental testing to determine concrete fracture energy using simple laboratory test setup. *ACI materials journal, 104*(6), 575.

Marzouk, H., & Chen, Z. (1995). Fracture energy and tension properties of high-strength concrete. *Journal of materials in civil engineering, 7*(2), 108-116.

Mohammed, H. (2015). *Mechanical Properties of Ultra High Strength Fiber Reinforced Concrete*. University of Akron.

Moreno, D. M., Trono, W., Jen, G., Ostertag, C., & Billington, S. L. (2014). Tension stiffening in reinforced high performance fiber reinforced cement-based composites. *Cement and Concrete Composites, 50*, 36-46.

Morin, D., & Maso, J. (1982). Fluage en traction des bétons ordinaires et des bétons légers. *Matériaux et Construction, 15*(5), 469-473.

Mu, R., & Forth, J. (2009). Modelling shrinkage of concrete from moisture lost using moisture diffusion theory. *Magazine of Concrete Research, 61*(7), 491-497.

Naaman, A. (2003). *Setting the Stage, Toward Performance Based Classification of FRC Composites*. Paper presented at the High Performance Fiber Reinforced Cement Composites (HPFRCC 4), Proc. of the 4th Int. RILEM Workshop, 2003.

Naaman, A. E., & Wille, K. (2012). The path to ultra-high performance fiber reinforced concrete (UHP-FRC): five decades of progress. *Proceedings of Hipermat*, 3-15.

Neville, A., Dilger, W., & Brooks, J. (1981). Creep of plain and structural concrete**. Construction press, Longman Group Ltd, England.

Østergaard, L., Lange, D. A., Altoubat, S. A., & Stang, H. (2001). Tensile basic creep of early-age concrete under constant load. *Cement and Concrete Research, 31*(12), 1895-1899.

Ouyang, C., Wollrab, E., Kulkarni, S., & Shah, S. P. (1997). Prediction of cracking response of reinforced concrete tensile members. *Journal of structural engineering, 123*(1), 70-78.

Ozawa, M. (2002). Evaluation of creep of high-strength concrete at early ages. *Control cracking in Early Age Concrete*, 255-264.

Persson, B. (1997). Basic Deformations of High-Performance Concrete at Early Ages. *Nordic Concrete Research, 20*, 59-74.

Plagué, T., Desmettre, C., & Charron, J.-P. (2017). Influence of fiber type and fiber orientation on cracking and permeability of reinforced concrete under tensile loading. *Cement and Concrete Research, 94*, 59-70.

Pyo, S., El-Tawil, S., & Naaman, A. E. (2016). Direct tensile behavior of ultra high performance fiber reinforced concrete (UHP-FRC) at high strain rates. *Cement and Concrete Research, 88*, 144-156.

Ranaivomanana, N., Multon, S., & Turatsinze, A. (2013a). Basic creep of concrete under compression, tension and bending. *Construction and building materials, 38*, 173-180.

Ranaivomanana, N., Multon, S., & Turatsinze, A. (2013b). Tensile, compressive and flexural basic creep of concrete at different stress levels. *Cement and Concrete Research, 52*, 1-10.

Ranzi, G., & Gilbert, R. I. (2010). *Time-dependent behaviour of concrete structures*: CRC Press.

Reddy, D. H., & Ramaswamy, A. (2018). Experimental and numerical modeling of creep in different types of concrete. *Heliyon, 4*(7).

Reinhardt, H.-W., & Rinder, T. (2006). Tensile creep of high-strength concrete. *journal of advanced concrete technology, 4*(2), 277-283.

Reviron, N., Nahas, G., Tailhan, J., Le Maou, F., Benboudjema, F., & Millard, A. (2008). Experimental study of uniaxial tensile creep of concrete. *Concreep, 8*, 453-457.

Rhodes, J. A., & Carreira+, D. J. (1982). Prediction of creep, shrinkage, and temperature effects in concrete structures: Hills, Unite States: American Concrete Institue.

Richard, P., & Cheyrezy, M. (1995). Composition of reactive powder concretes. *Cement and Concrete Research, 25*(7), 1501-1511.

Rossi, P., Charron, J. P., Bastien-Masse, M., Tailhan, J.-L., Le Maou, F., & Ramanich, S. (2014). Tensile basic creep versus compressive basic creep at early ages: comparison

between normal strength concrete and a very high strength fibre reinforced concrete. *Materials and Structures, 47*(10), 1773-1785.

Rossi, P., Godart, N., Robert, J., Gervais, J., & Bruhat, D. (1994). Investigation of the basic creep of concrete by acoustic emission. *Materials and Structures, 27*(9), 510.

Rossi, P., Tailhan, J.-L., & Le Maou, F. (2013). Comparison of concrete creep in tension and in compression: Influence of concrete age at loading and drying conditions. *Cement and Concrete Research, 51*, 78-84.

Rossi, P., Tailhan, J.-L., Le Maou, F., Gaillet, L., & Martin, E. (2012). Basic creep behavior of concretes investigation of the physical mechanisms by using acoustic emission. *Cement and Concrete Research, 42*(1), 61-73.

Roth, M., Eamon, C., Slawson, T., Tonyan, T., & Dubey, A. (2010). Ultra-high-strength, glass fiber-reinforced concrete: Mechanical behavior and numerical modeling. *ACI materials journal, 107*(2), 185.

Rößler, C., Bui, D.-D., & Ludwig, H.-M. (2014). Rice husk ash as both pozzolanic admixture and internal curing agent in ultra-high performance concrete. Cement and Concrete Composites, 53, 270-278.

Sobuz, H., Visintin, P., Ali, M. M., Singh, M., Griffith, M., & Sheikh, A. (2016). Manufacturing ultra-high performance concrete utilising conventional materials and production methods. *Construction and Building Materials, 111*, 251-261.

Soliman, A., & Nehdi, M. (2011). Effect of drying conditions on autogenous shrinkage in ultra-high performance concrete at early-age. *Materials and Structures, 44*(5), 879-899.

Sooriyaarachchi, H., Pilakoutas, K., & Byars, E. (2005). Tension stiffening behavior of GFRP-reinforced concrete. *Special Publication, 230*, 975-990.

Sturm, A., Visintin, P., Oehlers, D., & Seracino, R. (2018). Time-dependent tension-stiffening mechanics of fiber-reinforced and ultra-high-performance fiber-reinforced concrete. *Journal of structural engineering, 144*(8), 04018122.

Sturm, A. B., & Visintin, P. Local bond slip behavior of steel reinforcing bars embedded in ultra high performance fibre reinforced concrete. *Structural Concrete*.

Su, L., Wang, Y.-f., Mei, S.-q., & Li, P.-f. (2017). Experimental investigation on the fundamental behavior of concrete creep. *Construction and building materials, 152*, 250-258.

Switek, A., Denarié, E., & Brühwiler, E. (2009). *Tensile creep of UHPFRC under low and high stresses*. Paper presented at the 4th Internatioinal Conference on Construction materials: Performance, Innovations and Structural Implications ConMat" 09.

Tam, C. M., Tam, V. W., & Ng, K. M. (2012). Assessing drying shrinkage and water permeability of reactive powder concrete produced in Hong Kong. *Construction and Building Materials, 26*(1), 79-89.

Tam, V. W., Kotrayothar, D., & Xiao, J. (2015). Long-term deformation behaviour of recycled aggregate concrete. *Construction and Building Materials, 100*, 262-272.

Terrill, J., Richardson, M., & Selby, A. (1986). Non-linear moisture profiles and shrinkage in concrete members. *Magazine of Concrete Research, 38*(137), 220-225.

Vandamme, M., & Ulm, F.-J. (2009). Nanogranular origin of concrete creep. *Proceedings of the National Academy of Sciences, 106*(26), 10552-10557.

Vande Voort, T. L., Suleiman, M. T., & Sritharan, S. (2008). *Design and performance verification of ultra-high performance concrete piles for deep foundations*. Retrieved from

Visintin, P., Oehlers, D., & Haskett, M. (2013). Partial-interaction time dependent behaviour of reinforced concrete beams. *Engineering Structures, 49*, 408-420.

Wang, K., Shah, S. P., & Phuaksuk, P. (2001). Plastic shrinkage cracking in concrete materials-influence of fly ash and fibres. *ACI materials journal, 98*(6), 458-464.

Ward, M., & Cook, D. (1969). The mechanism of tensile creep in concrete. *Magazine of Concrete Research, 21*(68), 151-158.

Warner, R., Foster, S., Gravina, R., & Faulkes, K. (2017). *Prestressed concrete*: Pearson Education Austral.

Wei, S., Mandel, J. A., & Said, S. (1986). *Study of the interface strength in steel fiber-reinforced cement-based composites*. Paper presented at the Journal Proceedings.

Wille, K., El-Tawil, S., & Naaman, A. E. (2014). Properties of strain hardening ultra high performance fiber reinforced concrete (UHP-FRC) under direct tensile loading. *Cement and Concrete Composites, 48*, 53-66.

Woolson, I. H. (1905). Some remarkable tests indicating'flow'of concrete under pressure. *Engineering News, 54*(18), 459-460.

Wu, M. H. Q. (2010). *Tension stiffening in reinforced concrete–instantaneous and time-dependent behaviour*. UNIVERSITY OF NEW SOUTH WALES, SYDNEY.

Yang, S., Millard, S., Soutsos, M., Barnett, S., & Le, T. T. (2009). Influence of aggregate and curing regime on the mechanical properties of ultra-high performance fibre reinforced concrete (UHPFRC). *Construction and Building Materials, 23*(6), 2291-2298.

Yoo, D.-Y., Kim, S., & Kim, M.-J. (2018). CoMParative shrinkage behavior of ultra-high-performance fiber-reinforced concrete under ambient and heat curing conditions. *Construction and Building Materials, 162*, 406-419.

Yoo, D.-Y., Park, J.-J., Kim, S.-W., & Yoon, Y.-S. (2013). Early age setting, shrinkage and tensile characteristics of ultra high performance fiber reinforced concrete. *Construction and Building Materials, 41*, 427-438.

Yoo, D.-Y., Park, J.-J., Kim, S.-W., & Yoon, Y.-S. (2014). Influence of ring size on the restrained shrinkage behavior of ultra high performance fiber reinforced concrete. Materials and Structures, 47(7), 1161-1174.

Yu, R., Spiesz, P., & Brouwers, H. (2014). Mix design and properties assessment of ultra-high performance fibre reinforced concrete (UHPFRC). *Cement and Concrete Research, 56*, 29-39.

Zhang, M., Tam, C., & Leow, M. (2003). Effect of water-to-cementitious materials ratio and silica fume on the autogenous shrinkage of concrete. *Cement and Concrete Research, 33*(10), 1687-1694.

Zhao, G., Di Prisco, M., & Vandewalle, L. (2015). Experimental investigation on uniaxial tensile creep behavior of cracked steel fiber reinforced concrete. *Materials and Structures, 48*(10), 3173-3185.

Zhao, Q., Yu, J., Geng, G., Jiang, J., & Liu, X. (2016). Effect of fiber types on creep behavior of concrete. *Construction and Building Materials, 105*, 416-422.

Zheng, W., Kwan, A., & Lee, P. (2001). Direct tension test of concrete. *Materials Journal, 98*(1), 63-71.